FACULTY OF BIOSCIENCE ENGINEERING

VALORIZATION OF SOUTH KOREAN MARINE BIOWASTE VIA HYDROTHERMAL CARBONIZATION: HYDROCHAR SYNTHESIS AND INVESTIGATION OF ADSORPTION CAPACITY

Elisa Kooy
Student number: 01900719

Promotors: Prof. Dr. ir. Philippe M. Heynderickx, Prof. Dr. ir. Frederik Ronsse

Tutor: MSc. Tatwadhika Rangin Siddhartha

Master's Dissertation submitted to Ghent University in partial fulfilment of the requirements for the degree of Master of Science in Bioscience Engineering: Environmental Technology

Academic year: 2023-2024

GHENT UNIVERSITY

Ghent, 7th of June 2024

The promotors,

Prof. Dr. ir. Frederik Ronsse

Prof. Dr. ir. Philippe M. Heynderickx

The author,

Elisa Kooy

PREFACE

Time really flew by when I think that less than one year ago, I embarked on a plane to South Korea. Now, I am presenting my thesis and have almost reached the end of my master's studies. Writing this thesis has brought me many good memories and much knowledge. I am very thankful for the pleasant journey this thesis has been, mainly thanks to the support and involvement of several people, to whom I would like to express my gratitude.

I would like to thank my two promotors, Prof. Dr. ir. Philippe M. Heynderickx and Prof. Dr. ir. Frederik Ronsse, for their guidance throughout this past year. Prof. Dr. ir. Heynderickx's comments and reflections have challenged and encouraged me to push this thesis to a higher level. Thanks to him, I have learned the unlimited possibilities of Excel and that progress is not always linear. Prof. Dr. ir. Ronsse's feedback and encouragement were invaluable, giving me more confidence to persevere, finding explanations when faced with challenges, and motivating me to go the extra mile. Furthermore, I want to thank them for giving me the opportunity to do research abroad.

My stay in South Korea and my days in the lab would not have been as enjoyable had it not been for my tutor Dhika. Thank you for being a very empathetic tutor; no question was too much, and you always stayed optimistic and positive. I've learned to be more patient and not to let my perfectionism get in the way of progress.

A heartfelt thank you (감사합니다!) to the people I met during my stay in South Korea: for the friendship, laughs, and hardships we shared, and for encouraging each other. Also, to my friends at UGent (Lien, Elise, Heleen, Justine, Phara, Lotte), who have made the past five years unforgettable. I would also like to thank UGent and the Flemish government for supporting me financially during my studies and exchanges, and for opening doors that I and others may have otherwise found too heavy.

Lastly, I would like to thank my family. I am eternally grateful to them for encouraging me during my studies and supporting me unconditionally.

CONTENTS

ABSTRACT (EN)

This thesis addresses the pressing issue of marine biowaste generated from the consumption of fish and seafood, which poses significant environmental and socioeconomic challenges. With global population growth, the generation of such waste is expected to rise, necessitating responsible management strategies. Therefore, the valorisation potential through hydrothermal carbonization (HTC) was investigated. HTC on eight fish and crustacean species was performed at three different temperatures (T = 200, 220, 240°C, t = 5h, w/b = 7). The produced hydrochars (HC) were characterized through point zero charge (PZC), elemental and proximate analysis and FTIR. Their adsorption characteristics were evaluated using kinetic and adsorption models and using one-point adsorption experiments with an anionic (methyl orange, MO) and cationic (methylene blue, MB) dye. In addition, the influence of ionic strength on the adsorption performance was evaluated. Crustacean-HC showed higher yields (37-69%) than fish-HC (15-22%). Furthermore, crustacean-HC showed higher PZC than fish-HC (7.93 versus 6.49). The adsorption capacity of the HCs (MB: 2.7-10.8 mg/g and MO: 5.9-9.2 mg/g) showed a higher adsorption of MO for the crustacean-HCs. Difference in ionic strength in adsorption experiments was concluded to not yield significantly different adsorption results. The difference in yields, PZC and adsorption results were explained by the differences in feedstock composition, further emphasizing the importance of elucidating the inherent feedstock characteristics for waste utilization.

ABSTRACT (NL)

Deze masterthesis behandelt het groeiende probleem van marien bioafval dat wordt gegenereerd door de consumptie van vis en schaaldieren, wat aanzienlijke milieu en socio-economische uitdagingen met zich meebrengt. Met de groei van de wereldbevolking wordt verwacht dat de productie van dergelijk afval zal toenemen, waardoor verantwoorde beheerstrategieën nodig zijn. Daarom werd het valorisatiepotentieel via hydrothermale carbonisatie (HTC) onderzocht. HTC werd op acht vis- en schaaldiersoorten uitgevoerd bij drie verschillende temperaturen (T = 200, 220, 240°C, t = 5u, w/b = 7). De geproduceerde *hydrochars* (HC) werden gekarakteriseerd door middel van *point zero charge* (PZC), elementaire en proximate analyse en FTIR. Hun adsorptiekarakteristieken werden geëvalueerd met behulp van kinetische en adsorptiemodellen en via éénpuntsadsorptie-experimenten met een anionische (methyloranje, MO) en kationische (methyleenblauw, MB) kleurstof. Daarnaast werd de invloed van de ionsterkte op de adsorptiecapaciteiten geëvalueerd. HC van schaaldieren vertoonde een hoger rendement (37-69%) dan HC van vissen (15-22%). Bovendien vertoonde HC van schaaldieren een hogere PZC dan HC van vissen (7,93 versus 6,49). De adsorptiecapaciteit van de HCs (MB: 2,7-10,8 mg/g en MO: 5,9-9,2 mg/g) toonde een hogere adsorptiecapaciteit van MO voor de schaaldieren. De invloed van de ionsterkte in de adsorptie-experimenten werd aangetoond niet significant te zijn. Het verschil in opbrengst, PZC en adsorptieresultaten werd verklaard door de verschillen in de samenstelling van de soort vis en schaaldier, wat benadrukt hoe belangrijk het is om de inherente eigenschappen van de grondstof voor het gebruik van afval te achterhalen.

LIST OF FIGURES

LIST OF TABLES

NOMENCLATURE

Acronyms

BC	Biochar	-
CS	Carbon sequestration	-
DI	Deionized water	-
EBC	European Biochar Certificate	-
FA	Fatty acids	-
FAO	Food and Agriculture Organisation	-
FC	Fixed carbon	%
FFG	Frumkin-Fowler-Guggenheim isotherm	-
FTIR	Fourier Transform Infrared	-
FW	Food waste	-
HC	Hydrochar	-
HDB	Hill-de Boer isotherm	-
HHV	Higher heating value	kJ/g
HTC	Hydrothermal carbonization	-
MB	Methylene blue	-
MO	Methyl orange	-
MW	Molecular weight	g/mol
NED	Non-edible ratio	-
NLBM	Non-lignocellulosic biomass	-
NRMSE	Normalized root mean square error	-
NSD	Normalized standard error	-
OFG	Oxygen-containing functional groups	-
PFOM	Pseudo-first order kinetic model	-
PSOM	Pseudo-second order kinetic model	-
PZC	Point of zero charge	-
SC	Supercapacitor	-
SK	South Korea	-
SSE	Residual sum of squares	-
SST	Residual sum of total deviations	-
TGA	Thermogravimetric analysis	-
VM	Volatile matter	%
VOC	Volatile Organic Compounds	-

Latin symbols

$\mathcal{B}$	Buffer capacity	mol/L
C	Concentration	mg/L
f	Function	-
K	Equilibrium coefficient	-
k_1	Rate constant of PFOM	min^{-1}
K_2	Rate constant of PSOM	min^{-1}

K_a	Acid dissociation constant	mol/L
K_w	Ionic product of water	mol/L
m_{dry}	Mass of wet sample	g
m_{wet}	Mass of dry sample	g
n_p	Number of performed observations	-
p	Number of adjustable parameters	-
q_m	Maximum adsorption capacity	mg/g
R	Universal gas constant	kJ/mol/K
R^2	Square coefficient of correlation	-
R^2_{Adj}	Adjusted square coefficient of correlation	-
T	Temperature	°C
t	Residence time	s
V	Volume	L
W	Interaction energy between adsorbed molecules	kJ/mol
w	Moisture content	%
w_{add}	Added water to HTC container	g
w/b	Water-to-biomass ratio	g/g
wt.%	Weight percentage	%
x	Mass of conjugate base	g
y	Mass of acid	g
z	Charge of an ion	-

Greek symbols

α	Initial adsorption rate	mg/(g·h)
β	Desorption coefficient	g/mg
η	Removal efficiency	%
θ	Fractional coverage	-
μ	Ionic strength	mol/L
ρ_{AB}	Correlation between real variables A and B	-
σ	Standard deviation	-

Subscripts

0	Initial state
b	Base
c	Critical point
e	Equilibrium state
exp	Experimental value
F	Freundlich
i	A single component out of a group of components
L	Langmuir
max	Maximum
mod	Modelled value

1. INTRODUCTION

The consumption of aquatic foods has reached unprecedented levels, with individuals consuming approximately 20.5 kg/year per capita in 2020, more than double the consumption rate of half a century ago [1]. This expansion underscores why the United Nations' 2030 Agenda for Sustainable Development and the FAO recognize the critical role of fisheries and aquaculture in ensuring food security and nutrition [2]. However, the expansion of the sector results in increasing quantities of by-products. The FAO estimates that fish loss and waste account for 30% to 35% of total production in most regions worldwide [3]. Depending on size, species, and processing method, this may even constitute up to 70% of processed fish [1].

Fish and seafood consumption lies between 9.6 kg/capita/yr (Africa) and 24.7 kg/capita/yr (Asia). Considering this, South Korea positions itself as a major fish and seafood consumer with 55.27 kg/capita/yr in 2020 [4]. Given that approximately 80% of South Korea's land comprises of mountains and non-arable areas, aquatic resources play a vital role in meeting its food needs [5]. Consequently, effective waste management for marine biowaste holds paramount importance in South Korea. Especially when considering the potential hazards related to these by-products, such as wastewater leakage, unpleasant odours, illegal landfill disposal, and ocean dumping [6]. Moreover, in the era of circular economy, the generation of waste should be minimized by transitioning from a linear economy to a circular economy. This implies the creation of economic value, the creation of social value and the creation of value in terms of the environment from converting waste into secondary resources [7]. The conversion of fishery by-products into hydrochar (HC) presents an opportunity to align the management of marine biowaste with the principles of a circular economy.

Turning fishery by-products into HC using hydrothermal carbonization can be part of the solution in reconciling effective marine biowaste management and circular economy. Currently, there is a noticeable scarcity of research focused on exploring the potential of HTC for marine by-products, particularly those beyond algae. Therefore, this thesis aims to address the gaps in the literature and assess the feasibility of producing HC from marine biowaste. The possible applications will also be explored keeping the chemical composition and physical characteristics of the produced HC into account.

The general objective of this thesis is to identify the optimal parameters for hydrochar production specific to fish and crustacean waste, as well as exploring their potential applications. To achieve this, the thesis will begin with a literature review on feedstock streams and the production of HC. The potential applications will also be examined in regard to the characteristics inherent to the HC. The subsequent section will detail the experiments conducted to generate and characterize the HC. Finally, the findings will be discussed, conclusions will be drawn, and recommendations for future research will be provided.

2. LITERATURE REVIEW

2.1. Feedstock

Biomass is defined as all biological material obtained from living, or recently living organisms [8]. However, it is more often associated with plants or plant-derived materials, also called lignocellulosic biomass, which is composed of three main components: hemicellulose, cellulose, and lignin [9]. However, biomass can also encompass microorganisms, animals, specific parts of plants, and materials derived from them. These are defined as non-lignocellulosic biomass (NLBM) and are composed of proteins, lipids, carbohydrates, and inorganics with no or only a slight fraction of cellulose, hemicellulose, and lignin [10], [11]. For hydrothermal carbonization (HTC), both lignocellulosic and non-lignocellulosic streams can be valuable feedstocks.

It has been argued that both are convenient sources for HTC due to their widespread availability and potential to yield high-quality hydrochars [10]. However, the reaction mechanisms of HTC on lignocellulosic biomass have been elucidated more profoundly than on non-lignocellulosic biomass [12], [13], [14]. Thus, the widespread non-lignocellulosic biomass waste streams are still faced with considerable challenges and knowledge gaps for conversion into valuable products due to their complex and diverse composition. A big challenge when choosing non-lignocellulosic biomass in comparison to lignocellulosic biomass is -for example- the greater risk for toxicity due to the higher contents of heavy metals and heteroatoms such as nitrogen (N), phosphorus (P) and sulphur (S) [15], [16], [17]. The heavy metals contained in the biomass could dissolve in water, leading to water pollution and possible accumulation in the food chain [18], [19]. The presence of excessive N and P could also result in the eutrophication of water bodies [15].

Despite these challenges, the wide-ranging composition of non-lignocellulosic biomass could lead to different behaviours during thermochemical conversion, possibly yielding products of value. The mentioned elements (N, P, S, and metals) could be of benefit during hydrothermal conversion processes. During heating, the heteroatoms and metals could act as activators for the biomass decomposition which could lead to the formation of a carbon framework with high-value characteristics such as a high porosity and a great diversity in functional groups [11], [14].

The subsequent sections will provide an overview of various non-lignocellulosic feedstock options suitable for HTC. There will be a particular focus on marine biowaste as a unique feedstock for hydrochar production as this will be the feedstock used in the experimental work.

2.1.1. Non-lignocellulosic biomass

As mentioned previously, NLBM is mainly composed of proteins, lipids, carbohydrates, and inorganics with no or only a slight fraction of cellulose, hemicellulose and lignin [10]. Figure 1 shows the different NLBM streams which can be used for HTC as well as the main constituents they are composed of; these will be described in the following sections.

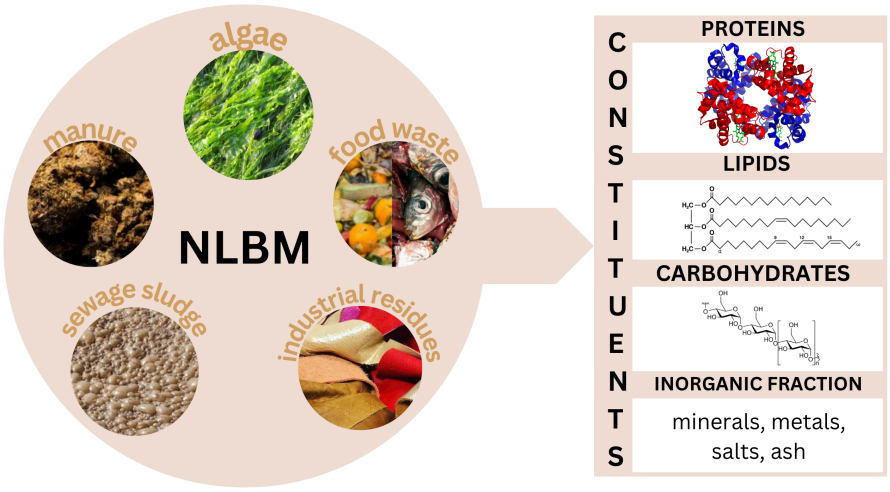

Figure 1: Schematic view of the main non-lignocellulosic biomass streams and their main constituents.

2.1.1.1. Proteins

Proteins are macromolecules that are present in all living things. There are 20 amino acids forming the building blocks of most proteins. Each amino acid contains a primary amine and carboxylic acid group, as can be seen in Figure 2. In the simplest case, R = H, which is glycine or aminoacetic acid. In other amino acids, R can be a group which is aliphatic, aromatic, heterocyclic, hydroxyl, acidic, amide, basic or which contains sulphur. Amino acids are linked covalently by connecting the α-carboxyl group of one amino acid and the α-amino group of another amino acid through an amide or peptide bond to form peptides, oligopeptides, polypeptides, and proteins. The amide linkage in proteins is a partial double bond. A protein is argued to be achieved when about 100 amino acids are linked. Proteins contain 50-55% carbon (C), 6-7% hydrogen (H), 20-23% oxygen (O), 12-19% nitrogen and 0.2-3% sulphur (all in wt.%) [20].

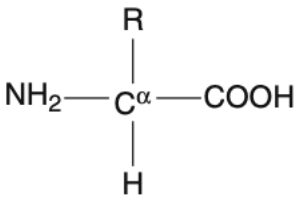

Figure 2: General structure of an amino acid [20].

2.1.1.2. Carbohydrates

Most natural carbohydrates are classified as simple sugars (mono- and disaccharides), oligomers (oligosaccharides), and polymers (polysaccharides). Monosaccharides are defined as simple carbohydrates containing three to eight carbon atoms, however, only those with five or six carbon atoms are common. Glucose and fructose (Figure 3(a-b)) are the two most important six-carbon monosaccharides with the general formula $C_6H_{12}O_6$. Oligosaccharides are formed when the reducing group of one monosaccharide connects to one of the hydroxyl groups on another through a glycosidic bond, to form disaccharides. Many glycosidic bonds can be established to form trisaccharides, tetrasaccharides, etc., and ultimately polysaccharides. Polysaccharides are formed when oligosaccharides have more than ten monosaccharides. Carbohydrates are susceptible to a wide range of chemical reactions with other compounds due to the presence of hydroxyl groups and in some cases carbonyl groups [21].

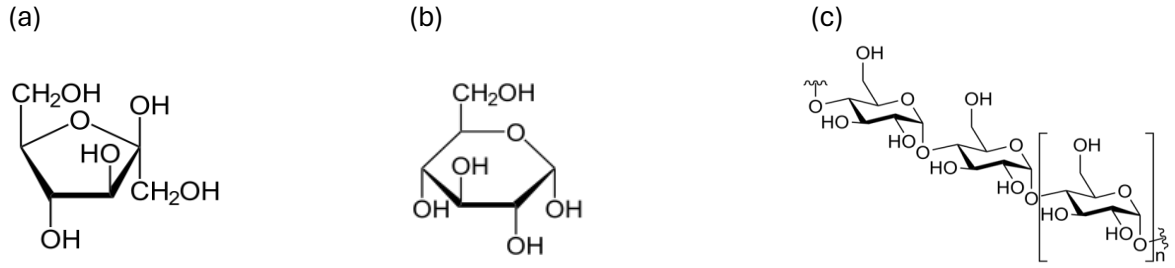

Figure 3: two monosaccharides: (a) fructose (β-d-fructofuranose) and (b) glucose (α-d-glucopyranose) and (c) a polysaccharide (amylose) [22], [23], [24].

2.1.1.3. Lipids

Lipids are hydrophobic molecules which include fatty acids (FA), glycerides, phospholipids, sterols, sphingolipids, and prenol lipids [25]. Fats and oils are triglycerides and are major components of certain NLBM residues; therefore, these will be explained in more detail. Glycerides have a glycerol molecule backbone joined to one or more FA molecules and the term includes mono-, di- and triglycerides. A triglyceride contains glycerol esterified to three fatty acid molecules, as can be seen on Figure 4 [26]. The arrangement and specific type of fatty acids on the glycerol determine the chemical and physical properties of a glyceride. FA are long hydrocarbon chains with a methyl group ($-CH_3$) at one end of the chain and a carboxylic acid group (-COOH) at the other end. Most natural FA contain 4 to 24 carbon atoms (and always an even number in the chain) and can be called saturated or unsaturated. FA are saturated when they only contain single carbon-to-carbon bonds and have the general formula $CH_3(CH_2)_nCOOH$, they are called unsaturated when they contain one or more double bonds [21]. The melting point-range is determined by the length of FA chains, number of double bonds and isomeric configuration [27]. Long-chain fatty acids have a higher melting point than short-chain fatty acids because there is more potential for attraction between long chains, which means a greater force of attraction between the molecules. The higher the number of double bonds, the lower the melting point. The isomeric configuration refers to the *cis* or *trans* configuration of the hydrogen atoms attached to the double-bonded carbon atoms. If they are located on the same side, they are in the *cis* configuration and have a lower melting point than *trans* double bonds. The lower melting point is

due to the formation of coil structures, creating less attraction between the molecules [20], [26]. Generally however, unsaturated fats have a low melting point and a liquid form at room temperature [28].

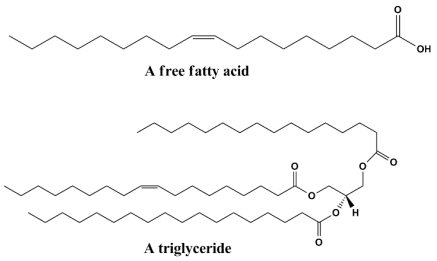

Figure 4: Chemical structure of an unsaturated fatty acid and triglyceride [29].

2.1.1.4. Inorganic fraction

Inorganic substances include all those that do not contain carbon-to-carbon or carbon-to-hydrogen bonds, i.e., those that are not classified as organic compounds [30]. Vassilev et al. (2012) have conducted a study on the inorganic matter of various biomass sources and found that it includes mostly mineral matter, especially mineral species and poorly crystallized mineraloids, as well as amorphous inorganic phases. The amount varies strongly depending on the biomass source, from 0.1 to 46% based on ash yield (dry basis). The inorganic phases in biomass can be categorized into: (i) silicates, (ii) oxides and hydroxides, (iii) sulphates, sulphites, and sulphides, (iv) phosphates, (v) carbonates, (vi) chlorides, (vii) nitrates and (viii) others. Depending on the biomass stream, these fractions can vary in abundance. However, minerals are chemically inert to heat, light, oxidizing agents, and extreme pH [31]. Therefore, the mineral composition of biomass and carbonization products have a strong impact on processing, application, and various environmental and technological considerations [32].

2.1.1.5. Non-lignocellulosic residues for HTC

In the previous section, the main constituents of NLBM were described. These constituents can be quantified for various NLBM waste streams. There is a big variety of non-lignocellulosic residues which can be broadly categorized into sewage sludge, manure, food waste, algal biomass, and industrial residues. Table 1 gives an overview of the main composition of these residues. The subsequent sections will provide further descriptions of these waste streams.

Table 1: Main constituents of different non-lignocellulosic biomass wastes, range is given.

Type	Lipids (%)	Carbohydrates (%)	Proteins (%)	Ash (%)	Ref.
Sewage sludge (n=3)	12-27.3	8.9-27.3	9.9-42.8	32.1-42.7	[33], [34], [35]
Manure (n=3)	2.1-8.7	34.5-52.6	18.1-31.6	12-15.9	[36]
Food waste (n=3)	15.2-15.7	50.2-51.4	16.1-27.5	5.4-16.1	[37], [38], [39]
Algal biomass					
Macroalgae (n=3)	0.6-3.9	30.5-33.6	9.3-12.2	17.1-35.8	[40], [41]
Microalgae (n=3)	1.1-51	7.4-24.8	14-45.2	8.9-14.4	[42], [43], [44]
Industrial biowaste (n=3) (Chicken feathers, leather fleshing waste, hog hair)	2.4-48.8	0-7.9	14.9-94.2	3.3-34.7	[45], [46], [47]

2.1.1.5.1. Sewage sludge

Sewage treatment has expanded in many countries, resulting in an increase of sludge that must be disposed of [48]. It is imperative to manage the sludge well as it contains nutrients, pathogens, heavy metals and other micropollutants that could cause harm if not disposed of responsibly [49], [50]. The global production rate of sewage sludge from municipal wastewater treatment plants in 2017 was determined as 45 dry MT per year [51]. This amount is bound to increase as new wastewater treatment plants are established. Therefore, sewage sludge can be a viable biomass feedstock. However, one of the main drawbacks is the presence of micropollutants and heavy metals, raising concerns for the environment. Another factor to consider is the high ash content (Table 1). This is due to the presence of many inorganic minerals and heavy metals. It was found that the major ash-forming elements in sewage sludge are Si, Al, Fe, Ca, and Mg as well as the alkali metals Na and K. In addition, some heavy metals have also been found in sewage sludge (Cr, Ni, Cu, Zn, Pb, Cd, and Hg). These heavy metals may originate from various sources such as industrial wastewater, run-off, corrosion, medicine, detergents, and cosmetics. This high ash content influences the characteristics of the products that can be yielded from sludge. Furthermore, it will lead to a dilution of the organic content, resulting in lower combustibility and undesirable ash deposition [52].

2.1.1.5.2. Manure

In the United States, 1.4 gigatons of manure are produced yearly, which is mainly used as a nutrient source for crop production [53]. However, with a shift to confined animal feeding operations, one type of animal is being produced in big numbers, leading to huge amounts of manure which cannot be applied to land. This means there is a surplus of manure which could be a valuable resource [36]. If manure is not disposed of correctly, it can lead to contamination of soil, air, and water surfaces due to run-off, as well as serious odour nuisances [54], [55], [56]. It can be observed from Table 1 that manure contains a high amount of carbohydrates and proteins. With the carbohydrates mainly consisting of hemicellulose and cellulose [36]. Livestock typically excrete 50-90% of the nutrients they are fed, depending on the feeding practices, stage of growth and livestock type, thus the manure composition can vary greatly. The ash content of manure likely holds substantial amounts of N, P (and K) as these are present in manure due to the excretion of the excess nutrients by the livestock and due to the microbial breakdown of complex molecules [57].

2.1.1.5.3. Food waste

The Food and Agriculture Organization (FAO) defines food waste (FW) as “any healthy or edible matters that are wasted, lost, or degraded throughout the food supply chain, including organic waste generated from various sources such as food processing plants, households and commercial kitchens” [58], [59], [60]. It is estimated that approximately 33.3% of food produced globally for human consumption is lost or wasted through the food supply chain, which leads to 1.6 gigatons of FW per year [61]. The composition of food waste varies by source, region, climate, season, and culture of the country [62]. It mainly consists of waste flour, meat, eggs, vegetables, fruit, rice, oil, and salt and thus exhibits high heterogeneity with diverse compositions of proteins, lipids, cellulose, hemicellulose, lignin, organic acids, vitamins, and minerals [63], [64], [65]. Due to the heterogeneous nature of the waste stream, it is difficult to give an average amount of lipids,

carbohydrates, proteins, and ash. However, in Table 1, the average was calculated from three FW streams containing; (i) cereal, vegetables, meat, eggs, oil, and salt (ii) waste from students' dining hall and (iii) canned green beans, canned baked beans, potato salad, canned chicken, and parmesan cheese. The carbohydrates make up the biggest portion of the biomass and the ash content is rather low in comparison to the other waste streams. This is probably due to the presence of more organics and for example, carbohydrate-rich FW such as food made from grains and cereals, legumes, and fruits. This is backed up by research, which has shown that vegetables (25%), cereals (24%) and fruit (12%) make up the biggest part of FW [66], [67]. Fish and seafood waste which will be used in the experimental part of this thesis could also be categorized as food waste, although it also fits in the category of industrial residues, as fish is not used solely for eating purposes (e.g. fish oil production, biomolecules, pets, livestock feed…).

2.1.1.5.4. Algal biomass

A lot of undesired algal waste is generated. Eutrophication or green tide events are bound to occur more frequently due to global warming, which generates huge amounts of undesired algal biowaste. An example was in Qingdao (China, 2008) where the largest green tide event in the world happened, causing 150 000 tons of wet algal biomass to be collected [68]. In Italy, 40 000 tons of algal biowaste are collected annually in the Venetian Lagoon [69]. The macroalgae for which the composition is given in Table 1 are brown, red and green macroalgae, respectively *Stoechospermum marginatum*, *Haloplegma duperreyi* and *Ulva lactuca*. The microalgae used to calculate the range were *Laminaria japonica*, *Cladophora sp.* and *Schizochytrium limacinum*. Microalgae have a much larger lipid concentration (1.1-51%) than macroalgae (0.6-3.9%). This is because microalgae can accumulate 20% to 80% of their dry weight in lipids [70]. Macroalgae generally do not contain lipids or only a very small fraction but have higher carbohydrate contents and are thus more favoured for the production of biogas or alcohol-based fuels [71].

2.1.1.5.5. Industrial biowaste

Industrial biowaste can include all other NLBM waste streams which don't fit in the other categories, this can be waste from leather processing, hair, bone, and feathers. Table 1 illustrates the compositional range of chicken feathers, hog hair and raw hide skin waste. Raw hide or skin waste (fleshing, trimmings, splits, scourings) constitutes a significant portion of waste generated by the leather industry. Currently considered as industrial waste, it commonly finds its way to landfills or incineration facilities [47]. Out of 1000 kg of raw hide, nearly 730 kg ends up as solid waste [72]. The leather waste used in the range represented in Table 1 had a considerably high lipid content (48.8%) and a high ash content (34.7%). Next to leather waste, hair is also a source of industrial biowaste. Hog hair constitutes up to 1% of total hog weight and is unfit for human consumption. It is difficult to degrade, and huge amounts are discarded yearly on landfills, reaching up to 34 kton/year in Spain alone. It is composed for 94.2% of protein, contains no carbohydrates and only small amounts of ash and fats [46]. Another NLBM waste stream with limited application possibilities are feathers. Annually, 40 million tons of chicken feathers are generated as a by-product of the poultry industry [73]. Furthermore, they are difficult to dispose of due to the generation of sulphur dioxide during incineration [74]. They are composed of mainly protein (74.2%) and ash (15.5%) and only small fractions of carbohydrates (7.9%) and lipids (2.4%) [45]. Although there has been some research into the hydrothermal carbonization of these NLBM industry biowaste sources, it remains in the early stages of development.

2.1.2. Marine biowaste as a unique feedstock: fish and seafood

Fish and seafood waste – which will be called marine biowaste for simplicity – can be a valuable feedstock due to its diverse chemical composition and the huge amount of waste that is generated annually. It is estimated that 35% of the global fisheries and aquaculture production is either lost or wasted annually, with production having reached 214 million tons in 2020, this resulted in approximately 75 million tons of marine biowaste [1]. Besides deterioration of marine products which leads to waste, fresh marine products also contain a considerable number of inedible parts such as heads (9-12% of total fish waste), viscera (12-18%), bones (9-15%), scales (5%) and skin (1-3%) resulting in the generation of substantial by-products throughout the food supply chain [1]. It is essential to manage these by-products responsibly to mitigate the risks associated with wastewater contamination, unpleasant odours, illegal disposal in landfills, and ocean dumping. Due to the potential for adverse environmental impacts, pollution, and substantial socioeconomic losses, it is important to avoid improper practices [6].

As can be seen on Figure 5, Europe, North America, Oceania, and Industrialized Asia have significant losses in the primary fisheries production phase of the food supply chain due to discard rates of 9 to 15%. Many consumer households also discard a significant portion of the fish and seafood they purchase. In the remaining regions, significant losses occur mostly during the distribution in the food supply chain. This can be explained by the deterioration occurring during fresh fish and seafood distribution. Overall, it can be concluded that 30 to 50% of the initial harvest is discarded, lost, or wasted throughout the food supply chain [3].

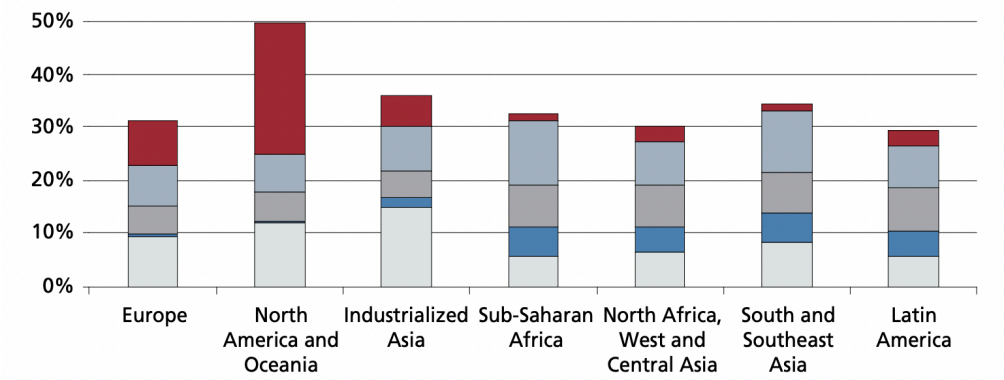

Figure 5: Part of the initial catchings (fish and seafood harvested) discarded, lost and wasted at different stages in the food supply chain: consumption (■), distribution (■), processing (■), post-catch (■), fisheries (□) [3].

A. Fish waste

Fish residues consist of various components, including whole waste fish, fish heads, viscera, skin, bones, blood, liver, gonads, guts, and some muscle tissue. The composition of these residues varies based on factors such as the species, sex, age, nutritional status, time of year, and health. Due to the heterogeneous nature of the waste, the average composition will vary [2], [75]. However, Table 2 illustrates the proportions of proteins, fats, fibre, and ash that are present on average. From the table it can be observed that fish waste contains a high amount of protein (58% dry matter) and lipids (19% dry matter), the relatively high ash content (22% dry matter) indicates that fish waste contains a high number of minerals. The high number of proteins leads

to high concentrations of nitrogen in the fish waste. Alvarez et al. (2010) measured ten times higher amount of Total Kjeldahl Nitrogen in fish waste compared to pig manure [76]. Elevated calcium (Ca) levels (5.80 ± 1.35%) are also often found as a result from the inclusion of fish bones in the gathered waste. The metals Fe, Zn, Mn, and Cu can be found at mean concentrations of 100, 62, 6 and 1 mg/kg, respectively. No toxic substances such as arsenic (As), lead (Pb), mercury (Hg), and cadmium (Cd) were detected in the waste samples. Additionally, no significant difference in nutritional composition of the waste due to seasonal variability was observed, except for the moisture content which was higher in the winter [75].

B. Crustacean waste

The high shell content in crustaceans, which can account up to 60% of a crab's weight, causes large amounts of waste. Most of this waste is currently disposed of in landfills or into the ocean due to their low monetary value and costly disposal. However, chitin, minerals, proteins, and pigments are components of this waste which can be converted into valuable products. The composition of crustacean shells was estimated to be: minerals (20-50%), proteins (20-40%), chitin (15-40%), and pigments (>2%). The mineral fraction consists mostly of $CaCO_3$; however, carbonates break down only at very high temperatures, i.e. 750°C [77]. As can be seen in Table 2, crab waste has an ash content of more than 25%, this can indicate the presence of a large fraction of $CaCO_3$. Shrimp and crab waste also exhibit a larger fraction of crude fibre than fish waste. This is due to the presence of a substantial amount of chitin. Chitin is a linear polysaccharide consisting of N-acetyl-D-glucosamine and the second most abundant biopolymer found in nature. Industrial chitin extraction from shells is already performed by a well-established protocol due to its economically viable production [78]. Chitin breaks down at approximately 250°C [79].

Table 2: Average composition of fish, shrimp and crab waste. Data is expressed in % on a dry matter basis.

Type	Protein (%)	Lipids (%)	Crude fibre (%)	Ash (%)	Moisture (% wet weight basis)	Ref.
Fish waste	57.92	19.10	1.19	21.79	73.85 ± 2.45	[75]
Shrimp waste	87.11	3.80	7.89	1.20	81.87 ± 2.11	[80]
Crab waste	33.89	10.28	21.04	26.49	79.41 ± 0.58	[81]

2.1.2.1. Availability in South Korea

The availability of marine biowaste in South Korea is of interest for this thesis as the feedstock which will be used, will be of Korean origin. Population growth and increased food demand have led to a rise in marine biowaste generation in South Korea. South Korea generates an estimated annual amount of 800 to 1200 kton of fishery by-products, categorized as fish, molluscs, and crustacean shells. Fish by-products primarily include bones, fins, intestines, and skin, while shellfish by-products include oyster, clam, and mollusc shells. Crustacean by-products consist mainly of crab shells and shrimp carapaces. The number of by-products which are treated as by-products and not as waste is unclear due to insufficient available statistics [6].

The management and disposal of fishery by-products in South Korea is regulated by the 'Waste Management Act' and the 'Act on the Promotion of Conservation and Recycling of Resources'. These regulations categorize fishery by-products into two distinct groups based on Article 2 of the

'Waste Management Act': waste and by-products. Article 2 defines waste as "materials no longer necessary for human life or business activities". Accordingly, fishery by-products that fall under this definition are considered waste and are subject to the prescribed disposal processes mandated by the Act. Consequently, most fishery by-products are treated as waste under these regulations. This is because all fishery by-products that originate from households and small seafood restaurants, are treated as food waste. According to Article 2, 'disposal' refers to intermediate and final disposal methods like crushing, neutralizing, solidification, incineration, landfilling and discharge into the ocean. However, exceptions exist for fishery by-products that are deemed "necessary for human life or business activities" at the site where they are initially generated. In such cases, these are classified as by-products rather than waste. For example, if fish processing by-products are transformed into products like salted fish or fish sauce, and they are registered as business products, they are excluded from the waste category. It should be noted that most fishery by-products that can be processed are transformed into fish meal and feed when it comes from large seafood markets and processing facilities [6].

Marine biowaste which could be subjected to HTC to produce hydrochar would be labelled as 'waste' according to the current South Korean 'Waste Management Act'. This categorization can invoke a negative perception on their value. Thus, a change in the legislation to categorize them as feedstocks could bring new life into the use of this NLBM stream.

2.1.2.2. Feedstock used in experiment

To familiarize the reader with the marine biowaste which will be used in the experiments of this thesis, a short description of the eight marine species which will be subjected to HTC will be given. These species comprise five from the subphylum Vertebrata: chub mackerel (*Scomber japonicus*), hairtail (*Trichiurus lepturus*), yellow corvina (*Larimichthys polyactis*), horse mackerel (*Trachurus japonicus*) and olive flounder (*Paralichthys olivaceus*) and three from the subphylum Crustacea: whiteleg shrimp (*Litopenaeus vannamei*), Gazami crab (*Portunus trituberculatus*) and tiger prawn (*Penaeus monodon*) as can be seen in Figure 6.

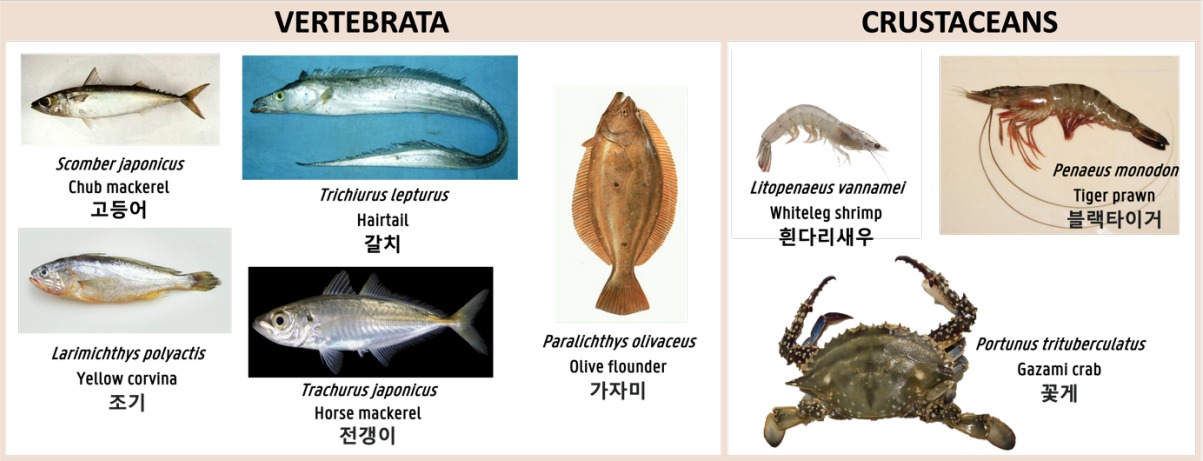

Figure 6: Species used in experimental part of this thesis [82], [83], [84], [85], [86], [87], [88].

In Table 3, the species' mass, length, non-edible ratio (NED), and production in the world and in South Korea can be found. The mass and length of the species varies greatly, the smallest being whiteleg shrimp (average of 20 g, 13 cm) and the biggest being hairtail (1250 g and 100 cm) [82], [89], [90], [91], [92], [93], [94], [95], [96], [97], [98], [99]. The non-edible ratio varies between 33 and 60%. In general, the crustaceans show higher non-edible ratios.

Most species considered in this thesis are native to the East China Sea and the Yellow Sea, their natural habitat is therefore near South Korea. Yellow corvina is almost exclusively produced in China, Korea, and Taiwan [100]. Olive flounder is also called the Korean halibut and Korea accounts for 75% of its worldwide production [100]. As can be seen, whiteleg shrimp has the highest world production, representing more than 50% of the total aquaculture species production. South Korea produced less than 5000 ton in 2021 but there is a rapid expansion of the species expected in Asia [89]. There is no tiger prawn being produced in South Korea currently, however there was about 2500 ton imported in 2021. The reason for the lack of tiger prawn production in South Korea is the surge of diseases affecting tiger prawn production in the world [101], [102].

Table 3: Marine species, their non-edible ratio (NED) [103]*, the world production and production in South Korea (SK) in 2021. Value marked with * is from 2020* [100].

Species	**Mass (g)**	**Length (cm)**	**NED (%)**	**2021 world production (ton)**	**2021 production in SK (ton)**	**Potential waste in SK (ton)**
Chub mackerel	370	32	41	2 355 523	152 951	62 710
Hairtail	1250	100	33	1 122 636	63 056	20 809
Yellow corvina	80	20	45	320 837	31 562	14 203
Horse mackerel	250	25	43	517 167	69*	30
Olive flounder	800	50	45	59 649	44 713	20 121
Whiteleg shrimp	20	13	47	6 348 622	4 607	2 118
Tiger prawn	200	25	47	883 686	-	-
Gazami crab	250	15	60	476 026	19 713	11 828
						TOTAL = 131 819

2.2. Hydrothermal conversion

In the following section, the different hydrothermal conversion processes will be described as well as the underlying chemical processes and the resulting reaction products. A more extensive portion will be dedicated to the hydrothermal carbonization of non-lignocellulosic biomass, as this process forms the core of the experimental work.

2.2.1. Hydrothermal conversion processes

Hydrothermal conversion is a complex process that can be broadly described as the chemical and physical transformation of carbon-rich compounds occurring in liquid water at high temperature and autogenic pressure [104]. The system's pressure needs to remain at or exceed the water vapor pressure in order to keep water in a liquid state. The physicochemical properties of water are then altered (its density, dielectric constant and ionic product as can be seen on Figure 7b) and thus valuable products can be produced [105]. Hydrothermal conversion can be classified into hydrothermal gasification, hydrothermal liquefaction, and hydrothermal carbonization according to the different regions above the pressure-temperature curve and the critical point (T_c = 374°C, P_c = 22.1 MPa) in the phase diagram of water (Figure 7a).

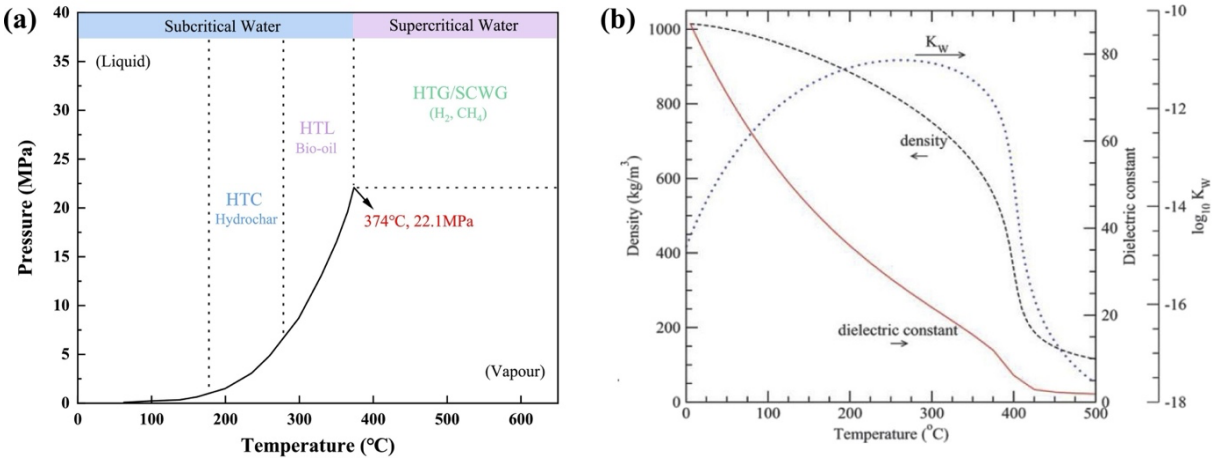

Figure 7: (a) Hydrothermal conversion processes with their main product on the pressure-temperature phase diagram of water [106]. *(b) Properties of water* [107] .

The hydrothermal processes operate in one of two states: subcritical and supercritical water. Subcritical water is characterized by water temperatures ranging from 100°C to 374°C, with sufficient pressure to maintain water in its liquid state. When water surpasses the critical point, it transitions into a new state known as supercritical water [108]. Sub- and supercritical water differ substantially from water at ambient conditions [109]. Figure 7b shows that there are temperature-dependent changes of the density, dielectric constant and ionic product of water. When water remains within the subcritical range, the ionic product (K_w) attains its maximum value at about 250°C whereas the density and dielectric constant of water decrease. The reduction of the dielectric constant implies a reduction of the polarity of water and thus the dissolution of non-polar compounds is facilitated [110]. Next to the reduction in polarity, it also weakens the hydrogen bonds. The increase in ion product on the other hand produces more acidic (H_3O^+) and basic (OH^-) ions [111]. It has also been observed that subcritical water contains a higher concentration of H^+ ions in comparison to water at ambient conditions, which promotes acid-

catalysed reactions of organic compounds [112], [113], [114]. It was also found that a small amount of water molecules in carbonization reactions could directly participate in hydrolysis, hydrogen exchange, condensation, and cracking reactions [114]. Generally, it can be said that subcritical water amplifies the solubility of organic compounds and enhances their reactivity, thus facilitating the decomposition and transformation processes [67], [115]. Furthermore, processes that use sub- or supercritical water, offer several advantages in comparison to other thermochemical conversion techniques like pyrolysis or gasification. These advantages include: (i) a cost-efficient method due to milder temperatures (< 350°C for subcritical water), (ii) compatible with various feedstocks and mixtures, (iii) low maintenance costs, (iv) suitable for wet or dry feedstock, and (v) lower energy consumption [105], [107], [116].

A) Hydrothermal gasification (HTG)

Hydrothermal gasification takes place at high temperatures and pressures higher than 22 MPa with typically the production of a syngas composed of carbon dioxide, methane and/or hydrogen as a result. The process is typically categorized in three main types: (i) aqueous phase reforming (215 to 265°C), (ii) near-critical catalytic gasification (350 to 400°C) and (iii) supercritical water gasification (600 to 700°C) [107], [117], [118].

B) Hydrothermal liquefaction (HTL)

Hydrothermal liquefaction usually takes place at a temperature of 300 to 350°C and a pressure of 15 to 25 MPa. The obtained products are a liquid “biocrude”, an aqueous solution with dissolved organics and a gas phase dominated by carbon dioxide. The obtained “biocrude” is often used to produce biofuels [117], [119].

C) Hydrothermal carbonization (HTC)

Hydrothermal carbonization occurs within a comparably low temperature range, typically between 160 and 250°C and autogenous pressure, which is typically between 1 and 5 MPa [120]. Within this temperature range, liquefaction and gasification are restricted, and a carbon-rich solid product dominates. This hydrothermal carbonization method allows various feedstocks to be transformed into a solid with a carbon content similar to lignite, with mass yields between 35 and 60%. The primary carbon losses arise from dissolved organics in the aqueous phase, while gas production is minimal. The distribution of products is primarily influenced by factors such as the nature of the feedstock, process temperature, reaction duration, and the solids load. Nevertheless, the principal product obtained from this process is hydrochar [117], [121], [122].

2.2.2. Hydrothermal carbonization of non-lignocellulosic biomass

In section 2.2.2.1, the effect of the following process parameters on the HTC process and products will be described: temperature, residence time, hydrous condition, water-to-biomass ratio and pressure. In section 2.2.2.2, the carbonization mechanism of NLBM constituents will be elaborated on to gain a comprehensive understanding of the chemical transformations occurring.

2.2.2.1. Effect of process parameters

The process parameters which will be discussed are temperature, residence time, water-to-biomass ratio and pressure. To understand the effect in terms of NLBM, some values from literature for various NLBM waste streams are summarized in Table 4.

2.2.2.1.1. Temperature

Temperature is a decisive parameter in HTC because it supplies the energy in the form of heat for the decomposition and fragmentation of the biomass. Due to the increase in energy supply with increasing temperature, the efficiency of the biomass conversion is proportional to the increase in temperature [123], [124]. This is because the viscosity of water is able to change more than one order of magnitude from 1.6 mPa·s at 0°C to 0.14 mPa·s at 350°C. Due to the change in viscosity, water at higher temperatures can more easily penetrate into the biomass and therefore accelerate the degradation [124]. In Table 4, it can be seen that the employed temperatures were between 160°C and 300°C. However, as mentioned in section 2.2.1, the temperature employed in HTC is typically between 160 and 250°C because these lower temperatures typically favour char yield. The temperature affects the number of compounds that undergo hydrolysis, which will be described more in section 2.2.2.2. However, generally it was observed in the experiments that an increase in temperature caused a decrease in hydrochar yield and an increase in carbon yield because the rate of waste solubilization was greater than the rate of char formation [124].

2.2.2.1.2. Residence time

Residence time influences the quantity and composition of the hydrochar. With longer reaction times usually increasing the severity of the reaction and decreasing the yield. As for the carbon content, this is initially seen to decrease at short reaction times due to the solubilization phase, which causes an increase in carbon content in the liquid phase. With longer reaction times, secondary charring can occur and thus the carbon content in the hydrochar can increase [124]. These trends were also observed in the experiments in Table 4, where the residence time varied from 30 minutes to 20 hours.

2.2.2.1.3. Hydrous condition and water-to-biomass ratio

A liquid medium is essential for HTC to occur. As the liquid medium avoids the combustion of the organic matter, which occurs in pyrolytic conditions. Furthermore, it has been observed that biomass above the liquid surface does not carbonize. The liquid medium is usually chosen as water as it is a good heat transfer and storage medium which avoids local temperature peaks that might result from exothermal reactions. However, it could also be possible to carbonize biomass

in oil even though it has been observed that the carbonization process is accelerated by water. This is because the thermal conductivity of water (0.609 W/(m·K)) is bigger than that of oil (0.1-0.15 W/(m·K)). Furthermore, the use of subcritical water as a solvent is cost-effective, easy to dispose of in comparison to hazardous organic solvents, and is non-aggressive [124], [125].

One of the advantages of HTC is the ability to work with wet feedstocks. However, it is still relatively unclear how naturally bound water versus externally added water influences the hydrochar characteristics. Soroush et al. (2023) investigated the effects of using fresh seaweed with and without additional water compared to soaked dry seaweed. They found that fresh seaweed with additional water showed higher adsorption capacity than soaked dry seaweed and that the former showed a higher amount of carboxyl functional groups. It was concluded that drying the feedstock and adding external water affects the hydrochar characteristics due to the drying process [126].

Table 4 summarises the used water-to-biomass ratio (w/b) for HTC of various NLBM waste streams, it can be seen that the ratio ranged from 1-20. In the two experiments carried out with varying w/b, it was observed that a lower w/b resulted in higher yields. This was explained due to the faster increase in concentration of monomers in the liquid phase at lower w/b content or higher solids content. This pushes polymerization to start earlier. Thus, for enhanced polymerization the solid load should be kept high, while still keeping all of the biomass submerged [127], [128].

2.2.2.1.4. Pressure

Hydrolysis and degradation are pushed by increasing the pressure, which makes sure the water remains in subcritical state. As pressure (in combination with the temperature) mainly affects the density and viscosity of the water and as explained in section 2.2.2.1.1, low viscosity solvents can more easily penetrate the biomass, thus accelerating the fragmentation. The pressure generated in HTC is autogenous and increases isotropically, as the temperature increases [125]. Thus, the pressure can be increased by increasing the temperature. Furthermore, Le Chatelier's principle applies in the reactor: to maintain equilibrium at higher pressures, the reaction equilibrium shifts between the solid and liquid phase, corresponding to the phase that has a smaller number of moles [124], [129]. This was observed as the dehydration and decarboxylation reactions occurred to a lesser extent at higher pressures whereas polymerization and condensation reactions occurred to a higher extent. However, this effect does not show a big impact on hydrothermal carbonization. At high pressures, it is assumed that extractables in biomass are more easily removed because encapsulated gases are compacted and therefore dissolved more easily in water, which allows better access of the liquid water [125].

Table 4: Process parameters and achieved yields of different sources of non-lignocellulosic biomass.

Non-lignocellulosic biomass						
Category	**Feedstock**	**T (°C)**	**Time (h)**	**w/b**	**Yield (%)**	**Ref.**
Sewage sludge	Sewage sludge	190-250	3	7.3	63-83	[130]
	Sewage sludge	190-220	1.4-4	7.3-19	53-68	[127]
	Anaerobic sludge	200-300	0.5-2	9	49-73	[131]
Manure	Swine and chicken manure	240	10	10	50-55	[132]
	Cattle manure	170-230	1	10	54-65	[133]
	Pig manure	180-260	1	10	42-53	[134]
Food waste	Food waste	200-250	1	10	40-44	[135]
	Food waste	250	20	4	41-47	[136]
	Beet pulp	180-220	1-4	20	37-56	[137]
Algal biomass	Microalgae	200-250	1	10	28-43	[135]
	Macroalgae	180-250	1-6	1-10	38-57	[128]
	Macroalgae	180-220	0.5-2	9	26-40	[138]
Industrial residues	Municipal solid waste	250	20	4	58-68	[136]
	Leather waste	180-300	0.5	10	70-86	[139]
	Chicken feathers	160-170	1-3	14.3	14-47	[140]

2.2.2.2. Carbonization mechanism

As mentioned in section 2.1.2, fish and crustaceans mainly consist of carbohydrates, lipids, proteins, and inorganics. It can be argued that lignocellulose is negligible in their composition. However, the components all undergo the carbonization mechanism of HTC. The hydrothermal reaction of carbohydrates, proteins, lipids, and inorganics will be described in the following sections and are schematically (except for lipids) given in Figure 8.

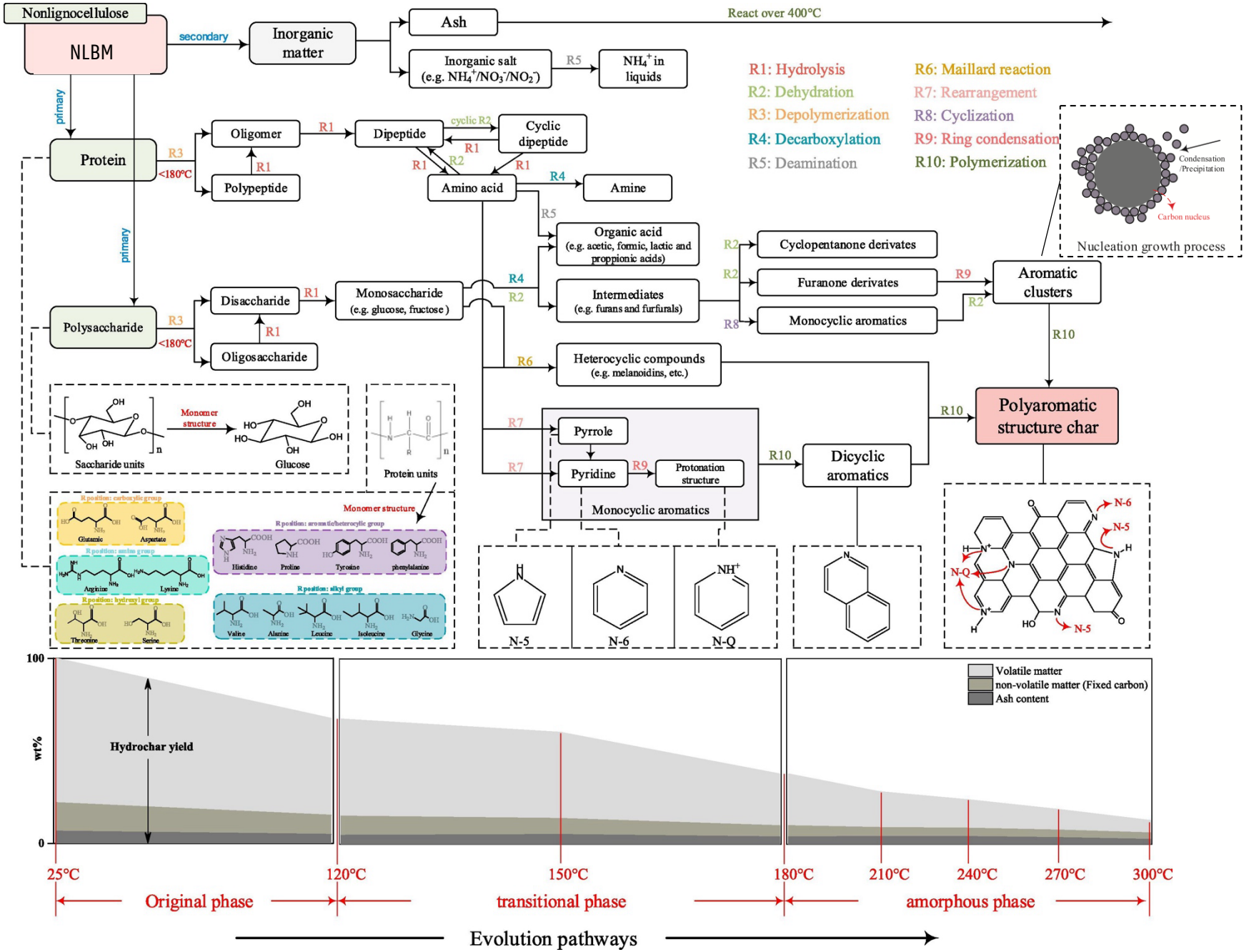

Figure 8: Reaction pathways of non-lignocellulosic biomass (excluding lipids) during hydrothermal carbonization, modified slightly from [141].

2.2.2.2.1. Hydrothermal reaction of carbohydrates

Carbohydrates are essentially monosaccharide polymers (such as polysaccharides, as depicted in Figure 8). Under hydrothermal conditions, polysaccharides get easily depolymerized and hydrolysed to monosaccharides [142]. The increasing HTC temperatures then lead to various reaction pathways of glucose and fructose, which are monosaccharides that cannot be hydrolysed further into smaller sugar molecules. The Lobry de Bruyn-Alberda van Ekenstein transformation isomerizes glucose to fructose, and vice versa [141]. It has also been observed that fructose is more reactive compared to glucose. Glucose is more inclined to undergo isomerization to fructose in subcritical water whereas the reverse process is not observed [143]. However, the rate of isomerization of monosaccharides, leading to the formation of different forms, is relatively slow compared to the degradation rate of glucose and fructose [144]. In general, glucose mainly decomposes into acetaldehyde, acetone, and other products, while fructose generates more dehydration products, such as 5-HMF [145]. These intermediates undergo further dehydration and sometimes cyclization and ring condensation, after which aromatic clusters are formed. These clusters are formed once the concentration of aromatics in the aqueous phase reaches a threshold value, after which a peak in the nucleation processes takes place, and a considerable number of aromatic clusters are concurrently accumulated. The aromatic clusters can undergo polymerization to form the polyaromatic structures typically sought after in hydrochar. However, it should be noted that the predominant shift from hydrolysis toward condensation and polymerization only occurs from 240°C. Thus, the reaction pathways during the process are significantly impacted by the temperature, with higher temperatures yielding more polyaromatic structures [67], [141].

2.2.2.2.2. Hydrothermal reaction of proteins

As mentioned in section 2.1.1.1, proteins consist of amino acids that are linked by peptide bonds formed between the carboxyl and amino groups of adjacent amino acids. The peptide bonds are susceptible to hydrolysis under hydrothermal conditions. Thus, when the temperature rises the polypeptides gradually undergo hydrolysis to form amino acids. Dehydration of amino acids to linear dipeptides could also take place, as can be seen in Figure 8 but this was observed to occur less [141]. The different amino acids characterized by their side chains lead to a variety of products via individual and synergistic reactions. The general decomposition of individual amino acids under hydrothermal conditions was determined as decarboxylation to produce CO_2 and amines and deamination to produce NH^{4+} and organic acids [146]. Additionally, self-rearrangement between amino acids can result in the formation of mono-cyclic aromatics and dicyclic aromatics at higher temperatures. There is also a synergistic reaction between amino acids and reduced sugars. This interaction is known as the Maillard reaction which produces N-containing heterocycles like melanoidin. When the temperature further increases above 240°C, it was found that aliphatic methylene or other O-containing functional groups on the aromatic or heterocyclic rings were thermally cracked, yielding more condensed structures via aromatization and ring condensation. Thus, polymerization of small aromatic and heterocyclic ring systems progressively formed polyaromatic structures [141], [147].

2.2.2.2.3. Hydrothermal reaction of lipids

A common form of lipids are the triglycerides, which consist of a glycerol backbone esterified with three fatty acid molecules, as mentioned in section 2.1.1.3 [107]. When the temperature of HTC increases, the polarity of the water in the HTC system decreases, making water more like non-polar organic solvents and causing lipids to dissolve in aqueous solutions. It was observed that the solubility of fats and oils in water increases, and when water reaches its supercritical state, fats and water become completely compatible [144]. Triglycerides can easily hydrolyse into glycerol and various types of long-chain fatty acids above temperatures of 280°C. Glycerol can then undergo secondary decomposition and generate alcohol compounds (methanol, ethanol, propylene glycol) and aldehyde compounds (formaldehyde, acetaldehyde, and trace amounts of organic gases) [148]. It was also observed that free fatty acids can be degraded at hydrothermal conditions and yield long-chain hydrocarbons [149]. Some long-chain fatty acids can yield alkanes with a carbon number greater than 16 under hydrothermal conditions through decarboxylation and dehydration reactions [67].

2.2.2.2.4. Hydrothermal reaction of inorganics

The inorganic fraction in raw materials has a certain influence on the hydrothermal conversion. The minerals within the inorganic fraction can have an influence. It was for example observed that there are higher concentrations of alkali (e.g., sodium salts) and alkaline (e.g., calcium salts) earth salts in biomass which can enhance (catalyse) the hydrolysis of carbohydrates [150]. It was also reported that iron ions in iron oxides have a high activity in HTC of starch, which promote the formation of hydrochar microspheres [151]. It was also observed that in algal biomass, noble metals usually promote the decarbonylation reaction activity whereas the non-precious metal nickel promotes the deoxygenation reaction of algal lipid groups [106], [152]. Next to the minerals, the ash content in general will usually only react at temperatures over 400°C but for some materials it was observed that the ash content in the hydrochar decreased with higher temperatures whereas with other materials the contrary was observed. This is due to the specific ash chemistry of the feedstock. An increase in ash content can occur if the feedstock has a smaller proportion of inorganic material removed in comparison to the proportion of organic material removed. Thus, even though inorganic material was removed it can become increasingly concentrated within the hydrochar [135].

2.3. Hydrochar

In the following sections, hydrochar (HC) will be defined through its chemical and physical characteristics. After which the characterization will be explored through the following techniques: the point of zero charge, elemental analysis through the van Krevelen diagram, and dye-adsorption. Specifically, the adsorption properties involving methylene blue and methyl orange will be described. The last section will focus on applications of hydrochar.

2.3.1. Characteristics

2.3.1.1. Chemical characteristics

Hydrochar is a carbonaceous solid product produced through HTC, as mentioned in section 2.2.1. The chemical characteristics vary according to the type of feedstock, HTC temperature and reaction time. This is especially true for NLBM sources, the composition of the raw feedstock is very diverse, leading to varying chemical characteristics of the resultant HC. However, some properties are deemed typical of all types of HC. When HTC occurs, it has been studied that the deoxygenation and dehydration reactions cause HC to have an increased carbon content compared to the raw feedstocks. This can be explained as the decrease in the number of low energy H-C and O-C bonds and increase of high energy C-C bonds leads to an improved energy density [153]. With regard to fuel applications, a high carbon and low oxygen content are preferable.

Besides elemental composition, surface functionality plays an important role in their application for surface-based phenomena, such as adsorption and catalysis [154]. The surface of HC shows a high degree of aromatization with abundant oxygen-containing functional groups (OFG), including hydroxyl, carboxyl, phenol, carbonyl groups and others, depicted in Figure 9 [11]. The HC microspheres generally present a core-shell chemical structure consisting of a highly hydrophobic aromatic nucleus (ether, quinone…) and a hydrophilic shell with many reactive OFG (hydroxyl, carbonyl, carboxyl, phenolic, ester, epoxy etc.) [155]. The presence of many hydrophilic OFG on the surface of HC explains its affinity for water; therefore, it could be used to increase the water retention capacity of the soil [9]. The abundance of OFG is also favourable for the design of carbon-based energy storage materials, such as supercapacitors [156].

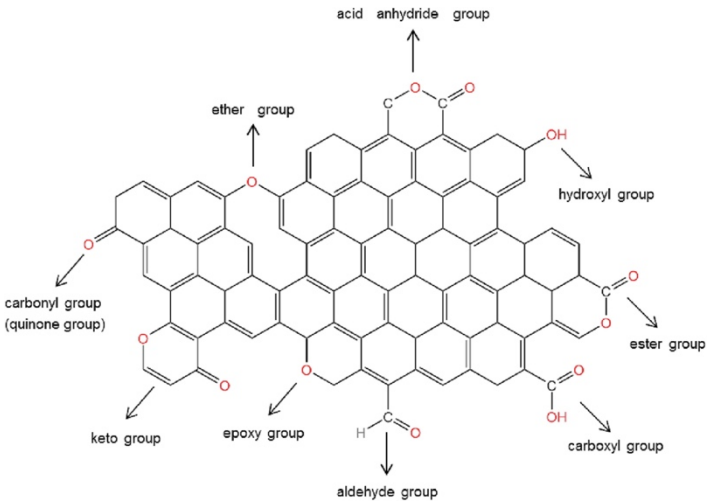

Figure 9: Oxygen-containing functional groups on carbon materials [156].

The pH of the HC is strongly dependent on the HTC conditions. It has been observed that lower temperatures produce more acidic HCs because acidic groups such as carboxyl and hydroxyl are lost when HTC temperatures increase [157]. The pH of the feed water was reported as having no influence on the hydrochar pH although biomass decomposition is different in acidic and alkaline media [158].

2.3.1.2. Physical characteristics

Hydrochar has low pore volume and BET surface area compared to activated carbon (1000 m^2/g and higher) or biochar (up to 100-400 m^2/g) [159], [160]. However, during the HTC process, pores with different sizes are created leading to an increasing internal surface area compared to the raw feedstock [9]. The pores can be classified based on their sizes: macropores (> 50 nm), mesopores (2-50 nm) and micropores (< 2 nm) [161]. Khoshbouy et al. (2019) produced hydrochar of wastewater sludge (260°C, 1 h, w/b = 8.9) and obtained a BET surface area of 6.3 m^2/g and a total pore volume of 0.015 cm^3/g, of which 98.68% were mesopores and the remainder were micropores. The average pore diameter was 2.98 nm [162]. The surface area of the HC is very low, scanning electron microscopy (SEM) images show a mostly non-porous surface (Figure 10a). However, chemical activation of the hydrochar (mixing KOH 1:1 w/w, 700°C, 1 h) can lead to increases in surface area and porosity with well-developed pore structures (Figure 10b). Another study which produced HC from food waste (mixtures of vegetables, fruits, staple foods and meat waste, at T = 200-300°C, t = 1 h, w/b = 3) obtained a BET surface area of 5.23 to 7.14 m^2/g [163]. Hydrochar produced from algae (T = 180-250°C, t = 1-6 h, w/b = 1-10) obtained a BET surface area of 4.9 to 51.7 m^2/g [128]. Despite their low surface area, the HCs gain their advantage in the great variety of OFG present on the surface.

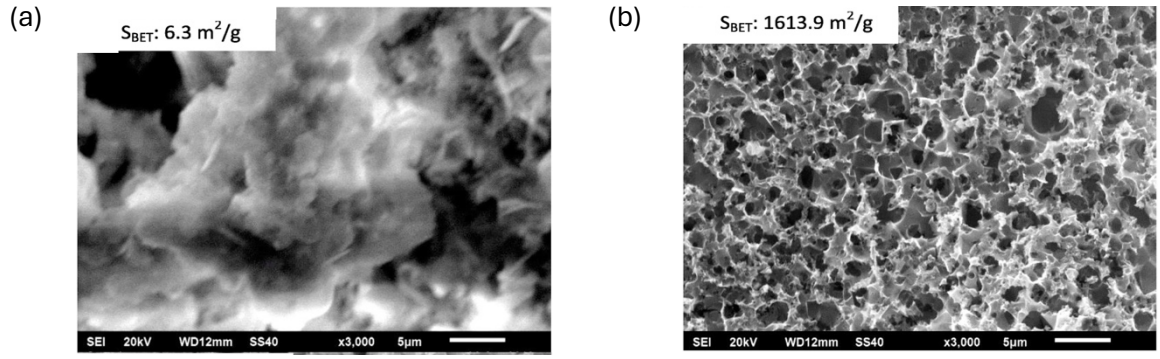

Figure 10: SEM images of (a) hydrochar produced at 260°C and (b) chemically activated hydrochar [162].

2.3.2. Characterization techniques

2.3.2.1. Point of zero charge

The point of zero charge provides important information on sorption mechanisms. Three different points of zero charge are described in literature: (i) point of zero charge (PZC), (ii) point of zero net charge (PZNC) and (iii) point of zero net proton charge (PZNPC). The PZC is the pH value at which the net surface charge is zero, and the diffuse ion swarm disappears [164]. The PZNC represents the pH at which the overall charge resulting from sorbed ions, other than H^+ and OH^-, equals zero. This aligns with the point where the anion exchange capacity and cation exchange capacity of the

substrate are in equilibrium [165], [166]. On the other hand, the PZNPC is the pH value at which the net charge, originating from H^+ and OH^- ions complexed by surface functional groups, becomes zero [167]. This section will focus on the first type (PZC) as this will be measured in the experimental part.

The PZC is a pH value at which the surface charge components become equal to zero at a given temperature, applied pressure and aqueous solution composition [168]. This means that there are equal amounts of positive and negative charges at the pH_{PZC}. Substrates characterized by low PZC values are most suitable for treating effluents contaminated with cations, whereas substrates with high PZC values are better suited for capturing anions [167]. This is because at a pH of the solution higher than the pH_{PZC}, the surface of the substrate is negatively charged whereas the surface charge is positive if the pH of the solution is lower than the pH_{PZC}.

The method usually used for measuring the PZC of organic substrates is the pH drift method due to its easy methodology. This technique should be performed by adding identical amounts of substrate to a set of solutions of the same ionic strength at different pH values and measuring the pH after equilibrium [167], [169], [170].

2.3.2.2. Elemental composition: van Krevelen diagram

For chemical characterization of the hydrochar, an elemental analysis can provide valuable insight. Van Krevelen proposed a diagram depicting the atomic H/C versus O/C ratio to analyse the chemical transformation of cellulose and glucose (mono- and polysaccharides) during HTC [171]. It has been observed that the H/C-O/C ratio decreases where the energy density increases with an increase in reaction time and temperature for the HTC process. For fuel applications, a fuel with low O/C-H/C atomic ratio is considered highly favourable because of the decreased water vapor, energy losses and smoke during combustion [172]. The European Biochar Certificate (EBC) requires that the molar ratios of O/C and H/C should be less than 0.4 and 0.7, respectively to qualify for the certification. Values that exceed these recommendations, indicate non-pyrolytic chars. No certificates have been made specifically for hydrochar yet [173].

Figure 11 was made using the data of different types of feedstock (willow, miscanthus, oak, greenhouse waste, food waste, municipal waste, secondary sewage sludge, AD press cake, macroalgae (*Laminaria hyperborea*) and microalgae (*Chlorella spp.*)) and hydrochars made at 200°C and 250°C with w/b = 10 for one hour [135]. It can be observed that the O/C and H/C ratios decrease with increasing reaction severity, indicating that decarboxylation, decarbonylation and dehydration reactions occurred during HTC. Decarboxylation degrades the carboxyl (-COOH), whereas decarbonylation degrades carbonyl groups (C=O), forming CO_2 and CO respectively. Dehydration removes hydroxyl groups (-OH) from the feedstock leading to less hydrophilic functional groups. Both reactions can therefore reduce the oxygen content significantly and thus improve the energy density [135].

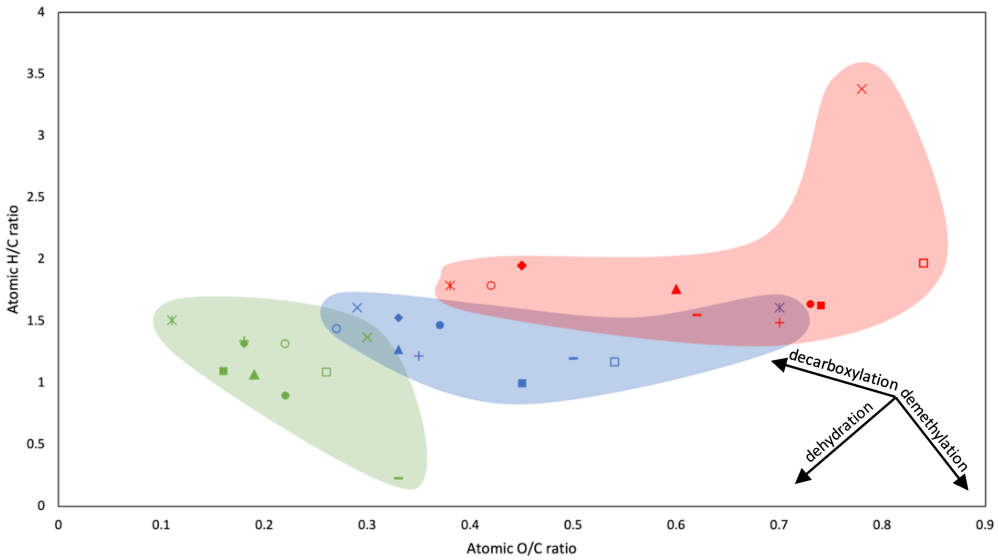

Figure 11: van Krevelen diagram of raw feedstock and produced hydrochars at 200°C and 250°C. Willow (●), miscanthus (+), oak wood (■), greenhouse waste (▲), food waste (◆), AD press cake (▬), municipal waste (✳), sewage sludge (✕), macroalgae (□), microalgae (○). Made with data from [135].

2.3.2.3. Dye adsorption

The adsorption process in the liquid phase comprises multiple steps: mass transport of the adsorbate in the bulk of the fluid phase, diffusion of adsorbate in the film at the solid-fluid interface, pore diffusion of the adsorbate through the adsorbent and surface reaction where the interactions between adsorbent and adsorbate take place [174].

Kinetic tests are performed to characterize the performance of an adsorbent. Fitting kinetic models to experimental data allows to estimate the rate of adsorption, indicating how fast the uptake of an adsorbate is. Additionally, it can help identify the steps in the adsorption process that control the entire process. The latter is known as the slowest step and provides information about the mechanism that drives sorption (e.g., diffusion or surface reactions). The interactions between the adsorbate and the adsorbent are governed by different phenomena such as: surface precipitation, surface complexation, ion exchange, cation-π and π-π interactions, Coulomb forces, van der Waals forces, hydrogen bonding, etc (Figure 12). The kinetic models cannot determine the kind of interaction that takes place but give an indication whether one or a combination of these interactions are controlling the adsorption [175].

The most used models to describe the adsorption kinetics, are the pseudo-first order kinetic model (PFOM) and the pseudo-second order kinetic model (PSOM). These are empirical models and are called pseudo due to: (i) the assumption that there is a constant concentration of the adsorbate in the solution and (ii) it is based on adsorption capacity of solids instead of the concentration in the liquid phase. PFOM assumes that the adsorption processes are mainly controlled by physisorption (low enthalpy of adsorption, formation of multilayers and reversibility) and diffusion; the PSOM assumes that the adsorption processes are controlled by the chemisorption (electron transfer, formation of ionic or covalent bonds, occurring on monolayers only and irreversible), mainly including the electronic sharing or exchange processes between adsorbate and adsorbent [175], [176], [177].

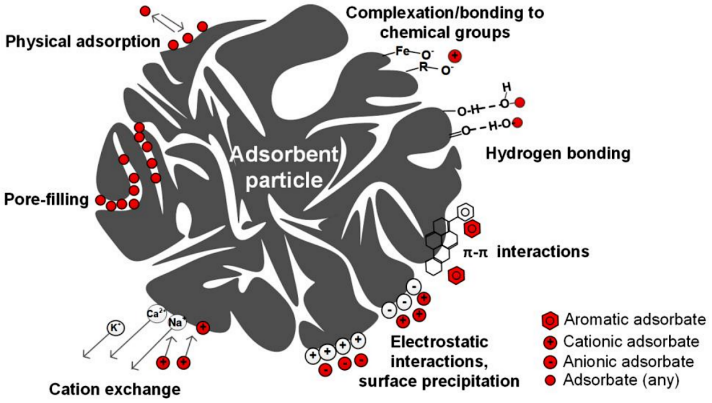

Figure 12: Examples of possible adsorption mechanisms on carbonaceous material [178].

2.3.2.3.1. Methylene blue

Methylene blue (MB) is a synthetic cationic thiazine dye with molecular formula $C_{16}H_{18}ClN_3S$ (Figure 13). It is a dark green powder with a deep blue colour in aqueous solution where it dissociates into an MB cation and a chloride anion. The dehydrated MB properties are: molecular weight (319.9 g/mol), width (14.3 Å), height (6.1 Å), thickness (4 Å), molecular volume (241.9 cm^3/mol), and molecular diameter 0.8 nm [179]. Its topological polar surface area is 43.9 $Å^2$ [180]. The overall pK_a of MB is 8.33. Thus, at a pH smaller than the pK_a, MB is positively charged whereas at a pH bigger than the pK_a, MB is negatively charged [181].

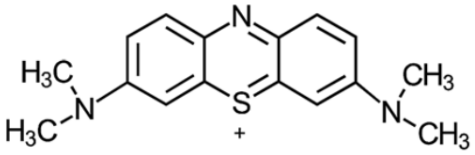

Figure 13: Chemical structure of methylene blue [182].

2.3.2.3.2. Methyl orange

Methyl orange (MO) is an anionic azo dye with molecular formula $C_{14}H_{14}N_3NaO_3S$. Its molecular weight is 327.34 g/mol and its topological polar surface area is 39.5 $Å^2$ [183]. The pK_a of methyl orange is 3.47. Thus, at a pH higher than 3.47, MO is negatively charged whereas it is positively charged at a pH below 3.47.

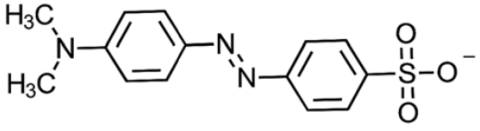

Figure 14: Chemical structure of methyl orange [182].

2.3.3. Applications of hydrochar

Hydrochar is considered a promising material which has potential for a range of applications. Literature has reported applications as low-cost adsorbent, for soil amendment and carbon sequestration, catalyst support and supercapacitors.

2.3.3.1. Low-cost adsorbent

Hydrochar usually has poor characteristics for adsorption due to its low surface area and pore volume which provide less sorption sites for contaminants (versus biochar for example) [184]. Furthermore, its negative surface charge is unconducive to adsorbing negatively charged substances [185]. Hydrochar also has a high volatile organic compound (VOC) content, which may leach into water. And even though most of the VOCs in hydrochar are water soluble, rinsing the HC is often not sufficient [186], [187]. However, some studies have shown that due to the diverse surface functionalities of HC, it has strong sorption capacities for both polar and non-polar organic contaminants [188], [189]. Thus, HC has been proposed as a low-cost adsorbent for contaminants in aqueous solutions [190]. These contaminants can be metals, dyes, organic pollutants (e.g. pesticides, pharmaceuticals), and some studies have even evaluated its adsorption potential for pathogens. However, for the removal of contaminants with HC it is crucial to determine the surface area, pore volume, surface charges and surface functionality [190].

To give hydrochar better characteristics for adsorption, activation can be carried out. Hydrochar can be activated with chemicals during HTC (1-step) or after HTC (2-step) [190], [191], [192]. Studies have shown that modified HCs have higher sorption capacities than their unmodified version [190]. A distinction between chemical and physical activation can be made, which will be briefly explained below.

Chemical activation

Chemical activation can be done by either adding chemicals directly in the HTC container or by washing the HC in a chemical solution after HTC. When washing the HC with a chemical solution, the HC can be used after rinsing with DI water or it can be further activated in an inert, heated environment [190]. Commonly used chemicals for chemical activation are: H_3PO_4, $ZnCl_2$, K_2CO_3, $FeCl_3$, NaOH, and KOH [193], [194], [195], [196]. These are dehydrating agents which leave deposits inside the matrix of the hydrochar, that becomes porous due to dehydration. The spent activation agent that is formed is then rinsed away which leads to the formation of meso- and micropores. Thus, the end product has a higher pore volume and surface area [190].

Physical activation

Physical activation relies on the carbonization of the HC in an inert atmosphere and/or activation with an oxidizing gas like CO_2 or steam, typically at temperatures above 600°C [197], [198]. This leads to the formation of larger surface areas and more pore volume, even though it requires more energy than chemical activation. Furthermore, physical activation is more effective, using less chemicals and water than chemical activation [198]. Fang et al. (2016) made HCs (T = 200°C, t = 6 h, w/b = 5.8) from hickory and peanut hull and activated them with CO_2 (m_{HC} = 5 g, t = 1-2 h, T = 600-900°C, CO_2 gas flow rate = 150 mL/min). The surface area increased from 7 m^2/g to 380-1300 m^2/g depending on the activation temperature, leading to a 50 to 190-fold increase [197].

2.3.3.2. Soil amendment and carbon sequestration

Hydrochar shows promising results in enhancing soil quality by improving its structure, nutrient cycling, and moisture retention capacities. These improvements are attributed to its well-developed pore structure, abundant OFGs, rich organic matter content, high aromaticity, and small O/C and H/C ratios [199], [200]. Many experiments have therefore been conducted to study the effect of hydrochar for soil improvement [200]. Although most HCs have a rather low nutrient content and thus cannot be used as fertilizer by themselves, they can be added to soil to strengthen the effect of fertilizers and thus reduce the amount of fertilizer that is lost through surface run-off [201]. This is because the nutrients are sorbed into the pores of the HC, which then slowly releases the nutrients into the soil for plant uptake. Thus, HC was found to have a synergistic effect with fertilizers by enhancing plant growth and improving nutrient use-efficiency [190].

However, some studies have shown a decrease in plant growth when HC was used, this was attributed to the immobilization of N in the soil due to the hydrochars decomposition activity [202], [203]. Since HC is more prone to biological degradation than biochar, it was also seen that fungal colonization on the surface of HC was sometimes observed, which reduced the water retention properties of HC [204], [205], [206]. Furthermore, HC has been seen to contain more hydrophobic areas, thus not improving the water holding capacity [207], [208]. However, in sandy soils (which naturally have low available water capacity), an improvement for water capacity was seen because HC addition to soil decreases the bulk density of the soil and increases the total pore volume, allowing more water retention in the soil [190], [209], [210].

An important aspect when considering HC for soil amendment is the possible phytotoxicity effects. As HC can often contain toxic compounds such as heavy metals, but also organic acids, phenols, furfurals, and their derivatives due to secondary charring, i.e. polymerization and condensation of dissolved intermediates [211], [212], [213]. The content of toxic compounds depends on both the feedstock and the HTC conditions [211], [213].

Another possible advantage of HC for soil amendment is its possibility to sequester carbon. Biochar (BC) has been proven to be a good material for carbon sequestration (CS) because pyrolysis turns the biomass into a more recalcitrant form. Thus, HC which obtains moderate stability by HTC, may also be a good material for CS, albeit for a shorter time than BC [214], [215]. Soils with added HC were monitored for their greenhouse gas (GHG) fluxes: N_2O, CO_2 and CH_4. The soils with added HCs showed considerably larger N_2O, CO_2 and CH_4 emissions than soils amended with BC and sometimes even compared to unamended soils. The increase of CO_2 was found to be due to the relatively low stability of the C in HC and due to the stimulated microbial activity as a result of its higher degradability [216], [217]. Baronti et al. (2017) determined that 47% of the added carbon through HC to the soil was lost due to decomposition in the first year after application. But it was also seen that more than half of the C did not decompose further. They found evidence that there was fast migration to deeper soil horizons where the low microbial density and oxygen content usually reduces decomposition. However, the assumption that translocation towards deeper soil horizons favours permanent CS is still under discussion [10], [218]. As such, CS with hydrochar still seems challenging and further testing is needed on different soils to come to a definite conclusion as well as considering the CO_2 emitted during the production of hydrochar, through for example a life cycle assessment [10].

Thus, even though many studies have proven the positive effect of HC application for soil amendment, some sidenotes can be made. Before considering HC for soil amendment, the phytotoxicity should be determined as well as the stability of the HC in the soil.

2.3.3.3. Material for supercapacitors or catalyst support

Supercapacitors

Supercapacitors (SC) are a promising electrochemical energy storage device due to their ability to rapidly charge and discharge, their high-power density, and long lifecycle. With the predicted growth in renewable energy sources (e.g. wind, solar power), the research for advanced energy storage and conversion technologies that enable a stable in- and output of energy is in full bloom, with SC being a good contender [219], [220]. The most common type of SC is the electric double-layer capacitor, which stores energy between the double layers through the phase interface of electrodes and electrolytes motivated by electrostatic interactions [221]. Vital to accumulate a huge amount of power is the layer thickness and the large electrode surface. Therefore, a critical component of the SC is the electrode, which should have excellent chemical stability, good conductivity, and a high specific capacitance [219], [222].

Thus, hydrochar has also been investigated for its possible utilisation as a low-cost material for electrodes in SC. As mentioned in section 2.3.3.1, the HC has to be activated in order to have the desired large specific surface area and large pore volume. In one study, HC was combined with nickel, with nickel acting as a graphitization catalyst which improved the specific capacity of HC by 149%. After activation, the HC-nickel composite had a specific capacitance of 175 F/g, which was higher than that of an activated carbon-nickel composite. This difference was attributed to the hierarchical porous structure in combination with the relatively high surface area and pore volume of the HC [223]. Another study made HC and BC from sewage sludge and activated those with $KHCO_3$ and also by further physical activation. A specific capacitance of 54 F/g was obtained for the activated HC versus 234 F/g for the activated BC at a current density of 1 A/g. The reason for the lower capacitance of the activated hydrochar was determined to be due to the substantially lower specific surface area (HC: 477 m^2/g, BC: 952 m^2/g) [224].

Catalysts

Biocatalysts and carbon-based catalysts, such as BC and HC, have a lower cost, reusable nature, large surface area, stable structure, good thermal and mechanical stability, and an improved acid density, which makes them a good alternative for the commonly used metal catalysts [225], [226]. As HCs directly after HTC have a relatively low specific surface area, activation or functionalization is needed to tune the HCs. As mentioned in section 2.3.3.1, chemical or physical activation can be done to increase the surface area. Functionalization can be done to obtain the desired surface functional groups. The most common modification method is sulfonation with concentrated H_2SO_4 or its derivatives. Following sulfonation, the modified hydrochars can be used as solid acid catalysts for polysaccharide hydrolysis, sugar dehydration, biodiesel production, etc [225].

Thus, HC used as low-cost material for SC or as catalyst support is a promising possible application. However, depending on the process parameters and the activation method, different results will be obtained which still needs to be further researched. Furthermore, the use of NLBM for these applications is only beginning to be evaluated [225].

3. MATERIALS AND METHODS

In the following sections, the materials and methods used during the experimental research will be described. This includes three main categories of experiments: the hydrothermal carbonization, the physicochemical characterization, and the experiments on adsorption. Figure 15 gives a schematic overview of the different steps. All experiments were carried out in the laboratory of the Centre on Green Chemistry and Environmental Biotechnology (GREAT) at Ghent University Global Campus in Songdo (GUGC) in South Korea, unless stated otherwise. ChatGPT was used throughout parts of this master thesis for structuring and rephrasing.

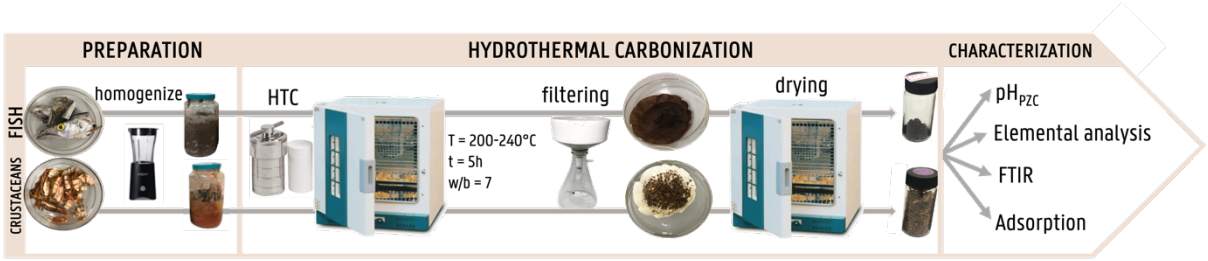

Figure 15: Schematic overview of feedstock preparation, HTC and hydrochar characterization.

3.1. Preparation of marine biowaste

The feedstock used in this research is waste from eight marine species collected at a local fish market called Sorae Pogu in Incheon, South Korea during the months of August and September 2023. These species comprise five from the subphylum Vertebrata: chub mackerel (*Scomber japonicus*), hairtail (*Trichiurus lepturus*), yellow corvina (*Larimichthys polyactis*), horse mackerel (*Trachurus japonicus*) and olive flounder (*Paralichthys olivaceus*), and three from the subphylum Crustacea: whiteleg shrimp (*Litopenaeus vannamei*), tiger prawn (*Penaeus monodon*) and Gazami crab (*Portunus trituberculatus*). The waste consisted primarily of the head, bones, tail, skin, and shell. The samples were stored in a cool transportation box and immediately stored in a freezer in the laboratory at a temperature below -10°C. Within 2 weeks after being put in the freezer, the waste was used. The frozen fish was thawed at room temperature and grinded using a food-grade blender to produce homogeneous fish and crustacean slurries. The moisture content of each of these species was then determined by drying approximately 5 g of the raw feedstock at 105°C for 24 hours in an electric oven (model JSOF-150). The moisture content w (%) was calculated by Eq. 3.1.1 with m_{wet} (g) and m_{dry} (g) being the mass of the wet sample before and after drying, respectively.

$$w = \frac{m_{wet} - m_{dry}}{m_{wet}} \cdot 100\% \qquad (3.1.1)$$

3.2. Hydrothermal carbonization

Hydrothermal carbonization was carried out in 50 mL non-stirred Teflon autoclave reactors heated in an electric oven (model JSOF-150). In previous research, a preliminary optimization protocol was carried out to determine the optimal process conditions. The temperature was determined as the most influential parameter. The hydrochars were produced using a constant water-to-biomass ratio (w/b) of 7, a constant residence time of 5 hours and varying temperatures of 200, 220 and 240°C. A lower temperature of 180°C was also considered if this might result in a higher hydrochar yield for certain feedstocks. From the determination of the moisture content of the different feedstocks, as described in the previous section, a precise amount of water was added to the wet slurry to obtain the chosen water-to-biomass ratio. The amount of wet feedstock used was dependent on the moisture content of the species, however, 4 grams of dry feedstock was used for all experiments. With the 4 grams of dry feedstock and an w/b of 7, the wet slurry always had a mass of 32.6 g for all samples. The extra water that must be added (w_{add} (g)) to the wet feedstock to obtain the desired water-to-biomass ratio could be calculated from Eq. 3.2.1, where w (%) is the initial moisture content of the feedstock and m_{wet} (g) is the mass of the wet feedstock.

$$w_{add} = (1 - w) \cdot m_{wet} \cdot w/b - w \cdot m_{wet} \tag{3.2.1}$$

After the HTC, the produced hydrochar slurry was cooled at room temperature and filtered using CHMLAB® Ashless Qualitative Analysis Filter grade F1001 (125 mm) using a porcelain Büchner funnel vacuum filtration setup. The hydrochar slurry was washed with acetone to remove any remaining oils from the marine biowaste. The washed and filtered hydrochar was then dried in an electric oven (model JSOF-150) for 3 hours at 105°C. The yield of the hydrochar was then determined by weighing the scraped dried solid product from the filter paper. Scraping the dry product from the filter paper was essential, as a lot of oily residue was adsorbed by the filter paper. The hydrochar yield (%) on dry basis was calculated using Eq. 3.2.2. All samples were done in triplicates and the produced hydrochars were stored in a fridge at 4°C until further characterization experiments were done.

$$Hydrochar\ yield = \frac{mass\ of\ dried\ hydrochar\ (g)}{mass\ of\ dried\ feedstock\ (g)} \cdot 100\% \tag{3.2.2}$$

The oily residue on the filter papers and after washing with acetone yielded a question as to the significance of this by-product. Thus, the oil and grease were recuperated for the fish waste. After acetone washing and filtering, the filtrate was put in a rotary evaporator at 60°C for 5 hours. The oil yield (%) was calculated using Eq. 3.2.3.

$$Oil\ yield = \frac{mass\ oil\ (g)}{mass\ of\ wet\ feedstock\ (g)} \cdot 100\% \tag{3.2.3}$$

3.3. Physicochemical characterization

3.3.1. Point of zero charge

The pH point of zero charge (pH_{PZC}) was used to characterize the electrical state of the adsorbent surfaces in dispersions. For the determination of the pH_{PZC} of the produced hydrochar, pH solutions of 2, 4, 6, 7, 8, 10 and 12 were made using 0.1 M NaCl solution adjusted with NaOH and HCl until the desired pH was reached. 5 mL of the 7 different pH solutions was then added to each sample of approximately 10 mg. These mixtures were then stirred with an electrical stirrer at 1200 rpm for 24 hours. After this time, the pH was assumed to stop changing and having reached equilibrium [227], [228]. The final pH was determined using a pH electrode with a pH meter S220 from METTLER TOLEDO. All measurements were done in duplicates. Plots were then drawn with initial pH (x-axis) and change in pH, ΔpH (y-axis). The intersecting point between the curve and the x-axis (where ΔpH was 0), was identified as pH_{PZC}.

The propagation of uncertainty was calculated using the standard deviation considering the covariance in case the uncertainties would be correlated. To calculate the PZC, a linear regression was made across three points on the obtained curve, closest to the intersecting point. These points were either two above and one below the x-axis or two below and one above the x-axis. The obtained first-order equation (Eq. 3.3.1) could then be used to calculate the PZC by solving for x, when y equalled 0.

$$y = Bx + A \tag{3.3.1}$$

The standard deviation (σ_f) of the function with the real variables A and B with standard deviations (σ_A and σ_B), covariance ($\sigma_{AB}=\rho_{AB}\sigma_A\sigma_B$) and correlation ($\rho_{AB}$) could then be determined. Eqs. 3.3.2-3.3.3 are the function and standard deviation, respectively [229].

$$f = \frac{-A}{B} \tag{3.3.2}$$

$$\sigma_f \approx |f| \sqrt{\left(\frac{\sigma_A}{A}\right)^2 + \left(\frac{\sigma_B}{B}\right)^2 - 2\frac{\sigma_{AB}}{AB}} \tag{3.3.3}$$

3.3.2. Elemental and proximate analysis

Elemental analysis (C, H, N, O and S) of the raw feedstocks and produced hydrochar was performed externally using a Vario-EL III (Elementar Analysensysteme GmbH, Germany). The ash content for the ultimate analysis was then calculated by using a mass balance (Eq. 3.3.4).

$$Ash\ content = 100 - (C + H + N + O + S) \tag{3.3.4}$$

Besides the calculated ash content, the ash content was also measured externally using a complete proximate analysis protocol (ASTM D7582) using a Leco TGA801. It should be noted that only the calculated ash content was used in the data analysis. For the proximate analysis protocol, all raw materials and produced hydrochars were put in ceramic crucibles in the

carousel of the TGA machine for a 3-step measurements process. The first stage was the moisture content measurement by increasing the temperature to 105°C under inert (N_2) atmosphere. The next stage was volatile matter (VM) measurement by increasing the temperature to 600°C. The final stage was to measure the ash content by increasing the temperature to 950°C with the atmosphere switched to an oxygen atmosphere. The heating rate was set for each step and each step was done after the previous step reached an equilibrium mass. The fixed carbon (FC) content of the produced hydrochars were calculated using the mass balance for the hydrochars total content, as expressed in wt.% in Eq. 3.3.5. Since the calculated fixed carbon content was sometimes negative, those values were replaced by 0 and the moisture content, VM, ash and FC were normalized.

$$Fixed\ carbon = 100 - (moisture + volatile\ matter + ash) \tag{3.3.5}$$

The higher heating value (HHV, kJ/g) was calculated using Dulong's formula (Eq. 3.3.6), as this is the most commonly used equation based on ultimate analysis [230].

$$HHV = 0.3383 \cdot C + 1.443\left(H - \left(\frac{O}{8}\right)\right) + 0.0942 \cdot S \tag{3.3.6}$$

3.3.3. FTIR

Analysis of surface functional groups of both the raw feedstock and hydrochar was conducted using Fourier Transform Infrared (FTIR) spectroscopy using a Bruker VERTEX v70 FTIR spectrometer within a wave number range of 400 to 4000 cm^{-1} at ambient temperature.

3.4. Adsorption

Experiments were carried out to determine the potential of the produced hydrochars for adsorption applications. The experiments were performed with methylene blue and methyl orange. The calibration curves for both can be found in Figure A.1 in Appendix A.

3.4.1. Considerations: pH and ionic strength

To compare the adsorption experiments when using different pH values, it was decided the ionic strength should be taken into consideration. Therefore, before starting any of the adsorption experiments, the ionic strength of each pH solution and the needed salt adjustments were calculated. The pH was decided to be fixed at 4, 7 and 9 using potassium phosphate buffers with a buffer capacity of 20 mM and salt adjustments were made using chemical-grade KCl. As can be seen on Figure 16, the inorganic phosphate speciation is in function of the pH. To make buffers at pH 4, 7 and 9, different combinations of potassium phosphate were needed. For pH 4, a combination of H_3PO_4 (as acid) and KH_2PO_4 (as base) were used, for pH 7 and 9, KH_2PO_4 (as acid) and K_2HPO_4 (as base) were used, all chemicals were bought from Daejung Chemicals & Metals Co., Ltd.

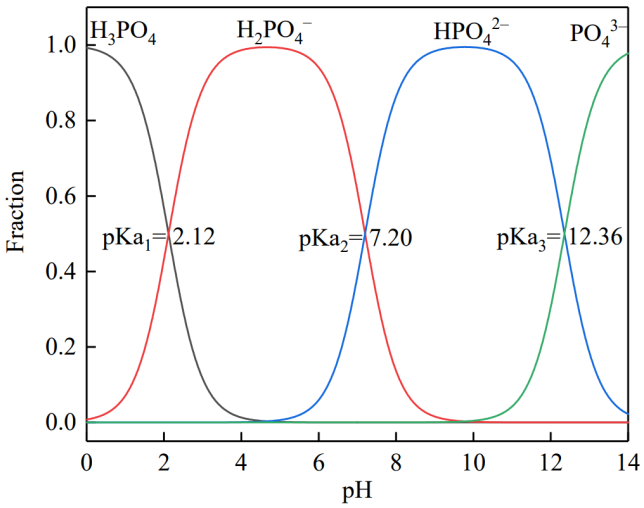

Figure 16: Inorganic phosphate speciation as a function of pH [231].

To calculate the ionic strength and thus the appropriate salt adjustments, the expression for buffer capacity was needed. This could be derived for a monoprotic acid, with the dissociation reaction noted in Eq. 3.4.1 and its equilibrium equation noted in Eq. 3.4.2. HX represents the acid, X^- the conjugate base, H^+ the proton and K_a the acid dissociation constant (mol/L). When the species are noted in square brackets, this indicates a concentration in mol/L.

$$HX \leftrightharpoons H^+ + X^- \tag{3.4.1}$$

$$K_a = \frac{[H^+][X^-]}{[HX]} \tag{3.4.2}$$

A mass and charge balance of a monoprotic acid and its conjugate base and a possible amount of base that is added (e.g., sodium salt) could then be made (Eq. 3.4.3 and 3.4.4) with $[X]_T$ (mol/L) the total concentration of acid and conjugate base.

$$Mass\ balance: [X]_T = [HX] + [X^-] \tag{3.4.3}$$

$$Charge\ balance: [H^+] + [Na^+] = [OH^-] + [X^-] \tag{3.4.4}$$

The substitution $[Na^+] = C_b$ could then be made and yields Eq. 3.4.5. C_b (mol/L) is the total concentration of base that must have been added.

$$C_b = [OH^-] - [H^+] + [X^-] \tag{3.4.5}$$

Substituting Eq. 3.4.3 in Eq. 3.4.2, yields an expression for $[X^-]$, Eq. 3.4.6. This could then be substituted in Eq. 3.4.5, to yield Eq. 3.4.7 and Eq. 3.4.8 when the ionic product of water ($K_w = [H^+][OH^-]$, with K_w (mol/L) the ionization constant for water) and the definition of pH is used, $pH = -\log([H^+])$.

$$[X^-] = [X]_T \frac{K_a}{K_a + [H^+]} \tag{3.4.6}$$

$$C_b = [OH^-] - [H^+] + [X]_T \frac{K_a}{K_a + [H^+]} \tag{3.4.7}$$

$$\Leftrightarrow C_b = \frac{K_w}{10^{-pH}} - 10^{-pH} + [X]_T \frac{K_a}{K_a + 10^{-pH}} \tag{3.4.8}$$

Eq. 3.4.8 could then be differentiated with respect to pH, with the assumption of a constant $[X]_T$. The expression for buffer capacity of a monoprotic acid is thus given by Eq. 3.4.9, with $\mathcal{B}$ (mol/L) the buffer capacity and dC_b (mol/L) the changes in the concentration of conjugate acid as strong monoprotic acid is added [232].

$$\mathcal{B} = \frac{dC_b}{d(pH)} = ln10\left(\frac{K_w}{[H^+]} + [H^+] + [X]_T \frac{K_a[H^+]}{(K_a + [H^+])^2}\right) \tag{3.4.9}$$

The first two terms in the logarithm represent the free hydroxide and hydrogen ions. However, these are only of interest when dealing with extremes, such as adding or subtracting strong Arrhenius bases or acids to change pH. Therefore, at very dilute strong acid or base concentrations, the auto-ionization of water is more important and $[H^+] \approx [OH^-]$. Furthermore, buffers usually function within a close range around the pK_a or pK_b of the chosen acid or base, thus in the envisaged region, the first two terms do not play a significant role. The maximum buffer capacity ($\mathcal{B}_{max}$) holds true for $pH = pK_a$, when the [HX] to $[X^-]$ ratio is exactly 1:1. This consequently means that $K_a = [H^+]$, and thus K_a can be replaced by $[H^+]$ in the last term within the logarithm. This leads to following equation (Eq. 3.4.10):

$$\mathcal{B}_{max} = \frac{ln10([X]_T)}{4} = 0.576[X]_T \tag{3.4.10}$$

$[X]_T$ can be replaced to include the mass of the conjugate base x (g) and the mass of the acid y (g) yielding Eq. 3.4.11. V (L) represents the volume and MW_{X^-} and MW_{HX} (g/mol) represent the molecular weight of the conjugate base and acid, respectively.

$$\mathcal{B}_{max} = 0.576\left(\frac{x}{MW_{X^-}} + \frac{y}{MW_{HX}}\right)\frac{1}{V} \tag{3.4.11}$$

The Henderson-Hasselbalch equation (Eq. 3.4.12) can be used to note x and y in function of the pH, yielding Eq. (3.4.13-15).

$$pH = pK_a + log\left(\frac{[X^-]}{[HX]}\right) \tag{3.4.12}$$

$$\Leftrightarrow pH = pK_a + log\left(\frac{\frac{x}{MW_{X^-}}}{\frac{y}{MW_{HX}}}\right) = pK_a + log\left(\frac{MW_{HX}}{MW_{X^-}}\right) + log\left(\frac{x}{y}\right) \tag{3.4.13}$$

$$\Leftrightarrow x = y \cdot 10^{pH - pK_a - log\left(\frac{MW_{HX}}{MW_{X^-}}\right)} \tag{3.4.14}$$

$$\Leftrightarrow y = x \cdot 10^{pK_a + log\left(\frac{MW_{HX}}{MW_{X^-}}\right) - pH} \tag{3.4.15}$$

Putting Eq. 3.4.11 and 3.4.14-15 together, formulas can be derived for x and y in function of $\mathcal{B}_{max}$, V, pH, and the molecular weights of the buffer components, yielding Eq. 3.4.16 and 3.4.17.

$$y = \frac{\mathcal{B}_{max}V}{0.576}\left(\frac{10^{pH - pK_a - log\left(\frac{MW_{HX}}{MW_{X^-}}\right)}}{MW_{X^-}} + \frac{1}{MW_{HX}}\right)^{-1} \tag{3.4.16}$$

$$x = \frac{\mathcal{B}_{max}V}{0.576}\left(\frac{1}{MW_{X^-}} + \frac{10^{pK_a + log\left(\frac{MW_{HX}}{MW_{X^-}}\right) - pH}}{MW_{HX}}\right)^{-1} \tag{3.4.17}$$

After having calculated the mass of each buffer component needed, the ionic strength of the solution can be determined with the formula for ionic strength (Eq. 3.4.18), with c_i the concentration and z_i the charge of ion i.

$$\mu = \frac{1}{2}\Sigma c_i (z_i)^2 \tag{3.4.18}$$

The difference in ionic strength between the different buffer solutions (Eq. 3.4.19) can be calculated and the lowest ionic strengths can be made the same as the highest one by adding salts. The difference in ionic strength of buffer j, $\Delta\mu_j$ (mol/L), is calculated by subtracting the biggest μ of all the buffers with the ionic strength of buffer j, μ_j (mol/L). The mass of salt $m_{salt,add}$ (g) that should be added to buffer solution j can then be calculated by Eq. 3.4.20.

$$\Delta\mu_j = \max(\mu) - \mu_j \tag{3.4.19}$$

$$m_{salt,add} = \Delta\mu_j \cdot MW_{salt} \cdot V \tag{3.4.20}$$

3.4.2. Adsorption kinetics

The time at which equilibrium occurs was determined by mixing 160 mg of whiteleg shrimp hydrochar with 80 mL of 50 mg/L MB solution. The pH was fixed at 9 using phosphate buffer. The solution was mixed at 150 rpm and kept at room temperature. Samples of 1 mL were taken at certain time intervals and filtered using Hyundai Micro Nylon Syringe filters with a pore size of 0.2 µm. The MB concentration in the filtrate was then determined by UV-Vis spectrometry (K LAB CO., LTD) at a wavelength of 664 nm. The adsorbed amount of MB was calculated by Eq. 3.4.21, with q_e the adsorbed MB amount (mg/g), C_0 the initial concentration (mg/L), C_e the equilibrium concentration (mg/L), V the volume of MB solution (L) and m the hydrochar dosage (g). The removal efficiency η (%) was calculated using Eq. 3.4.22.

$$q_e = \frac{(C_0 - C_e)V}{m} \tag{3.4.21}$$

$$\eta = \frac{(C_0 - C_e)}{C_0} \cdot 100\% \tag{3.4.22}$$

The adsorption and desorption kinetic rate constants for the whiteleg shrimp-HC were evaluated by the Lagergren's pseudo-first-order model (PFOM), as expressed in Eq. 3.4.23.

$$Q(t) = Q_{m,1}(1 - \exp(-k_1 t)) \tag{3.4.23}$$

The pseudo-second-order kinetics model (PSOM) was evaluated using Eq. 3.4.24.

$$Q(t) = \frac{K_2 Q_{m,2}^2 t}{1 + K_2 Q_{m,2} t} \tag{3.4.24}$$

The Elovich model (Eq. 3.4.25) with α representing the initial adsorption rate (mg/(g·h)) and β the desorption coefficient (g/mg).

$$Q(t) = \frac{\ln(\alpha \cdot \beta) + \ln(t)}{\beta} \tag{3.4.25}$$

To determine which model had the best fit, the parameter precision was estimated using nonlinear least-squares routine based on the Levenberg-Marquardt algorithm (Solver) which comes with Microsoft Excel®. The parameters of the models were estimated by minimising the residual sum of squares (SSE) (Eq. 3.4.26).

$$SSE = \sum_{i=1}^{n} \left(y_{i,exp} - y_{i,mod}\right)^2 \tag{3.4.26}$$

The standard deviations σ_i of the parameters a_i were then calculated using Eq. 3.4.27. With n_p the number of performed observations, p the number of adjustable parameters a_i and m_{ii}^{-1} the i^{th} diagonal term of the inverse of a p·p matrix containing the partial differentials of the fitting function $\delta F_n/\delta a_i$ with $F_n = y_{i,mod}$ [233].

$$\sigma_i = \sqrt{\frac{m_{ii}^{-1} \cdot SSE}{n_p - p}} \tag{3.4.27}$$

Since PSOM, PFOM and Elovich equations contain the same number of adjustable parameters and the same dataset was used on all 3 models, it is not necessary to use adjusted or normalized statistical indicators of the quality of fit [234]. Therefore, coefficient of determination (R^2, Eq. 3.4.28) and the residual sum of squares (SSE, Eq. 3.4.26) suffice and were calculated. With $y_{i,exp}$ being the experimental value of the independent variable, $y_{i,mod}$ is the modelled value, $\overline{y_{i,exp}}$ is the mean of observed values and SST is the sum of square of total deviations.

$$R^2 = 1 - \frac{\sum_{i=1}^{n}\left(y_{i,exp} - y_{i,mod}\right)^2}{\sum_{i=1}^{n}\left(y_{i,exp} - \overline{y_{i,exp}}\right)^2} = 1 - \frac{SSE}{SST} \tag{3.4.28}$$

3.4.3. Isotherms

An amount of 10 mg of hydrochar was added to 5 mL of MB dye solution with different concentrations of 5, 30, 50 and 100 mg/L (and 200 mg/L for yellow corvina-HC at pH 9). The samples were stirred at 150 rpm in a shaking water bath (Model MaXturdy 45, DAIHAN Scientific Co., LTD) during 6 hours at 25°C. The pH was fixed to 4, 7 and 9 using potassium phosphate buffers with a buffer capacity of 20 mM to study the effect of pH on adsorption. For all pH solutions, the ionic strengths were made constant by adding chemical grade potassium chloride salt. After the adsorption experiment, the solid and liquid phases were separated using Hyundai Micro Nylon Syringe filters with a pore size of 0.2 µm. The MB concentration in the filtrate was determined by UV-Vis spectrometry (K LAB CO., LTD) at a wavelength of 664 nm. The adsorption capacity of HC was calculated by Eq. 3.4.21. The equilibrium adsorption data was fitted with Langmuir and Freundlich isotherms, using Eq. 3.4.29 and 3.4.30 respectively. The amount of MB adsorbed at equilibrium is represented by q_e (mg/g), q_m is the maximum MB adsorption capacity (mg/g), K_L (L/mg) and K_F ($mg^{1-1/n}L^{1/n}/g$) are the Langmuir and Freundlich equilibrium coefficients. The factor 1/n is the adsorption intensity or heterogeneity factor of the adsorption. The Langmuir adsorption isotherm assumes that adsorption takes place at a fixed number of homogeneous sites within the hydrochar and is mainly used for reversible monolayer adsorption [235]. In contrast, the Freundlich adsorption isotherm considers a heterogeneous adsorption surface that has unequal available sites with different adsorption energies [236].

$$q_e = \frac{q_{max} K_L C_e}{1 + K_L C_e} \tag{3.4.29}$$

$$q_e = K_F C_e^{1/n} \tag{3.4.30}$$

When computing these isotherms, an inflection point was observed for yellow corvina-HC at pH 9. This inflection point was an indication of possible lateral interactions during adsorption. Thus, two additional models were evaluated: Frumkin-Fowler-Guggenheim and Hill-de Boer.

The Frumkin-Fowler-Guggenheim (FFG) model is given by Eq. 3.4.31, where k_{FG} is the FG equilibrium coefficient of adsorption (L/mg), theta is the fractional coverage (-) and W is the interaction energy between adsorbed molecules (kJ/mol). R is the universal gas constant (8.314 kJ/mol/K), and T is the temperature (298 K) [237].

$$k_{FG} \cdot C_e = \frac{\theta}{1-\theta} \cdot \exp\left(\frac{2 \cdot W \cdot \theta}{R \cdot T}\right) \; and \; \theta = \frac{q_e}{q_{max}} \tag{3.4.31}$$

Hill-de Boer (HDB) model can be seen in Eq. 3.4.32, where K_1 is the Hill-de Boer constant (L/mg), K_2 is the interaction energy between adsorbed molecules (kJ/mol) and theta is the fractional coverage (-). A K_2 that is positive, negative or zero means attraction, repulsion, or lack of attraction between adsorbed molecules, respectively [238], [239].

$$K_1 \cdot C_e = \frac{\theta}{1-\theta} \cdot \exp\left(\frac{\theta}{1-\theta} - \frac{K_2 \cdot \theta}{R \cdot T}\right) \; and \; \theta = \frac{q_e}{q_{max}} \tag{3.4.32}$$

Convergence issues using simultaneous estimation of the three parameters in the FFG and HDB model persisted, therefore values for the lateral interaction parameter (W in FFG and K_2 in HDB) were varied and the SSE was evaluated. The value of W or K_2 where SSE was minimal (depending on W or K_2), was then used to re-evaluate the two remaining adjustable parameters (q_{max} and k_{FG} (FFG) or K_1 (HDB), thus convergence issues were solved.

As the FFG and HDB models are 3-parameter models and Langmuir and Freundlich are 2-parameter models, it was decided to use adjusted and normalised statistical indicators. Because Wang et al. pointed out that relying solely on R^2 makes distinctive model selection difficult because R^2 values of different models always have small differences [240]. Thus, the adjusted square coefficient of correlation (R^2_{Adj}, Eq. 3.4.33), normalized root mean square error (NRMSE, Eq. 3.4.34) and normalized standard deviation (NSD, Eq. 3.4.35) were calculated [177], [237].

$$R^2_{Adj} = 1 - (1 - R^2) \cdot \left(\frac{n_p - 1}{n_p - p - 1}\right) \tag{3.4.33}$$

$$NRSME = \sum_{i=1}^{n} \frac{\left(y_{i,exp} - y_{i,mod}\right)^2}{y^2_{i,exp}} \tag{3.4.34}$$

$$NSD = 100 \cdot \sqrt{\frac{\sum_{i=1}^{n} \frac{\left(y_{i,exp} - y_{i,mod}\right)^2}{y^2_{i,exp}}}{n_p - p}} \tag{3.4.35}$$

3.4.4. One-point adsorption

For one-point adsorptions, an amount of 10 mg of hydrochar for the eight species was added to 5 mL of 50 mg/L MB dye or 50 mg/L MO dye. The samples were stirred at 150 rpm in a shaking water bath (Model MaXturdy 45, DAIHAN Scientific Co., LTD) during 6 hours at 25°C. The pH was fixed at 7 with potassium phosphate buffer with a buffer capacity of 20 mM. The ionic strength μ was fixed at 103 mM by adding chemical grade potassium chloride. The experiment was repeated without adding salt, and thus the ionic strength at pH 7 was 61.2 mM. All samples were done in duplicates. The point adsorptions were repeated for yellow corvina-HC and whiteleg prawn-HC at pH 4 and 9 with a buffer capacity of 20 mM. The experiments were done with and without the addition of salt, all in duplicates. After the adsorption experiment, the samples were filtered using Hyundai Micro Nylon Syringe filters with a pore size of 0.2 μm. The MO and MB concentration in the filtrate were determined by UV-Vis spectrometry (K LAB CO., LTD) at a wavelength of 464 nm for MO and 664 nm for MB. To determine whether a different ionic strength yielded a significantly different adsorption capacity, the independent two sample t-test was conducted.

4. RESULTS AND DISCUSSION

In the following sections, the results of the experiments are presented and described. The experiments are divided into a section about the characteristics of the feedstock, the performed HTC, the characterization of the hydrochar and lastly, the adsorption experiments. The outcomes were analysed to attempt a comprehensive understanding of the findings. All data analysis was done in Excel ® (version 16.77.1.).

4.1. Characteristics of marine biowaste

As can be seen on Figure 17, the moisture content reached a stable value at the 6-hour mark after drying at a temperature of 105°C. Overall, the crustacean waste showed a higher moisture content (75-81%) than the fish waste (67-73%). Tiger prawn waste showed the highest moisture content (81±1%) whereas horse mackerel waste showed the lowest moisture content (67±2%). The exact moisture content of each species can be found in Table B.1 in Appendix B.

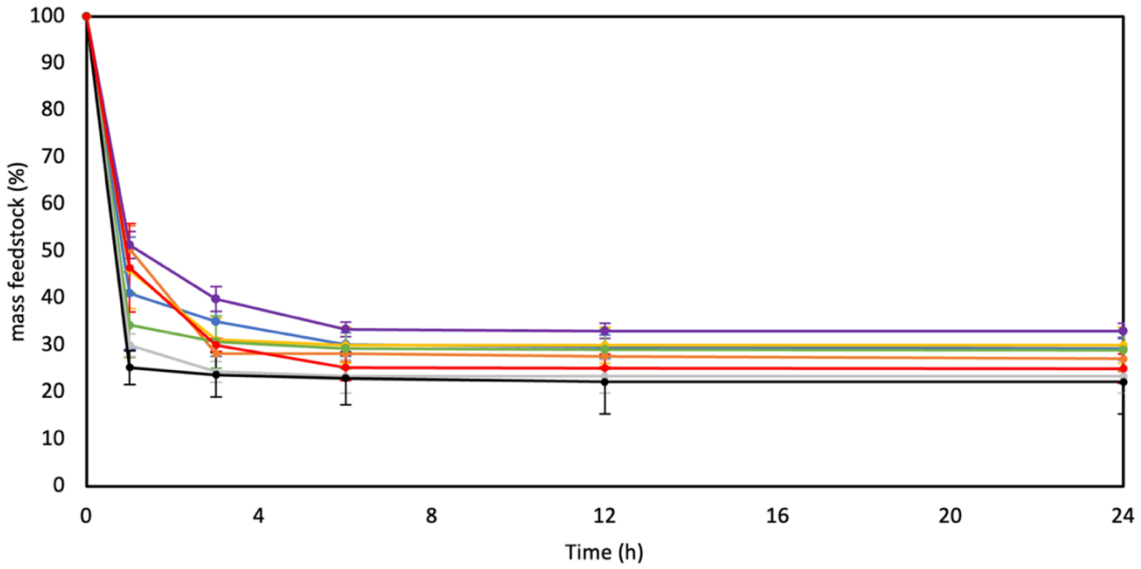

Figure 17: Mass decline over time during drying at 105°C of feedstock. Chub mackerel (—), hairtail (—), yellow corvina (—), horse mackerel (—), olive flounder (—), whiteleg shrimp (—), tiger prawn (—) and gazami crab (—). Lines are added to guide the eye.

The exact moisture content enabled to calculate the amount of deionized water (DI) that had to be added to obtain a constant water-to-biomass ratio of 7, which was used for all HC production experiments. Thus, the initial solid (12.3%) and liquid (87.7%) composition was the same for all variations, with 4 g taken as the initial dry feedstock. The liquid portion was different in composition for each species depending on the naturally occurring moisture content of each species and the added DI water, as calculated using Eq. 3.2.1 and visualized in Figure 18. The most DI water was added to horse mackerel waste and the least amount was added to tiger prawn waste. Using wet feedstocks prevented an unnecessary drying step (i.e. which would otherwise be needed in for instance pyrolysis). However, the naturally occurring moisture may have a different influence on the HTC compared to using added DI water. The effect of this naturally occurring moisture in comparison to purely deionized water is unclear. However, the location of the water could have a small effect on the conversion, as the natural water is present within the

cells of the biomass whereas the added water is always external. The effect could be negligible, or the naturally occurring moisture could act as a catalyst for increased pore formation or could, on the other hand, hinder this formation. Further research could be done to determine this.

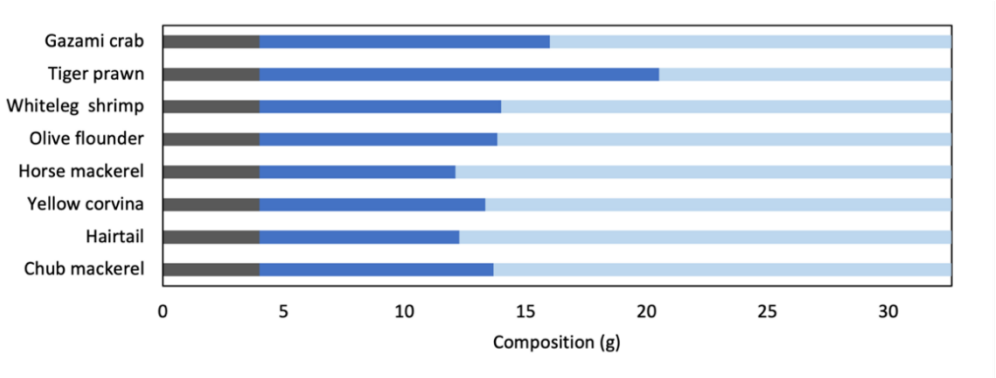

Figure 18: Feedstock composition in the HTC reactors prior to conversion. Dry feedstock (■), naturally occurring moisture (■), added distilled water (■).

When homogenizing the different marine species, as can be observed for whiteleg shrimp in Figure 19, some observations could be made. All the fish were easily blended with the blender; however, the fishbone of olive flounder was nearly impossible to break with the blender. Thus, the bones visually bigger than 2 cm were omitted from the slurry. As for Gazami crab, the shells were first broken in a mortar before blending them further.

Figure 19: Whiteleg shrimp before and after homogenizing.

4.2. Hydrothermal carbonization

Figure 20 shows the yield obtained for the hydrochars (HC) produced at 200°C, 220°C and 240°C (the exact yield-values can be found in Table B.2 in Appendix B). Crustaceans were subjected to HTC at 180°C in addition to temperatures of 200-240°C. This extra experiment at 180°C was prompted by the observation that crustaceans obtained the highest yield at 200°C, suggesting the potential for even higher yields at lower temperatures. Meanwhile, fish exhibited the highest yield at 220°C. Overall, it can be observed that the crustacean-HC achieved higher yields (37-69%) than the fish-HC (15-22%). This is a striking difference which could possibly be attributed to the greater amount of chitin and $CaCO_3$ in crustaceans. These compounds only break down at temperatures above 250 and 750°C, respectively, as mentioned in section 2.1.2. Thus, a higher portion of initial feedstock may remain unconverted. It can also be noted that all fish species have the highest HC yield at 220°C, whereas the crustacean-HC show the highest yield at 200°C. Chub mackerel showed the lowest yield (16 ± 2%), with only very few changes in yield with a change in temperature. Gazami crab showed the highest yield (69 ± 6%), with a decrease in yield with rising carbonization temperatures. Overall, most species showed an increase in yield with higher

temperatures, until 200°C for crustaceans or 220°C for fish, after which a rising temperature resulted in decreasing hydrochar yields. This decrease in solid yield with increasing reaction temperature after the optimum, was probably due to greater initial feedstock solubilization (hydrolysis) and increasing degradation reactions which could also be called secondary decomposition. The intermediates formed during biomass conversion then undergo hydrolysis, dehydration, decarboxylation, and other degradation reactions [241].

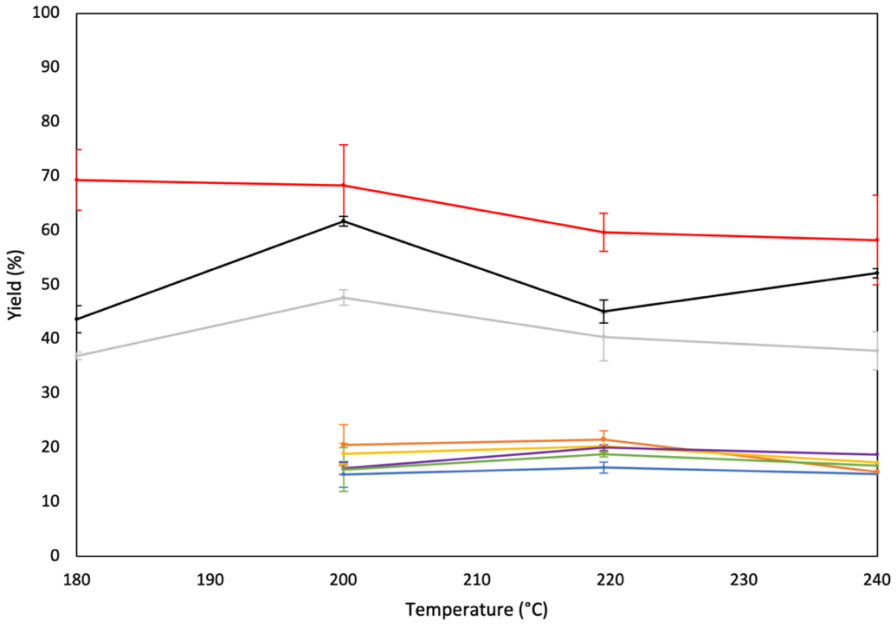

Figure 20: Hydrochar yield of the different species for various HTC temperatures. Chub mackerel (—), hairtail (—), yellow corvina (—), horse mackerel (—), olive flounder (—), whiteleg shrimp (—), tiger prawn (—) and Gazami crab (—). Lines are added to guide the eye.

After HTC, a solid, liquid and gas fraction were obtained. Within the liquid fraction of the fish-HC, oil and grease were observed (oil yield can be found in Table B.3 in Appendix B). In Figure 21 the oil/grease yield after HTC can be seen, on a wet feedstock basis. Higher temperatures resulted in higher amounts of oil or grease. This is due to the increased biomass decomposition with increasing temperature which leads to higher liquid and oil yields [242]. Furthermore, the oil yield is very similar between the different fish species, ranging from 17.8% for yellow corvina-HC (200°C) to 29.8% for horse mackerel-HC (240°C).

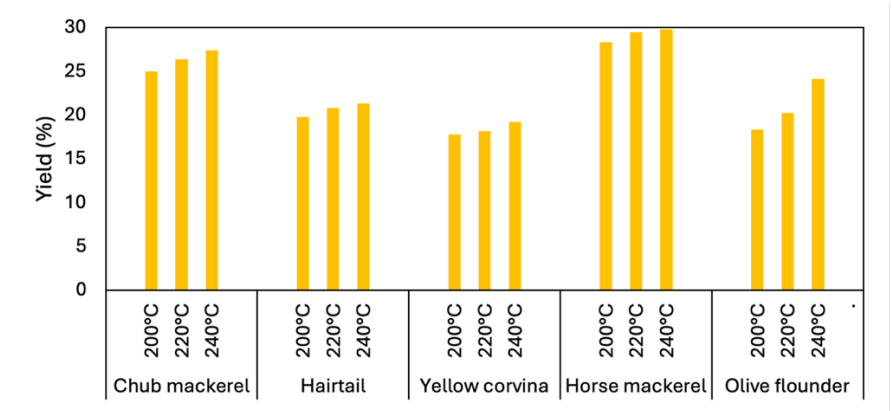

Figure 21: Oil/grease (■) yield on wet feedstock base of hydrochars.

4.3. Physicochemical characterization

4.3.1. Point of zero charge

As mentioned in section 2.3.2.1, the PZC reveals information about sorption mechanisms and surface charges. At the PZC, there are equal amounts of positive and negative charges. Therefore, at a pH of a solution higher (lower) than the PZC, the surface of the substrate is negatively (positively) charged. Figure 22 represents the PZC plot of HC from (a) chub mackerel and (b) whiteleg shrimp. The plots of all species can be found in Figure A.2 in Appendix A.

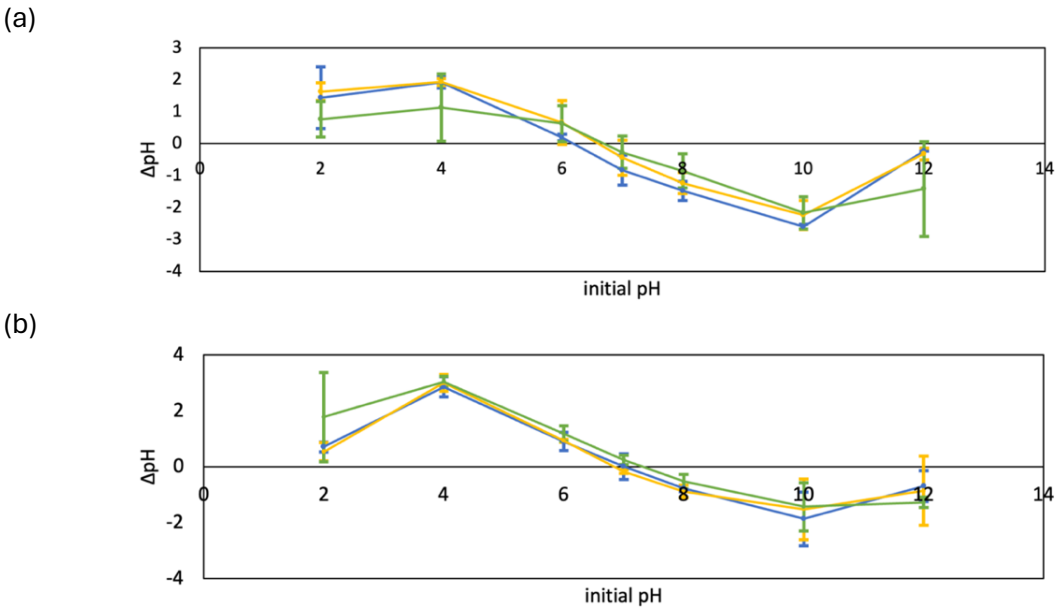

Figure 22: Point of zero charge graphs (200°C, 220°C, 240°C). (a) chub mackerel, (b) whiteleg shrimp based hydrochars.

In Table 5, the obtained PZC of the different hydrochars is given. It can be observed that all pH_{PZC} lie between 6 and 9, with the fish and the crustaceans each occupying a specific region. The fish-HCs showed lower PZC values (average of 6.48) than the crustacean-HCs (average of 7.93). This means that at neutral solution pH, the HCs from fish are negatively charged whereas the HCs from the crustaceans are positively charged.

Table 5: Point of zero charge of the hydrochars at the different HTC temperatures.

Point of zero charge	200°C	220°C	240°C
Chub mackerel	6.15 ± 0.21	6.64 ± 0.23	6.77 ± 0.27
Hairtail	6.56 ± 0.03	6.92 ± 0.07	7.02 ± 0.04
Yellow corvina	6.18 ± 0.11	6.35 ± 0.12	6.37 ± 0.07
Horse mackerel	6.20 ± 0.17	6.14 ± 0.18	6.30 ± 0.07
Olive flounder	6.56 ± 0.09	6.49 ± 0.04	6.60 ± 0.12
Whiteleg shrimp	7.05 ± 0.14	6.95 ± 0.07	7.35 ± 0.11
Tiger prawn	7.72 ± 0.06	8.12 ± 0.16	8.48 ± 0.14
Gazami crab	8.76 ± 0.13	8.32 ± 0.33	8.58 ± 0.18

A slight increase in pH_{PZC} was observed for increasing temperature for all species except for Gazami crab-HC. This increase in pH_{PZC} could be due to concentration of inorganic elements in the HCs with increasing HTC temperatures, such as the accumulation of alkaline salts (Na, K, Ca, Mg…) from the organic matrix in the feedstock [243], [244]. The highest PZC values were obtained for the crustaceans, with HC made from Gazami crab at 240°C showing the highest pH_{PZC} of all species. This highest pH value and the hypothesis that this is due to the concentration of inorganic elements, can be supported by FTIR results in Figure A.4(f) in Appendix A. For crab, the peak at 1400-1450 cm^{-1} was the highest amongst all produced HCs. This peak represents the asymmetric stretching of carbonate groups. This could indicate the presence of calcite ($CaCO_3$) in the samples. Thus, the higher PZC values for the crustacean-HCs could be attributed partly to the presence of this inorganic compound, which represents a large portion of the crustacean composition, as mentioned in section 2.1.2. This increasing trend with increasing reaction temperature was also observed by Shinogi and Kanri (2003), they argued however that this increase due to the inorganic components (ash) renders the surface more alkaline due to the plugging of pores with ash. They argue that for the pH to indicate the surface conditions, the ash should be removed with acid [244]. Even though treating the HCs with acid will leach the minerals, it will inevitably also alter the surface functional groups. Therefore, there is no way to completely uncouple the effect of minerals versus the surface functional groups.

4.3.2. Elemental analysis

To chemically characterize the produced hydrochars, the elemental composition was analysed. The exact values of the elemental composition can be found in Table B.4 and are visualised in Figure A.3 in the Appendices. The elemental composition of chub mackerel and whiteleg shrimp HCs are represented in Figure 23a and b, respectively. HTC had a clear impact on the elemental composition of chub mackerel-HC, whereas for whiteleg shrimp-HC the impact is less clear. The ash content increased for all species, compared to the raw feedstock. This is probably due to the accumulation of minerals in the HCs or the leaching of organics to the aqueous phase, resulting in concentration of inorganics in the HCs [245]. Remarkably, the carbon content decreased for all the species except whiteleg shrimp and tiger prawn with increasing HTC temperature. This could be because (i) the mass loss rate (in the solid phase) exceeds the rate of carbon enrichment in the hydrochar with increased reaction temperature, (ii) the shorter chain organic molecules which were produced dissolved into the aqueous phase, (iii) a higher transfer of carbon to the gas phase through decarboxylation reactions at higher temperatures resulted in a decrease in the carbon content of the hydrochar [246], [247], [248], [249]. The carbon content of whiteleg shrimp and tiger prawn HCs stayed relatively stable, this difference with the fish-HC can probably be explained due to the fat in the fish. The fatty acids will decarboxylate, producing CO_2 and long chain hydrocarbons which will end up in the oil/grease phase. Thus, the removal of oil/grease with acetone leads to a fraction of the C not ending up in the fish hydrochar. The stable carbon content in the crustacean-HCs may also be due to the presence of chitin and $CaCO_3$, which remain stable. Next to the decrease of carbon, all species also show a decrease in nitrogen, hydrogen, and sulphur with increasing reaction temperature. All fish-HCs also show a decreasing oxygen content, due to enhanced decarboxylation and dehydration reactions. For all the crustacean-HCs, an increase in oxygen content is observed with increasing reaction temperature. This can be attributed to $CaCO_3$, which stays unreacted during HTC and thus concentrates within the HC. This O-increase is something that is not typically observed with HCs from lignocellulosic biomass.

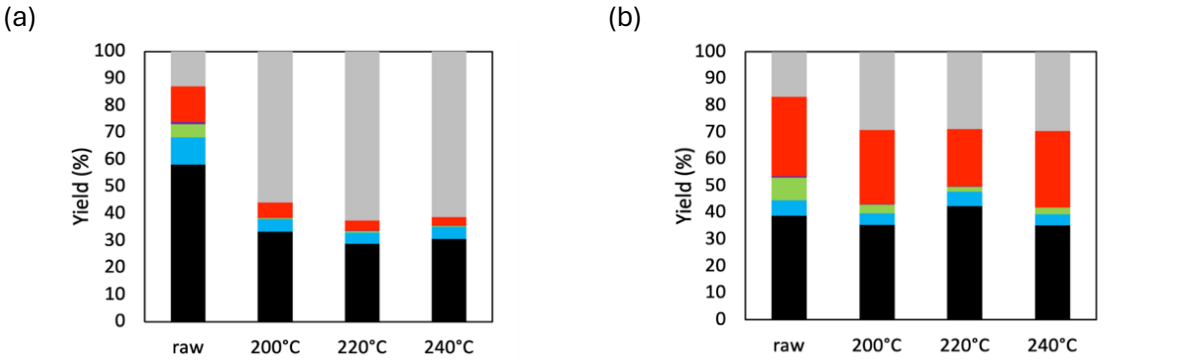

Figure 23: Effect of HTC temperature on elemental composition of hydrochar: carbon (■), hydrogen (■), nitrogen (■), sulphur (■), oxygen (■) and ash (■). (a) chub mackerel, (b) whiteleg shrimp.

4.3.2.1. Higher Heating Value

The Higher Heating Value (HHV) is an important property which is used to evaluate the fuel quality. Dulong's formula is the most commonly used equation based on the ultimate analysis and is used to determine the HHV of anthracitic, semi-anthracitic and bituminous coals, with only a 1.5% error compared to values obtained by using an oxygen-bomb calorimeter. And as the formula was approximated by using actual heating values of coal, it is only accurate in a narrow range around 30 kJ/g [250]. Thus, other estimation equations may give a more accurate result for HCs. The HHV values (Table B.4, Appendix B) range from 31.9 kJ/g (raw chub mackerel) to 4.7 kJ/g (Gazami crab-HC produced at 200°C). The average HHV of the HCs is 12.9 kJ/g, whereas the average HHV of the raw biomass is 22.1 kJ/g. As the HHV values of the HCs are much lower than typical solid fuels, they would not be optimal for fuel-related applications. The HHV values for the raw feedstocks from fish are much higher in comparison to crustaceans, this was to be expected, as fish contain a lot of fat and oil (triglycerides).

4.3.2.2. van Krevelen diagram

The elemental analysis of the biomass and HCs provides essential insights into the characterization of the feedstock and products as well as into the carbonization mechanism. As said in section 2.3.2.2, the reactions involved are primarily deoxygenation, dehydration, and decarboxylation, which overall decrease the amounts of H and O in the HC. Simultaneously, the carbon content of the HC increases due to condensation and aromatisation reactions [251]. The progression of these reactions can be visualised in the van Krevelen diagram, with the atomic H/C and O/C ratios on the y- and x-axis respectively. The polarity of the material is reflected by the O/C ratio, where a higher ratio indicates a greater presence of polar functional groups. Likewise, the aromaticity of the HC is assessed through the H/C ratio [252]. Consequently, the extent of key reactions - such as dehydration, decarboxylation, and demethylation - occurring during HTC is determined by the direction and length of the vector drawn from the raw material to the specific HC [253]. The van Krevelen diagram of the HCs from the marine biowaste is shown in Figure 24. Immediately, it is noticeable that the raw feedstock has a higher H/C ratio than the HCs, this indicates that dehydration and aromatization took place during HTC. The O/C ratio of the raw feedstock is higher than the fish-HCs (indicating decarboxylation took place), but lower than the

crustacean-HCs. This difference is possibly due to the high oxygen content in the crustacean-HCs due to the concentration of $CaCO_3$, which leads to a higher O/C ratio. The O/C ratios of the crustacean-HCs also show a broader range than for the fish-HC, with Gazami crab having the highest O/C ratio. This further proves that concentration of $CaCO_3$ and chitin in the HC took place, as crab waste contains a much higher amount of crude fibre (mostly chitin) and ash (mostly $CaCO_3$) than the shrimp and fish waste as mentioned in section 2.1.2, and thus has the highest O/C ratio. The change in O/C ratio also does not follow the same path for the different species with increasing temperature. This may indicate that the HC already obtained a relatively stable composition after 200°C, not leading to further changes at higher temperatures. The slight differences in O/C ratios could therefore be attributed to the heterogeneous nature of the feedstock. This is also noticeable in the H/C ratio, which is relatively stable for the HC of each species, independent of the reaction temperature. In comparison to Figure 11 in the literature review, where different HCs (T = 200-250°C, w/b = 10, t = 1h) from various feedstocks were plotted, the HCs produced in this thesis achieve very comparable O/C and H/C ratios.

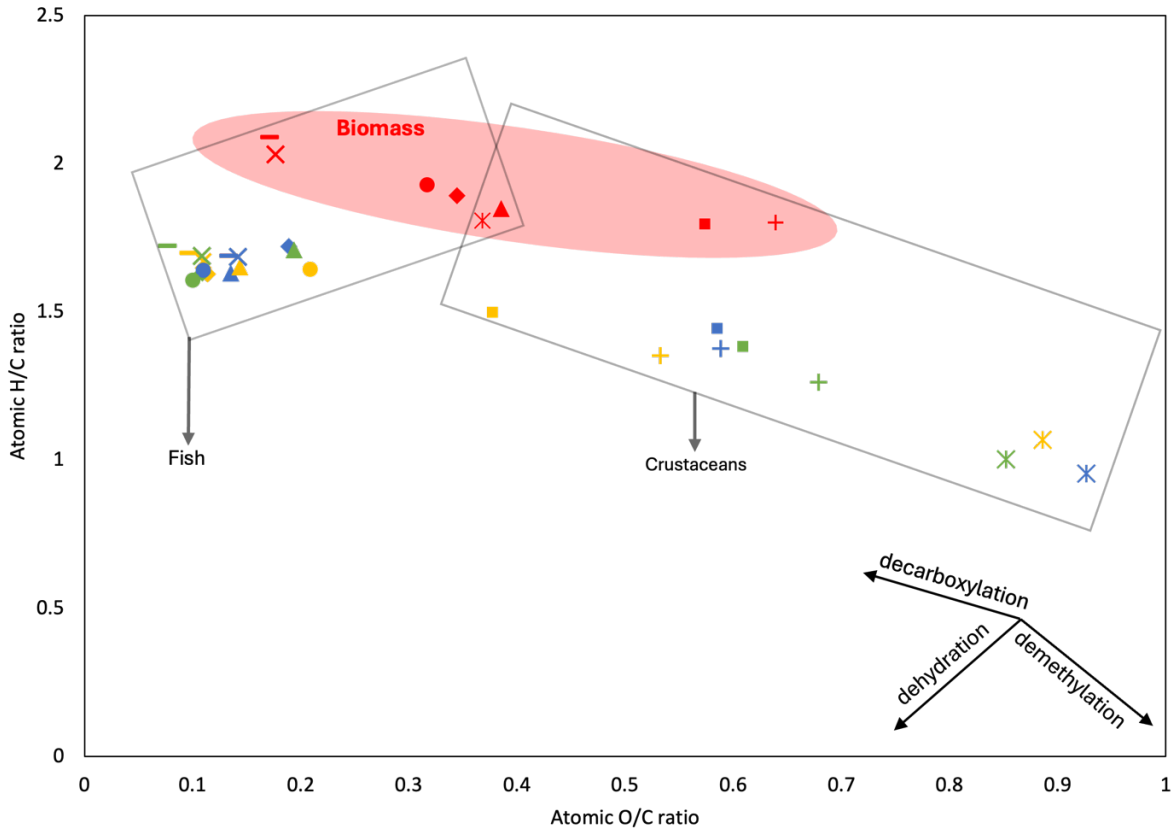

Figure 24: van Krevelen diagram with the raw feedstock and all the hydrochars. Each colour corresponds to an HTC temperature (raw, 200°C, 220°C, 240°C). Chub mackerel (▬), hairtail (◆), yellow corvina (▲), horse mackerel (✕), olive flounder (●), whiteleg shrimp (■), tiger prawn (✚) and Gazami crab (✱).

4.3.2.3. Proximate analysis

In addition to the ultimate analysis, the proximate analysis was also carried out and is visualised in Figure 25 (exact values in Table B.5). The ash content shows a big increase after HTC for all HCs, as expected and explained previously. Additionally, the VM decreased after HTC, but the FC did not increase with a decrease in VM. This may indicate that VM was also converted to other

products such as CO_2 or aqueous phase products [136], [254]. The decrease in FC is not what is expected from carbonization but was explained by the decarboxylation of the oil/grease. For the crustacean-HCs, the FC stays relatively stable expect for Gazami crab. For the Gazami crab-HC, the values were made 0 due to the calculated FC content being negative, which may indicate wrong data or the chitin registering as VM even though it does not degrade. Furthermore, as the feedstock is heterogeneous, the fluctuations could also be due to the nature of the feedstock.

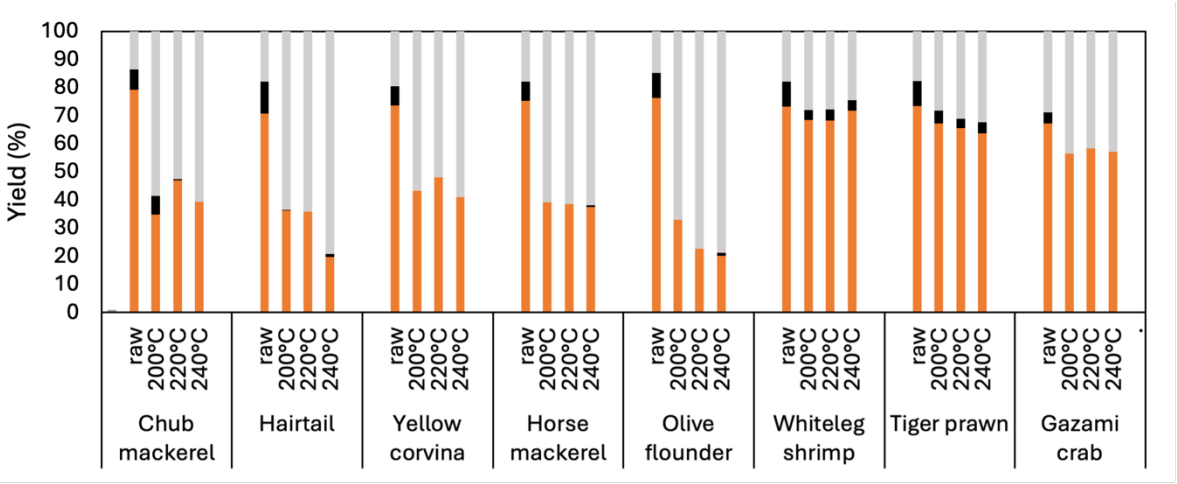

Figure 25: Effect of HTC temperature on the proximate analysis of HC: VM (dry basis) (■), FC (dry basis) (■), ash (■).

4.3.3. FTIR

FTIR spectral analysis was conducted to study the functional groups of the HCs and elucidate the difference with the raw feedstock. Table 6 summarizes the characteristic functional groups related to the spectral bands found in the hydrochars and raw feedstock.

Table 6: Characteristic functional groups of the FTIR spectra of hydrochar, based on [255].

	Range (cm^{-1})	Characteristic functional group	Ref.
1	820 - 940	O-H bending bands from clay minerals associated with hydrochar	[256]
2	960 - 970	Alkene trans-C-H out-of-plane bend	[257]
3	1020 - 1030	OH representative of oxygenated functional groups of polysaccharides	[258]
4	1020 - 1160	C-O from polysaccharide, carbohydrate region	[259], [260], [261]
5	1200 - 1280	Carboxylic acid C-OH stretch, O-H deformation	[260], [262]
6	1310 - 1390	Phenolic O-H bend, -C(CH_3) C-H deformation	[263]
7	1400 - 1450	Carbonate (v3; asymmetric stretch)	[256]
8	1440 - 1480	CH_2 deformation (scissor vibration)	[263]
9	1520 - 1590	COO- carboxylate anions	[264], [265]
10	1650 - 1740	C=O from carboxylic acids, esters, and ketones	[263]
11	2840 - 2870	Symmetric aliphatic CH from terminal CH_3 groups	[263], [266], [267]
12	2920 - 2950	Asymmetric aliphatic CH from terminal CH_2 groups	[263]
13	3200 - 3600	OH from sorbed water and hydrogen-bonded hydrochar O-H groups	[258]

In Table B.6 and Table B.7 in Appendix B, the different HCs and raw feedstocks are evaluated on the presence of these bands. In Figure A.4 in Appendix A, the FTIR spectra of the raw feedstocks and HCs of the different species can be found. In Figure 26, the FTIR spectrum of chub mackerel-HC and raw feedstock is shown, with a zoom on the absorbance between 0 and 0.04. The two peaks at 2840-2870 and 2920-2950 cm^{-1} (number 11 and 12 on Figure 26) indicate asymmetric and symmetric aliphatic v(CH) from terminal -CH_3 groups respectively. It is interesting to note that these peaks increase with temperature from 200°C to 220°C and then decrease with a further increase to 240°C. This decrease could be attributed to the dehydration and demethylation which occurs at higher temperatures. The peak at 1650-1740 cm^{-1} (number 10) corresponds to C=O in carboxylic acid. Additionally, the peak at 1520-1590 cm^{-1} (number 9) indicates the presence of carboxylate anions, which are the conjugate base of the carboxylic acid. These peaks are a lot more pronounced for the raw feedstock. This could indicate that decarboxylation took place, to produce CO_2, as mentioned in section 2.2.2.2.2. The absorbance band between 3200 and 3600 cm^{-1} (number 13) indicates the presence of v(OH) of sorbed water and hydrogen bonded O-H groups. These are usually related to the presence of O-H groups in carboxylic acid, proteins or polysaccharides. Again, this peak is only present for the raw feedstock, indicating dehydration took place. The peak at 960-970 cm^{-1} (number 2) indicates the presence of alkenes in trans-C-H out-of-plane bend configuration. This may originate from the oils present in the HC which increased with increasing reaction temperature. When looking at Table B.7 in Appendix B it can be observed that this band was absent in all crustaceans, which further validates the assumption. The band at 1020-1030 cm^{-1} (number 3), which is present for all HCs and absent for the raw feedstock, shows the highest intensity, almost 10 times bigger than the next peak. It is indicative of -OH groups of oxygenated functional groups of polysaccharides. The peak at number 4 is also typically observed for polysaccharides. These two peaks are most prominent for HC produced at 240°C. In section 2.2.2.2.1, it was mentioned that the shift from hydrolysis toward condensation and polymerization reactions only occurs from 240°C, with higher temperatures yielding more polyaromatic structures. This could explain the highest peak at 240°C.

Figure 27 shows the FTIR spectra of whiteleg shrimp-HC and raw feedstock. All peaks present in chub mackerel-HC can also be found in the HC from whiteleg shrimp. Additionally, a new peak at 820-940 cm^{-1} can be observed. This represents -OH bending bands from clay minerals associated with hydrochar. This peak is only found in the HCs from crustaceans. The peak at around 1424 cm^{-1} (number 7, Figure 27) corresponds to asymmetric stretchings of carbonate groups. This could indicate the presence of $CaCO_3$ in the samples. This chemical compound thermally degrades from 750°C upwards, thus the HTC temperatures are assumed to have limited influence on calcite. The differences in peak height could be attributed to the heterogeneous nature of the feedstock or to the release of more calcite.

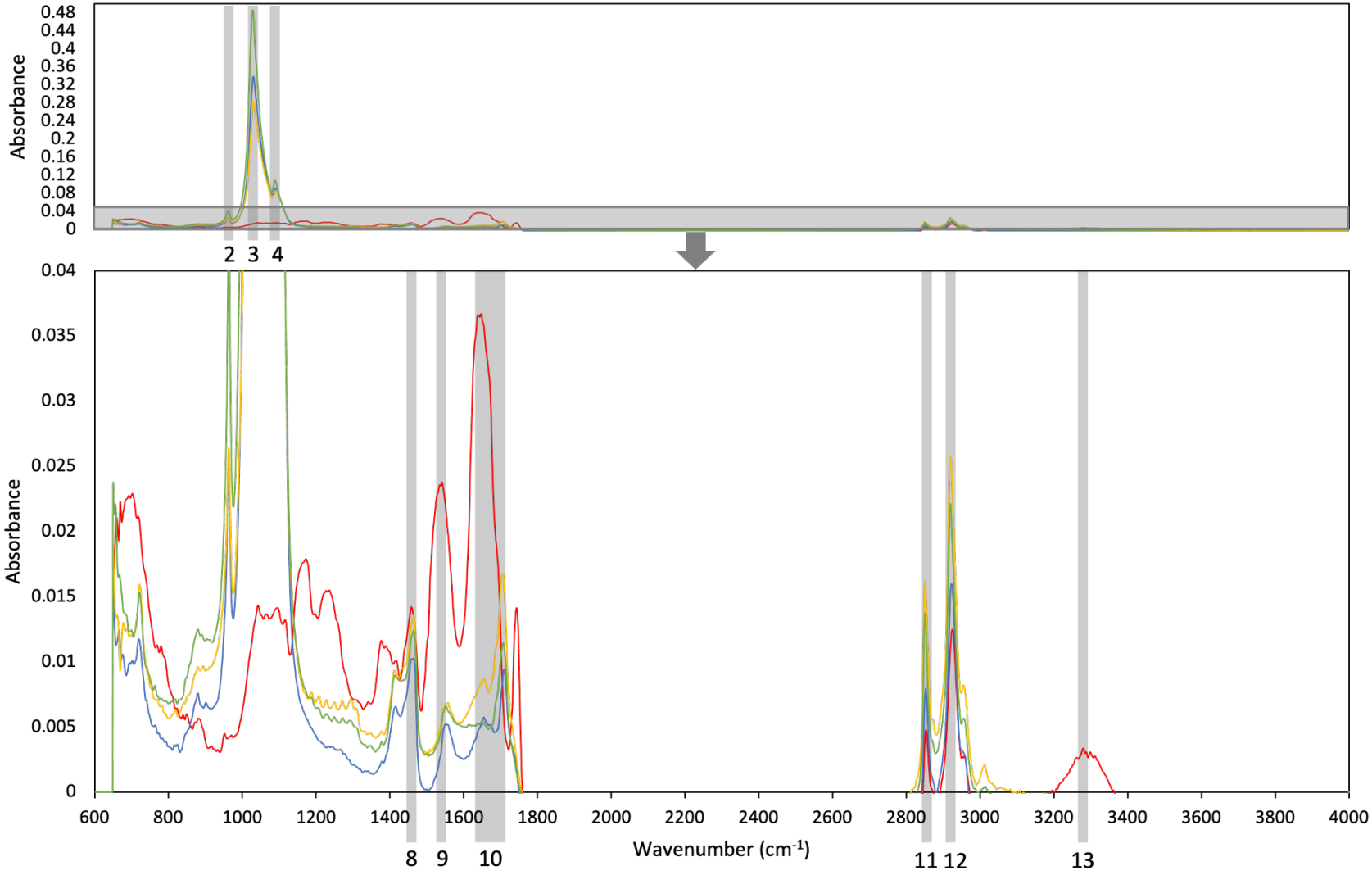

Figure 26: FTIR spectrum of chub mackerel raw feedstock and hydrochar produced at 200°C, 220°C, 240°C.

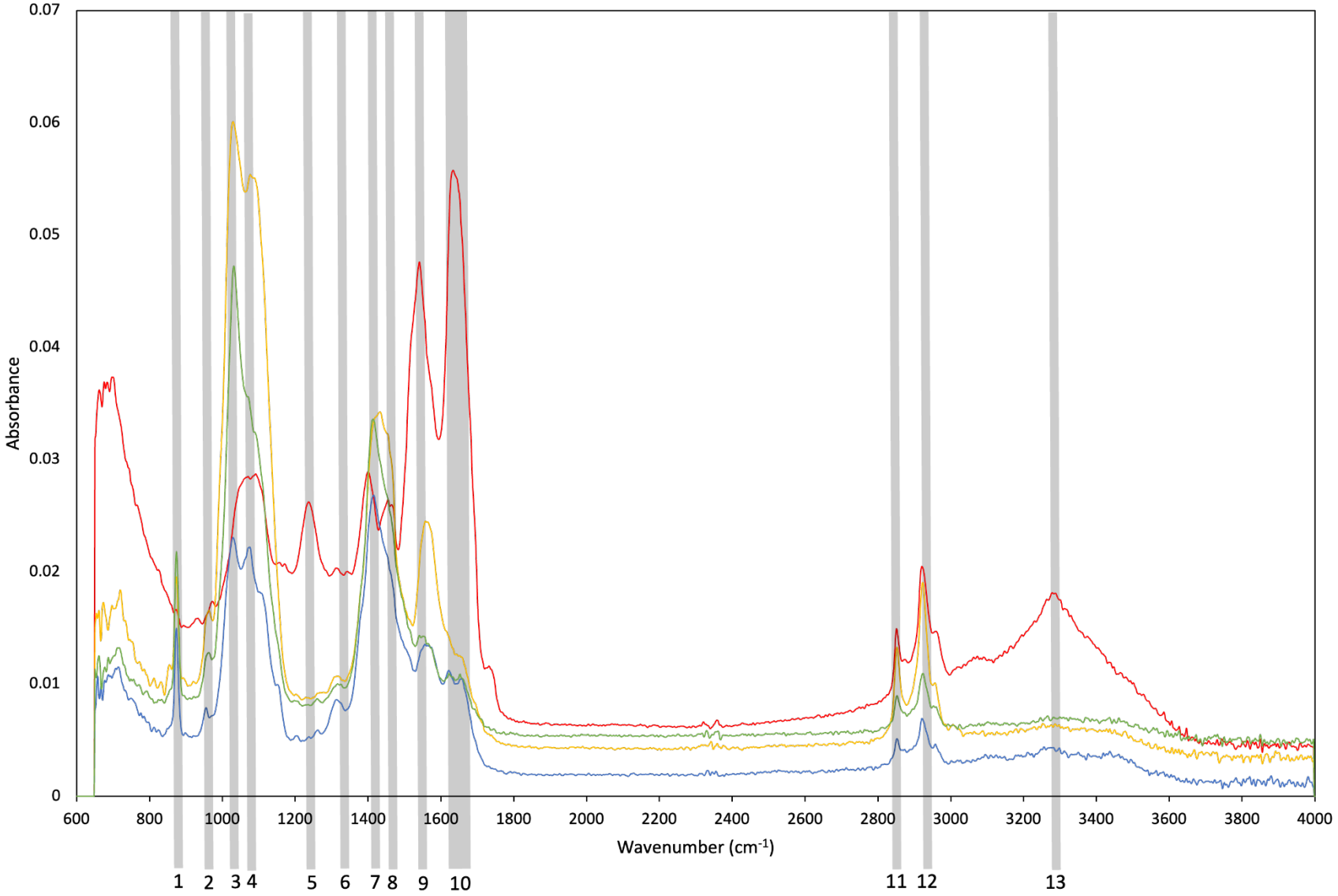

Figure 27: FTIR spectrum of whiteleg shrimp raw feedstock and hydrochar produced at 200°C, 220°C, 240°C.

4.4. Adsorption

4.4.1. Adsorption kinetics

As mentioned in section 2.3.2.3, fitting kinetic models to experimental data allows to estimate the rate of adsorption and can help identify the controlling sorption mechanisms. PFOM assumes that the adsorption processes are mainly controlled by physisorption and diffusion; the PSOM assumes that the adsorption processes are controlled by chemisorption, mainly including the electronic sharing or exchange processes between adsorbate and adsorbent [175], [176], [177]. Elovich model assumes that the activation energy increases with adsorption time and that the surface of the adsorbent is heterogeneous [240].

Figure 28(a-c) show the PFOM, PSOM and Elovich model fitted to experimental data of MB (C_0 = 50 mg/L) adsorbed by whiteleg shrimp-HC (220°C). Table 7 summarises the obtained model parameters as well as statistical parameters. The highest R^2 and lowest SSE were observed for the Elovich model, indicating the better fit. The adsorption of MB on the whiteleg shrimp-HC was thus best described by the Elovich model, which indicates the HC has a heterogeneous surface and that the activation energy increases with adsorption time.

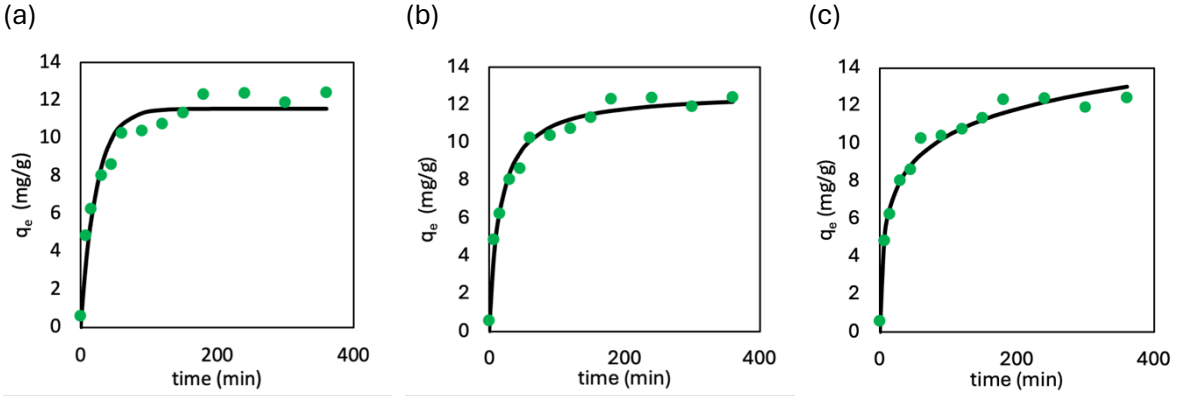

Figure 28: (a) PFOM, (b) PSOM, (c) Elovich adsorption kinetics modelled on experimental data of MB (C_0 = 50 mg/L) adsorption by whiteleg shrimp hydrochar (220°C).

Table 7: Adsorption pseudo-first-order model (PFOM) and pseudo-second-order model (PSOM) kinetics parameters for MB (C_0 = 50 mg/L) adsorbed onto whiteleg shrimp hydrochar (HTC temperature of 220°C).

Adsorption kinetics – Whiteleg shrimp				
PFOM	**$q_{m,1}$ [mg/g]**	**K_1 [1/min]**	**R^2 [-]**	**SSE [-]**
	11.56 ± 0.028	$(4.33 \pm 0.55)\cdot10^{-2}$	0.93	9.80
PSOM	**$q_{m,2}$ [mg/g]**	**K_2 [mg/(g·min)]**	**R^2 [-]**	**SSE [-]**
	12.68 ± 0.29	$(5.06 \pm 0.71)\cdot10^{-3}$	0.98	3.12
Elovich	**α [mg/(g·h)]**	**β [g/mg]**	**R^2 [-]**	**SSE [-]**
	3.61 ± 1.07	0.50 ± 0.040	0.98	2.79

4.4.2. Removal efficiency

Figure 29 represents the removal efficiency (η) of MB in function of the initial MB concentration at pH 4, 7 and 9 for whiteleg shrimp (a) and yellow corvina (b) hydrochar. For whiteleg shrimp-HC, the removal efficiency drops with increasing initial MB concentration. This may be due to the saturation of adsorption sites on the surface. For yellow corvina-HC, an overall decrease in MB concentration is observed with increasing C_0, except at pH 9. At pH 9, an initial increase in removal efficiency is observed whereafter it stabilizes from C_0 = 100 mg/L on. Despite the overall declining η at pH 4 and 7, HC from yellow corvina shows a fluctuating removal efficiency at these pH values. These increases could be explained by the high driving force for mass transfer at higher initial dye concentrations [236], [268].

Despite the differences in η in function of C_0 between both HCs, the effect of pH is the same for both. With increasing pH, an increase in removal efficiency is achieved. The pH influences the degree of ionization of methylene blue, or any adsorptive molecule, as well as the surface properties of the adsorbent [269]. This can be linked to the pH_{pzc}, where adsorption of a cationic dye is favoured when pH > pH_{pzc}, in other words when the surface becomes negatively charged. As mentioned in section 4.3.1, the pH_{pzc} of whiteleg shrimp-HC and yellow corvina-HC is 6.95 and 6.35, respectively. Thus, at pH 4 both HC surfaces can be assumed positively charged, and at pH 7 and 9 negatively charged. MB has a pK_a of 8.33 and thus at a pH below 8.33, MB is positively charged and negatively charged at a pH above 8.33. Thus, at pH 4, there is a repulsion between MB and the hydrochar, at pH 7 there is attraction. At pH 9, MB is slightly negatively charged, but as the adsorption capacity increases, we can assume that the attraction between the more negatively charged HC (due to the increasing pH) and the remaining positively charged MB molecules outweigh the slight change in ionization of MB. This explains the increasing removal efficiency of MB with increasing pH.

It should be noted that the removal efficiencies are rather low, never achieving adsorption capacities higher than 90% except at pH of 9. Thus, the hydrochars as such don't have a large enough surface area and the needed functional groups for good adsorption of MB. The adsorption could be enhanced in the future by activating the HC chemically or physically, as explained in section 2.3.3.1.

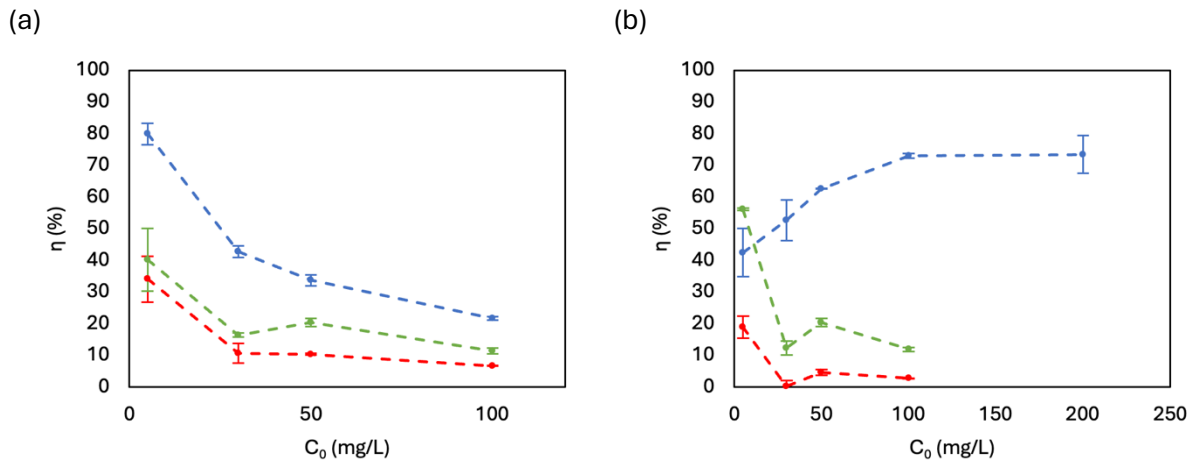

Figure 29: Removal efficiency in function of initial MB concentration for pH 4, 7 and 9 on hydrochar (T = 220°C) from (a) whiteleg shrimp and (b) yellow corvina. Dashed lines were added to guide the eye.

4.4.3. Isotherms

The Langmuir and Freundlich isotherms were used to describe the adsorption mechanisms of MB molecules by the HC. Figure 30 shows the isotherms plotted to the experimental data and Table 8 summarizes the parameters. As mentioned in section 3.4.3, the Langmuir adsorption isotherm assumes that adsorption takes place at a fixed number of homogeneous sites within the HC and is mainly used for reversible monolayer adsorption whereas the Freundlich adsorption isotherm considers a heterogeneous adsorption surface that has unequal available sites with different adsorption energies [235], [236]. It can be seen that for whiteleg shrimp-HC, the Freundlich isotherm has a better fit as the R^2_{Adj} is higher than for the Langmuir isotherm and the NRSME and NSD are smaller. This indicates that there is a heterogeneous adsorption surface. Like with the removal efficiencies, it can be seen that an increasing adsorption capacity is reached with increasing pH, this is in accordance with the charge of the MB molecule and the dyes, like explained above. For yellow corvina-HCs, the isotherms don't fit the experimental data. Visually, the isotherms don't have the expected curvature and the calculated statistics show very low R^2_{Adj}. For pH 9 of the yellow corvina-HC, the Langmuir isotherm shows a higher R^2_{Adj} but an unrealistic q_{max}, therefore we can conclude the isotherms are not a good match. An inflection point is noticeable, this gives an indication that adsorption with lateral interactions might occur, thus two additional models were implemented.

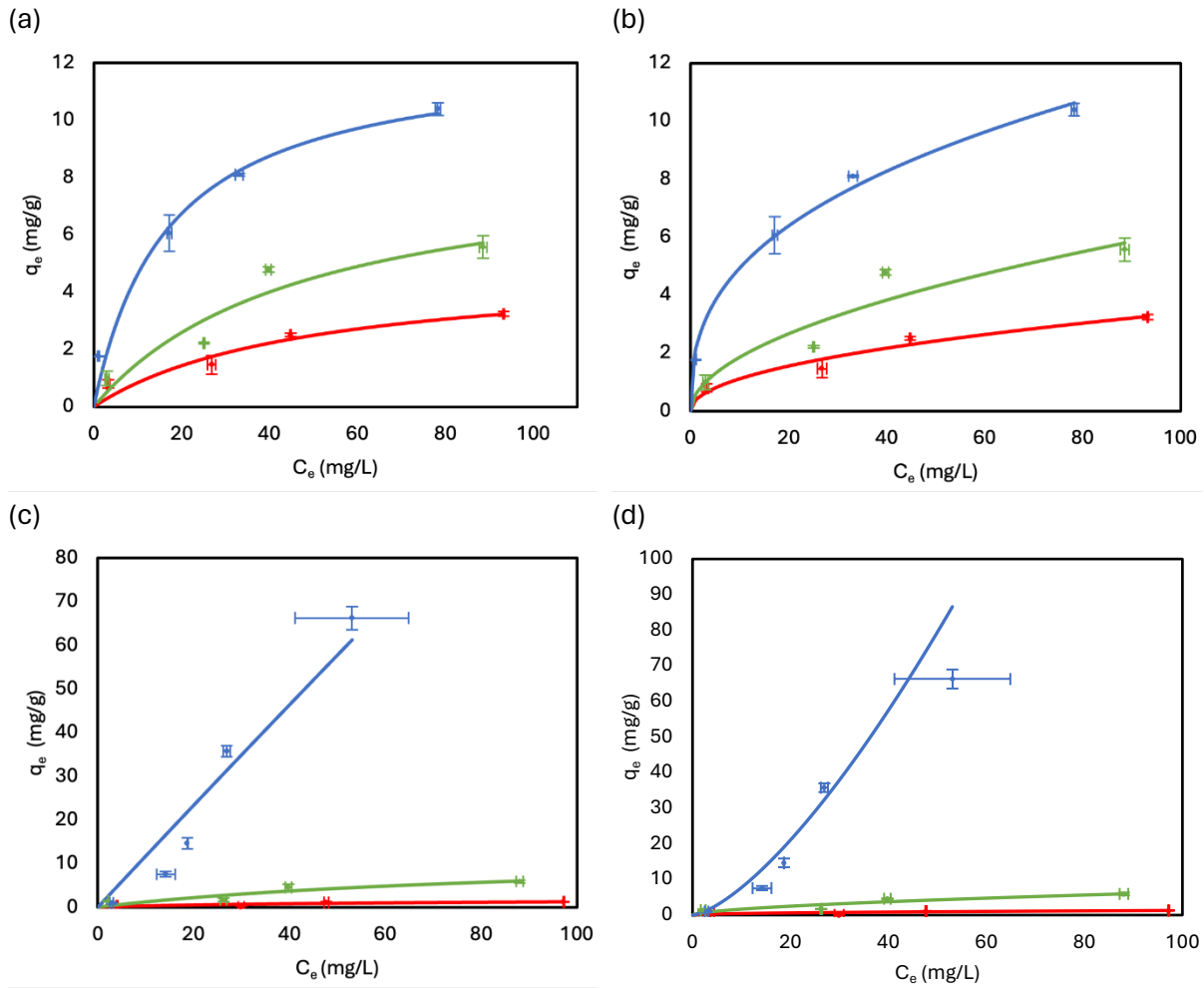

Figure 30: Langmuir and Freundlich adsorption isotherms for hydrochar produced at 220°C, with pH of 4 (——), 7 (——), 9 (——): (a) Langmuir and (b) Freundlich isotherms for whiteleg shrimp, (c) Langmuir and (d) Freundlich isotherms for yellow corvina.

Table 8: Adsorption isotherm parameters for MB adsorption onto hydrochar from whiteleg shrimp (220°C) and yellow corvina (220°C) at different pH strengths.

species	Whiteleg shrimp-HC			Yellow corvina-HC		
pH [-]	4	7	9	4	7	9
q_e [mg/g]	3.24 ± 0.08	5.57 ± 0.39	10.39 ± 0.22	1.29 ± 0.04	5.95 ± 0.35	69.09 ± 0.15
Langmuir						
q_m [mg/g]	4.93 ± 0.30	8.83 ± 0.77	12.44 ± 0.44	2.12 ± 0.12	12.50 ± 1.36	3355.3 ± 399.68
K_L [L/mg]	0.02 ± 0.02	0.02 ± 0.02	0.06 ± 0.03	0.02 ± 0.03	$0.01 \pm 4.87 \cdot 10^{-3}$	$(3.51 \pm 0.14) \cdot 10^{-4}$
R^2_{Adj} [-]	0.838	0.833	0.946	0.469	0.684	0.854
NRSME [-]	0.916	0.780	0.762	5.285	2.283	19.222
NSD [-]	21.03	11.85	22.92	28.62	32.16	62.17
Freundlich						
n [-]	2.07 ± 0.11	1.91 ± 0.26	2.68 ± 0.22	2.12 ± 0.12	1.70 ± 0.30	0.69 ± 1.09
K_F [$mg^{1-1/n}L^{1/n}/g$]	0.36 ± 0.31	0.56 ± 0.41	2.09 ± 0.19	0.15 ± 0.82	0.43 ± 0.49	0.28 ± 0.52
R^2_{Adj} [-]	0.901	0.824	0.979	0.557	0.714	-0.28
NRSME [-]	0.316	0.468	0.090	5.364	1.857	4.506
NSD [-]	1.27	11.92	9.61	10.17	20.11	0.28

As mentioned above, two additional models were implemented that include adsorption with lateral interactions. Figure 31 shows both models implemented on the adsorption experiment done on yellow corvina-HC at pH 9. Visually, it is clear these fit better than Langmuir or Freundlich and this is also reflected in the statistics (Table 9), with an R^2_{Adj} of 0.918 for the HDB model, this showed the best fit. Additionally, the W (FFG) and K_2 (HDB) parameters are negative, indicating that the interaction between the adsorbate molecules was repulsive [239]. It should also be noted that the difference between the Langmuir and Freundlich isotherms for the HC of the fish versus the shrimp is quite striking. Further experiments could try to elucidate the reason. A possible hypothesis could be that the oil at pH 9, underwent a chemical transformation (e.g., emulsification) which led to a change in the MB or HC properties, leading to enhanced adsorption or to clogging of the filter, leading to skewed results.

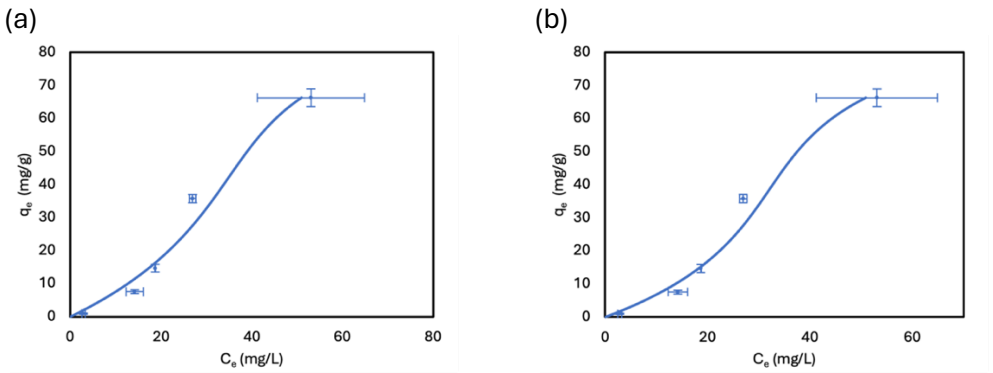

Figure 31: Frumkin-Fowler-Guggenheim (a) and Hill-de Boer (b) isotherms for yellow corvina-HC produced at 200°C, adsorption at pH 9.

Table 9: Adsorption isotherm (FFG and HDB) parameters for MB adsorption onto whiteleg shrimp hydrochar (220°C) at pH 9.

Yellow corvina-HC – pH 9			
Frumkin-Fowler-Guggenheim		**Hill-de Boer**	
q_{max} [mg/g]	95.84 ± 36.50	q_{max} [mg/g]	128.42 ± 36.20
k_{FG} [g/(mg·h)]	$(6.97 \pm 1.84) \cdot 10^{-3}$	K_1	$(4.54 \pm 1.10) \cdot 10^{-3}$
W [kJ/mol]	$-3.25 \cdot 10^{3} \pm 8.97 \cdot 10^{-1}$	K_2	$-1.23 \cdot 10^{4} \pm 1.23$
R^2_{Adj} [-]	0.914	R^2_{Adj} [-]	0.918
NRSME [-]	7.29	NRSME [-]	5.75
NSD [-]	33.16	NSD [-]	25.47

4.4.4. One-point adsorption

It is clear from the one-point adsorption graph (looking only at the values without added salt) on Figure 32 that the three crustacean-HCs (whiteleg shrimp, tiger prawn and Gazami crab) show a higher adsorption for MO. When looking at section 4.3.1., their pH_{PZC} is higher than 7 (except for whiteleg shrimp-HC which has a pH_{PZC} close to 7), therefore at the pH 7 of the dye-solution, the HC is positively charged, thus adsorbing the anionic MO better. The fish-HCs each show less difference between adsorption of MO or MB. As their PZCs are closer to pH 7, MO and MB compete for adsorption, thus showing a less clear preference for either dye. The independent two-sample t-test showed no significance difference in the adsorption capacity with or without added salt. Thus, we can conclude that the ionic strength does not have a significant impact on the adsorption dynamics.

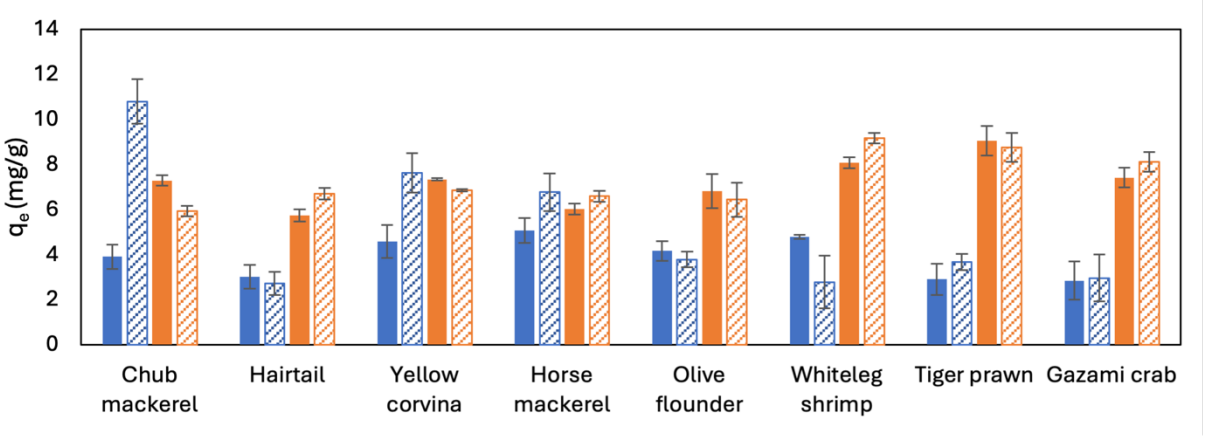

Figure 32: One-point adsorptions of MB and MO (C_0 = 50 mg/L) with and without addition of salt at pH 7, for each type of hydrochar, produced at 220°C. MB adsorption with (■) and without (▨) addition of salt. MO adsorption with (■) and without (▨) addition of salt.

At pH levels below 7, the surface of the HC underwent protonation by H^+, therefore strengthening the electrostatic attraction between HC and MO (anionic). This led to an increase in the adsorption capacity of HC for MO. Conversely, at pH levels above 7, OH^- competed with MO for adsorption, resulting in a decrease of the adsorption capacity for MO. The impact of pH on the removal of MB (cationic) followed an opposite trend, as can be observed on Figure 33.

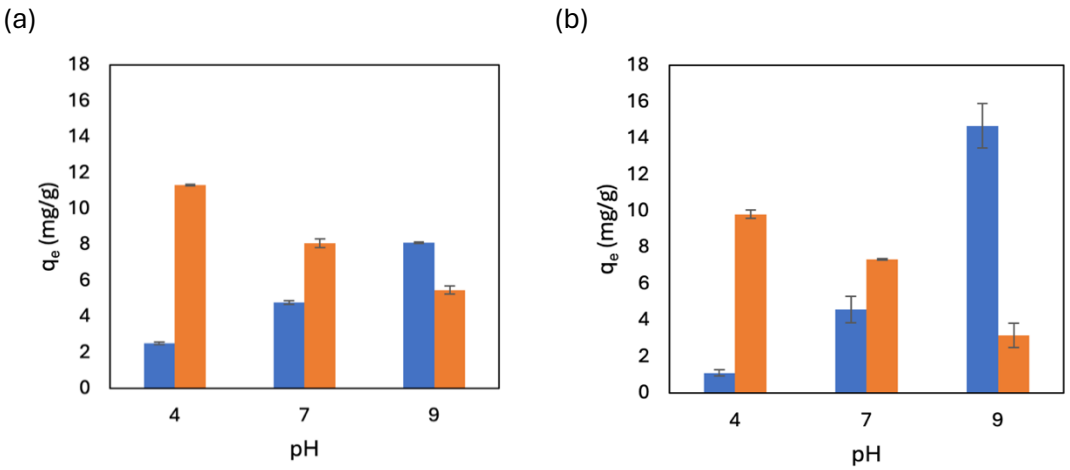

Figure 33: One-point adsorptions of MB (■) and MO (■) with varying pH for whiteleg shrimp (a) and yellow corvina (b).

5. CONCLUSION

In this thesis, the aim was to assess the valorisation potential of marine biowaste into hydrochar and fill the knowledge gaps concerning the hydrothermal conversion of non-lignocellulosic biomass such as fish and crustaceans. The investigation consisted of quantifying the potential biomass stream, producing, and characterising hydrochar and evaluating its potential for adsorption applications.

The waste from eight fish and crustacean species (*Scomber japonicus*, *Trichiurus lepturus*, *Larimichthys polyactis*, *Trachurus japonicus*, *Paralichthys olivaceus*, *Litopenaeus vannamei*, *Penaeus monodon* and *Portunus trituberculatus*) from South Korea were quantified to generate 130 kton of waste annually. With the obtained hydrochar yields, this could generate 30.5 kton of hydrochar annually. From the literature review, it was made clear that the responsible management of marine biowaste is essential to avoid environmental and socioeconomic losses. Before being able to use marine biowaste, a change in legislation will have to occur in South Korea. Marine biowaste is currently regarded as waste and should be disposed of accordingly, however categorizing it as a "by-product" could open doors to valorisation in useful products.

Hydrothermal conversion (HTC) is a possible valorisation pathway for marine biowaste. The literature review showed that HTC holds some advantages in comparison to pyrolysis, mainly being able to use wet feedstock and having lower energy costs due to milder temperatures. Hydrochar (HC) was produced at three different temperatures (between 200-240°C), constant residence time (t = 5h) and constant water-to-biomass ratio (w/b = 7). The optimal reaction temperature with regards to maximal yield was different for fish (220°C) versus crustacean (200°C) species. Additionally, crustacean-HCs showed a much higher yield (37-69%) than fish-HCs (15-22%), which was attributed to the inherent composition of both subphyla. During the production of HC, it was observed that the fish-HC also yielded a substantial amount of oil (17.8-29.8% on a wet feedstock basis). This product could be a precursor for other applications (i.e. liquid fuels).

The produced hydrochars were then characterized through their point of zero charge (PZC), their ultimate and proximate analysis and FTIR. The PZC ranged from 6.14-8.76, with the crustacean-HCs showing higher PZC values (average 7.93) in comparison to fish-HCs (average of 6.48). This difference was attributed to the accumulation of inorganics in the hydrochars of crustaceans, and was further proven by the rising PZC values with rising temperatures. With rising temperatures, the HC yields decreased, and the ash content increased, resulting in an accumulation of inorganics. The ultimate analysis showed a remarkable decrease in carbon content, for fish-HC which was argued to be mostly due to the decarboxylation of oil/grease (and subsequent separation from the solid/hydrochar phase) and for crustaceans this was argued to be mostly due to accumulation of inorganics. This was concluded to be a typical characteristic of hydrochar from non-lignocellulosic biomass. The FTIR analysis supported the conclusions made, with adsorption bands for alkenes showing only in the fish-HCs and being an indication of oils. For the crustacean-HCs, an adsorption band for $CaCO_3$ was found, which was absent in fish-HCs.

Lastly, the potential of the produced hydrochar as a low-cost adsorbent was assessed. The kinetics of the whiteleg shrimp-HC was best described by the Elovich model, indicating adsorption on a heterogeneous surface and increasing activation energy with adsorption time. As for the isotherms, the whiteleg shrimp-HC showed the best fit by the Freundlich isotherm, indicating a heterogeneous adsorption surface with unequal available sites and different adsorption energies. Yellow corvina-HC showed indications of adsorption with lateral interaction. Two additional models were implemented and showed a better fit to the data. Lastly, one-point adsorption experiments were done and the effect of ionic strength on the adsorption capacity was assessed. The adsorption capacity of the HCs (MB: 2.7-10.8 mg/g and MO: 5.9-9.2 mg/g with C_0 = 50 mg/L) showed a higher adsorption of MO for the crustaceans. This difference could be explained using PZC results. Differences in ionic strength was concluded not to yield significant differences in adsorption capacity. In conclusion, the adsorption experiments elucidated the adsorption mechanisms associated with hydrochars made from fish and crustacean waste and that the adsorption capacity is rather low, almost never achieving removal efficiencies above 50%, except at low initial dye concentration (5 mg MB/L) at pH 9.

Thus, considering all the results from the experiments, using the HC as such as a low-cost adsorbent, does not seem the most viable option. In the next section, recommendations are made for future research, to further elucidate the potential of HC from fish and crustacean waste.

Overall, this thesis demonstrated: that marine biowaste can be utilised as feedstock for HTC, what the inherent characteristics of the produced HCs were, how it acts as an adsorbent of cationic and anionic dyes and that future research is needed for the determination of a possible application.

6. RECOMMENDATIONS

Some recommendations can be made for future research involving hydrochar production from fish and crustacean waste. While doing HTC, the wet feedstock was used to produce the hydrochar. However, the impact of the naturally occurring water versus the added deionized water is unclear, further research could try to assess the impact of using wet feedstock versus added water. In relation to this, the feedstock storage should be optimized and unified. In this thesis, the feedstock was gathered from a fish market and transported in a cool box, after which it was blended, and stored in a freezer at -10°C. Every time HTC was carried out, the frozen slurry was thawed at room temperature and the remaining slurry was frozen again. However, it was noticed that this subsequent thawing and freezing led to a change in moisture content of the wet slurry. Thus, in the future, freezing the feedstock in smaller portions to avoid multiple thawing and freezing cycles is recommended.

After HTC, only the solid product was analysed. In the future, the liquid and gas phases could also be analysed for future possible applications. Of particular interest is the obtained oil after HTC of the fish species. A significant amount of oil was obtained but no analysis of its characteristics was done. This oil could be a starting point for new experiments and possible applications.

While doing the adsorption experiments, the impact of ionic strength on adsorption capacity was tested. It was concluded that the ionic strength did not yield a significantly different adsorption capacity. However, this was only tested with a buffer capacity of 20 mM. Doing new experiments with bigger buffer capacities or/and bigger ionic strengths, might yield different results.

Another important factor to note is that the adsorption experiments were carried out using Hyundai Micro Nylon Syringe filters with a pore size of 0.2 µm. It was tested if MB and MO were able to go through without leaving residues, and therefore this filter was chosen. However, the impact of the hydrochar on this filter is not clear. Especially, with the HC from yellow corvina, it is possible that the oil clogged the pores of the filter, leading to skewed results. Therefore, pre-filtering may alleviate this problem or give an indication of whether the clogging of pores occurs.

Further experiments are also needed to determine the best application for the produced hydrochar. For using the hydrochar as a low-cost adsorbent, physical or chemical activation is recommended to increase its surface area, however, this will increase its price. Using the HC as a catalyst support or as a part of supercapacitors will also necessitate activation. For the application of the HC for soil amendment, the first step would be to determine its phytotoxicity. As the hydrochar has a low C-content, it is not optimal for carbon sequestration.

7. BIBLIOGRAPHY

[1] FAO, "The State of World Fisheries and Aquaculture 2022," *The State of World Fisheries and Aquaculture 2022*, Jun. 2022, doi: 10.4060/CC0461EN.

[2] T. Maschmeyer, R. Luque, and M. Selva, "Upgrading of marine (fish and crustaceans) biowaste for high added-value molecules and bio(nano)-materials," *Chem Soc Rev*, vol. 49, no. 13, pp. 4527–4563, Jul. 2020, doi: 10.1039/C9CS00653B.

[3] FAO, *Global food losses and food waste - Extent, causes and prevention*. Rome, 2011.

[4] "FAOSTAT." Accessed: Sep. 27, 2023. [Online]. Available: https://www.fao.org/faostat/en/#data/FBS

[5] FAO, "Country profile-Democratic People's Republic of Korea," Rome, 2011. Accessed: Oct. 11, 2023. [Online]. Available: www.fao.org/

[6] D.-Y. Kim and J.-S. Lee, "Directions for Eco-friendly Utilization and Industrialization of Fishery By-products," *Journal of Fisheries and Marine Sciences Education*, vol. 27, no. 2, pp. 566–575, Apr. 2015, doi: 10.13000/jfmse.2015.27.2.566.

[7] N. van Buren, M. Demmers, R. van der Heijden, and F. Witlox, "Towards a Circular Economy: The Role of Dutch Logistics Industries and Governments," *Sustainability 2016, Vol. 8, Page 647*, vol. 8, no. 7, p. 647, Jul. 2016, doi: 10.3390/SU8070647.

[8] A. A. Khan, W. de Jong, P. J. Jansens, and H. Spliethoff, "Biomass combustion in fluidized bed boilers: Potential problems and remedies," *Fuel Processing Technology*, vol. 90, no. 1, pp. 21–50, Jan. 2009, doi: 10.1016/J.FUPROC.2008.07.012.

[9] H. S. Kambo and A. Dutta, "A comparative review of biochar and hydrochar in terms of production, physico-chemical properties and applications," *Renewable and Sustainable Energy Reviews*, vol. 45, pp. 359–378, May 2015, doi: 10.1016/J.RSER.2015.01.050.

[10] M. Cavali *et al.*, "A review on hydrothermal carbonization of potential biomass wastes, characterization and environmental applications of hydrochar, and biorefinery perspectives of the process," 2022, doi: 10.1016/j.scitotenv.2022.159627.

[11] D. C. Li and H. Jiang, "The thermochemical conversion of non-lignocellulosic biomass to form biochar: A review on characterizations and mechanism elucidation," *Bioresour Technol*, vol. 246, pp. 57–68, Dec. 2017, doi: 10.1016/J.BIORTECH.2017.07.029.

[12] W. J. Liu, H. Jiang, and H. Q. Yu, "Thermochemical conversion of lignin to functional materials: a review and future directions," *Green Chemistry*, vol. 17, no. 11, pp. 4888–4907, Jul. 2015, doi: 10.1039/c5gc01054c.

[13] W. J. Liu, W. W. Li, H. Jiang, and H. Q. Yu, "Fates of Chemical Elements in Biomass during Its Pyrolysis," *Chem Rev*, vol. 117, no. 9, pp. 6367–6398, May 2017, doi: 10.1021/ACS.CHEMREV.6B00647/ASSET/IMAGES/MEDIUM/CR-2016-00647Y_0021.GIF.

[14] W. J. Liu, H. Jiang, and H. Q. Yu, "Development of Biochar-Based Functional Materials: Toward a Sustainable Platform Carbon Material," *Chem Rev*, vol. 115, no. 22, pp. 12251–12285, Nov. 2015, doi: 10.1021/ACS.CHEMREV.5B00195/ASSET/ACS.CHEMREV.5B00195.FP.PNG_V03.

[15] T. T. Qian and H. Jiang, "Migration of phosphorus in sewage sludge during different thermal treatment processes," *ACS Sustain Chem Eng*, vol. 2, no. 6, pp. 1411–1419, Jun. 2014, doi: 10.1021/SC400476J/SUPPL_FILE/SC400476J_SI_001.PDF.

[16] W. Shi *et al.*, "Immobilization of heavy metals in sewage sludge by using subcritical water technology," *Bioresour Technol*, vol. 137, pp. 18–24, Jun. 2013, doi: 10.1016/J.BIORTECH.2013.03.106.
[17] K. Tian, W. J. Liu, T. T. Qian, H. Jiang, and H. Q. Yu, "Investigation on the evolution of N-containing organic compounds during pyrolysis of sewage sludge," *Environ Sci Technol*, vol. 48, no. 18, pp. 10888–10896, Sep. 2014, doi: 10.1021/ES5022137/SUPPL_FILE/ES5022137_SI_001.PDF.
[18] W. Shi, C. Liu, Y. Shu, C. Feng, Z. Lei, and Z. Zhang, "Synergistic effect of rice husk addition on hydrothermal treatment of sewage sludge: Fate and environmental risk of heavy metals," *Bioresour Technol*, vol. 149, pp. 496–502, Dec. 2013, doi: 10.1016/J.BIORTECH.2013.09.114.
[19] X. Wang, C. Li, B. Zhang, J. Lin, Q. Chi, and Y. Wang, "Migration and risk assessment of heavy metals in sewage sludge during hydrothermal treatment combined with pyrolysis," *Bioresour Technol*, vol. 221, pp. 560–567, Dec. 2016, doi: 10.1016/J.BIORTECH.2016.09.069.
[20] C. H. Wijaya, W. Wijaya, and B. M. Mehta, "General Properties of Major Food Components," *Handbook of Food Chemistry*, pp. 15–54, Jan. 2015, doi: 10.1007/978-3-642-36605-5_35/FIGURES/9.
[21] O. Fennema, *Food Chemistry*. Boca Raton: CRC Press, 1996.
[22] "Polysaccharide - Wikipedia." Accessed: Dec. 14, 2023. [Online]. Available: https://en.wikipedia.org/wiki/Polysaccharide
[23] "Fructose - Wikipedia." Accessed: Dec. 14, 2023. [Online]. Available: https://en.wikipedia.org/wiki/Fructose
[24] "Glucose - Wikipedia." Accessed: Dec. 14, 2023. [Online]. Available: https://en.wikipedia.org/wiki/Glucose
[25] M. Markovic, S. Ben-Shabat, A. Aponick, E. M. Zimmermann, and A. Dahan, "Lipids and Lipid-Processing Pathways in Drug Delivery and Therapeutics," *International Journal of Molecular Sciences 2020, Vol. 21, Page 3248*, vol. 21, no. 9, p. 3248, May 2020, doi: 10.3390/IJMS21093248.
[26] S. F. O'Keefe, "Nomenclature and Classification of Lipids," in *Akoh CC, Min DB (eds) Food lipids, chemistry, nutrition and biotechnology*, CRC Press, 2002, pp. 20–59. doi: 10.1201/9780203908815-4.
[27] T. J. Weiss, *Food oils and their uses*, 2nd ed. Westport: AVI Pub. Co, 1983. Accessed: Dec. 14, 2023. [Online]. Available: https://books.google.com/books/about/Food_Oils_and_Their_Uses.html?hl=nl&id=91gkAQAAIAAJ
[28] A. G. Marangoni and S. S. Narine, *Physical properties of lipids*. Marcel Dekker, 2002.
[29] "Lipid - Wikipedia." Accessed: Dec. 14, 2023. [Online]. Available: https://en.wikipedia.org/wiki/Lipid
[30] D. A. Vallero and T. M. Letcher, "Minerals," *Unraveling Environmental Disasters*, pp. 235–273, Jan. 2013, doi: 10.1016/B978-0-12-397026-8.00010-0.
[31] B. M. Mehta and P. C. K. Cheung, "Overview of Food Chemistry," *Handbook of Food Chemistry*, pp. 3–13, Jan. 2015, doi: 10.1007/978-3-642-36605-5_34/COVER.
[32] S. V. Vassilev, D. Baxter, L. K. Andersen, C. G. Vassileva, and T. J. Morgan, "An overview of the organic and inorganic phase composition of biomass," *Fuel*, vol. 94, pp. 1–33, Apr. 2012, doi: 10.1016/J.FUEL.2011.09.030.

[33] N. Parmar, A. Singh, and O. P. Ward, “Characterization of the combined effects of enzyme, pH and temperature treatments for removal of pathogens from sewage sludge,” *World J Microbiol Biotechnol*, vol. 17, no. 2, pp. 169–172, 2001, doi: 10.1023/A:1016606020993/METRICS.

[34] W. Ma *et al.*, “Supercritical water pyrolysis of sewage sludge,” *Waste Management*, vol. 59, pp. 371–378, Jan. 2017, doi: 10.1016/J.WASMAN.2016.10.053.

[35] P. Supaporn, H. V. Ly, S.-S. Kim, and S. H. Yeom, “Bio-oil production using residual sewage sludge after lipid and carbohydrate extraction,” *Environmental Engineering Research*, vol. 24, no. 2, pp. 202–210, Jul. 2018, doi: 10.4491/eer.2017.178.

[36] S. M. Heilmann *et al.*, “Phosphorus reclamation through hydrothermal carbonization of animal manures,” *Environ Sci Technol*, vol. 48, no. 17, pp. 10323–10329, Sep. 2014, doi: 10.1021/ES501872K/SUPPL_FILE/ES501872K_SI_001.PDF.

[37] O. Li, J. Liang, Y. Chen, S. Tang, and Z. Li, “Exploration of Converting Food Waste into Value-Added Products via Insect Pretreatment-Assisted Hydrothermal Catalysis,” *ACS Omega*, vol. 8, no. 21, pp. 18760–18772, May 2023, doi: 10.1021/ACSOMEGA.3C00762/SUPPL_FILE/AO3C00762_SI_001.PDF.

[38] B. Motavaf and P. E. Savage, “Effect of Process Variables on Food Waste Valorization via Hydrothermal Liquefaction,” *ACS ES and T Engineering*, vol. 1, no. 3, pp. 363–374, Mar. 2021, doi: 10.1021/ACSESTENGG.0C00115/ASSET/IMAGES/LARGE/EE0C00115_0012.JPEG.

[39] Y. Q. Tang *et al.*, “Ethanol production from kitchen waste using the flocculating yeast Saccharomyces cerevisiae strain KF-7,” *Biomass Bioenergy*, vol. 32, no. 11, pp. 1037–1045, Nov. 2008, doi: 10.1016/J.BIOMBIOE.2008.01.027.

[40] P. Verma, M. Kumar, G. Mishra, and D. Sahoo, “Multivariate analysis of fatty acid and biochemical constitutes of seaweeds to characterize their potential as bioresource for biofuel and fine chemicals,” *Bioresour Technol*, vol. 226, pp. 132–144, Feb. 2017, doi: 10.1016/J.BIORTECH.2016.11.044.

[41] B. Maddi, S. Viamajala, and S. Varanasi, “Comparative study of pyrolysis of algal biomass from natural lake blooms with lignocellulosic biomass,” *Bioresour Technol*, vol. 102, no. 23, pp. 11018–11026, Dec. 2011, doi: 10.1016/J.BIORTECH.2011.09.055.

[42] J. Fang, L. Zhan, Y. S. Ok, and B. Gao, “Minireview of potential applications of hydrochar derived from hydrothermal carbonization of biomass,” *Journal of Industrial and Engineering Chemistry*, vol. 57, pp. 15–21, Jan. 2018, doi: 10.1016/J.JIEC.2017.08.026.

[43] V. Anand, R. Gautam, and R. Vinu, “Non-catalytic and catalytic fast pyrolysis of Schizochytrium limacinum microalga,” *Fuel*, vol. 205, pp. 1–10, Oct. 2017, doi: 10.1016/J.FUEL.2017.05.049.

[44] X. J. Lee, H. C. Ong, Y. Y. Gan, W. H. Chen, and T. M. I. Mahlia, “State of art review on conventional and advanced pyrolysis of macroalgae and microalgae for biochar, bio-oil and bio-syngas production,” *Energy Convers Manag*, vol. 210, p. 112707, Apr. 2020, doi: 10.1016/J.ENCONMAN.2020.112707.

[45] A. Adelina, F. Feliatra, Y. I. Siregar, I. Suharman, and N. A. Pamukas, “Fermented chicken feathers using Bacillus subtilis to improve the quality of nutrition as a fish feed material,” *IOP Conf Ser Earth Environ Sci*, vol. 348, no. 1, p. 012008, Nov. 2019, doi: 10.1088/1755-1315/348/1/012008.

[46] M. B. Esteban, A. J. García, P. Ramos, and M. C. Márquez, “Sub-critical water hydrolysis of hog hair for amino acid production,” *Bioresour Technol*, vol. 101, no. 7, pp. 2472–2476, Apr. 2010, doi: 10.1016/J.BIORTECH.2009.11.054.

[47] J. Lee, J. Hong, D. Jang, and K. Y. Park, “Hydrothermal carbonization of waste from leather processing and feasibility of produced hydrochar as an alternative solid fuel,” *J Environ Manage*, vol. 247, pp. 115–120, Oct. 2019, doi: 10.1016/J.JENVMAN.2019.06.067.

[48] P. Drechsel, M. Qadir, and D. Wichelns, “Wastewater: Economic asset in an urbanizing world,” *Wastewater: Economic Asset in an Urbanizing World*, pp. 1–282, Jan. 2015, doi: 10.1007/978-94-017-9545-6/COVER.

[49] A. Gherghel, C. Teodosiu, and S. De Gisi, “A review on wastewater sludge valorisation and its challenges in the context of circular economy,” *J Clean Prod*, vol. 228, pp. 244–263, Aug. 2019, doi: 10.1016/J.JCLEPRO.2019.04.240.

[50] F. Merzari, M. Langone, G. Andreottola, and L. Fiori, “Methane production from process water of sewage sludge hydrothermal carbonization. A review. Valorising sludge through hydrothermal carbonization,” *Crit Rev Environ Sci Technol*, vol. 49, no. 11, pp. 947–988, Jun. 2019, doi: 10.1080/10643389.2018.1561104.

[51] N. Gao, K. Kamran, C. Quan, and P. T. Williams, “Thermochemical conversion of sewage sludge: A critical review,” *Prog Energy Combust Sci*, vol. 79, p. 100843, Jul. 2020, doi: 10.1016/J.PECS.2020.100843.

[52] C. Peng *et al.*, “Production of char from sewage sludge employing hydrothermal carbonization: Char properties, combustion behavior and thermal characteristics,” *Fuel*, vol. 176, pp. 110–118, Jul. 2016, doi: 10.1016/J.FUEL.2016.02.068.

[53] P. Pagliari, M. Wilson, and Z. He, “Animal Manure Production and Utilization: Impact of Modern Concentrated Animal Feeding Operations,” *Animal Manure: Production, Characteristics, Environmental Concerns, and Management*, pp. 1–14, Jan. 2020, doi: 10.2134/ASASPECPUB67.C1.

[54] M. E. Sanchez, M. Otero, X. Gómez, and A. Morán, “Thermogravimetric kinetic analysis of the combustion of biowastes,” *Renew Energy*, vol. 34, no. 6, pp. 1622–1627, Jun. 2009, doi: 10.1016/J.RENENE.2008.11.011.

[55] O. E. Saunders, A. M. Fortuna, J. H. Harrison, C. G. Cogger, E. Whitefield, and T. Green, “Gaseous nitrogen and bacterial responses to raw and digested dairy manure applications in incubated soil,” *Environ Sci Technol*, vol. 46, no. 21, pp. 11684–11692, Nov. 2012, doi: 10.1021/ES301754S/SUPPL_FILE/ES301754S_SI_001.PDF.

[56] J. Venglovsky, N. Sasakova, and I. Placha, “Pathogens and antibiotic residues in animal manures and hygienic and ecological risks related to subsequent land application,” *Bioresour Technol*, vol. 100, no. 22, pp. 5386–5391, Nov. 2009, doi: 10.1016/J.BIORTECH.2009.03.068.

[57] Manitoba, “Properties of Manure,” Nov. 2015.

[58] C. Rohini, P. Geetha, R. Vijayalakshmi, M. Mini, and E. Pasupathi, “Global effects of food waste,” *J Pharmacogn Phytochem*, vol. 9, no. 2, pp. 690–699, 2020, Accessed: Dec. 19, 2023. [Online]. Available: https://www.phytojournal.com/archives/2020.v9.i2.10936/global-effects-of-food-waste

[59] H. Chen, H. Shen, H. F. Su, H. Z. Chen, F. R. Tan, and J. F. Lin, “High-efficiency bioconversion of kitchen garbage to biobutanol using an enzymatic cocktail procedure,” *Bioresour Technol*, vol. 245, pp. 1110–1121, Dec. 2017, doi: 10.1016/J.BIORTECH.2017.09.056.

[60] M. V. L. Chhandama, A. C. Chetia, K. B. Satyan, Supongsenla Ao, J. V. Ruatpuia, and S. L. Rokhum, “Valorisation of food waste to sustainable energy and other value-added products: A review,” *Bioresour Technol Rep*, vol. 17, p. 100945, Feb. 2022, doi: 10.1016/J.BITEB.2022.100945.

[61] S. K. Pramanik, F. B. Suja, S. M. Zain, and B. K. Pramanik, “The anaerobic digestion process of biogas production from food waste: Prospects and constraints,” *Bioresour Technol Rep*, vol. 8, p. 100310, Dec. 2019, doi: 10.1016/J.BITEB.2019.100310.

[62] C. Negri *et al.*, “Anaerobic digestion of food waste for bio-energy production in China and Southeast Asia: A review,” *Renewable and Sustainable Energy Reviews*, vol. 133, p. 110138, Nov. 2020, doi: 10.1016/J.RSER.2020.110138.

[63] L. Alibardi *et al.*, “Organic waste biorefineries: Looking towards implementation,” *Waste Management*, vol. 114, pp. 274–286, Aug. 2020, doi: 10.1016/J.WASMAN.2020.07.010.

[64] C. Ma, J. Liu, M. Ye, L. Zou, G. Qian, and Y. Y. Li, “Towards utmost bioenergy conversion efficiency of food waste: Pretreatment, co-digestion, and reactor type,” *Renewable and Sustainable Energy Reviews*, vol. 90, pp. 700–709, Jul. 2018, doi: 10.1016/J.RSER.2018.03.110.

[65] C. Tirapanampai, N. Toewiwat, N. Weeranoppanant, P. Chaiyen, and T. Wongnate, “Processing of palm oil mill effluent (POME) into food waste digesting microbes: An investigation of acclimatization strategies,” *Sustainable Energy Technologies and Assessments*, vol. 52, Aug. 2022, doi: 10.1016/J.SETA.2022.102287.

[66] C. H. Chen *et al.*, “Understanding and modelling the interactions of peptides with membranes: from partitioning to self-assembly,” *Curr Opin Struct Biol*, vol. 61, pp. 160–166, Apr. 2020, doi: 10.1016/J.SBI.2019.12.021.

[67] S. Wu *et al.*, “Hydrothermal carbonization of food waste for sustainable biofuel production: Advancements, challenges, and future prospects,” *Science of The Total Environment*, vol. 897, p. 165327, Nov. 2023, doi: 10.1016/J.SCITOTENV.2023.165327.

[68] W. Han, W. Clarke, and S. Pratt, “Composting of waste algae: A review,” *Waste Management*, vol. 34, no. 7, pp. 1148–1155, Jul. 2014, doi: 10.1016/J.WASMAN.2014.01.019.

[69] V. Cuomo, A. Perretti, I. Palomba, A. Verde, and A. Cuomo, “Utilisation of Ulva rigida biomass in the Venice Lagoon (Italy): biotransformation in compost,” *J Appl Phycol*, vol. 7, no. 5, pp. 479–485, Oct. 1995, doi: 10.1007/BF00003932/METRICS.

[70] X. M. Sun, L. J. Ren, Q. Y. Zhao, X. J. Ji, and H. Huang, “Microalgae for the production of lipid and carotenoids: a review with focus on stress regulation and adaptation,” *Biotechnol Biofuels*, vol. 11, no. 1, p. 272, Oct. 2018, doi: 10.1186/S13068-018-1275-9.

[71] T. Cai, S. Y. Park, and Y. Li, “Nutrient recovery from wastewater streams by microalgae: Status and prospects,” *Renewable and Sustainable Energy Reviews*, vol. 19, pp. 360–369, Mar. 2013, doi: 10.1016/J.RSER.2012.11.030.

[72] K. Fela, K. Wieczorek-Ciurowa, M. Konopka, and Z. Woźny, “Present and prospective leather industry waste disposal,” *Polish Journal of Chemical Technology*, vol. 13, no. 3, pp. 53–55, Jan. 2011, doi: 10.2478/V10026-011-0037-2.

[73] M. Peydayesh, M. Bagnani, W. L. Soon, and R. Mezzenga, “Turning Food Protein Waste into Sustainable Technologies,” *Chem Rev*, vol. 123, no. 5, pp. 2112–2154, Mar. 2023, doi: 10.1021/acs.chemrev.2c00236.

[74] W. L. Soon *et al.*, “Renewable Energy from Livestock Waste Valorization: Amyloid-Based Feather Keratin Fuel Cells,” *ACS Appl Mater Interfaces*, vol. 15, no. 40, pp. 47049–47057, Oct. 2023, doi: 10.1021/ACSAMI.3C10218/ASSET/IMAGES/LARGE/AM3C10218_0004.JPEG.

[75] M. B. Esteban, A. J. García, P. Ramos, and M. C. Márquez, “Evaluation of fruit–vegetable and fish wastes as alternative feedstuffs in pig diets,” *Waste Management*, vol. 27, no. 2, pp. 193–200, Jan. 2007, doi: 10.1016/J.WASMAN.2006.01.004.

[76] J. A. Álvarez, L. Otero, and J. M. Lema, “A methodology for optimising feed composition for anaerobic co-digestion of agro-industrial wastes,” *Bioresour Technol*, vol. 101, no. 4, pp. 1153–1158, Feb. 2010, doi: 10.1016/J.BIORTECH.2009.09.061.
[77] K. S. P. Karunadasa, C. H. Manoratne, H. M. T. G. A. Pitawala, and R. M. G. Rajapakse, “Thermal decomposition of calcium carbonate (calcite polymorph) as examined by in-situ high-temperature X-ray powder diffraction,” *Journal of Physics and Chemistry of Solids*, vol. 134, pp. 21–28, Nov. 2019, doi: 10.1016/J.JPCS.2019.05.023.
[78] J. L. Vidal, T. Jin, E. Lam, F. Kerton, and A. Moores, “Blue is the new green: Valorization of crustacean waste,” *Current Research in Green and Sustainable Chemistry*, vol. 5, p. 100330, Jan. 2022, doi: 10.1016/J.CRGSC.2022.100330.
[79] S. S. Kim, J. Kim, Y. Duk, and Y. M. Lee, “Thermal characteristics of chitin and hydroxypropyl chitin,” *Polymer (Guildf)*, vol. 35, no. 15, 1994.
[80] S. Mandeville, V. Yaylayan, and B. K. Simpson, “Proximate analysis, isolation and identification of amino acids and sugars from raw and cooked commercial shrimp waste,” *Food Biotechnol*, vol. 6, no. 1, pp. 51–64, Jan. 1992, doi: 10.1080/08905439209549821.
[81] L. Ferdousi *et al.*, “Biochemical analysis of commonly consumed fishes and shell fishes from the Tista and the Baral River in Bangladesh,” *J Agric Food Res*, vol. 14, p. 100671, Dec. 2023, doi: 10.1016/J.JAFR.2023.100671.
[82] “Atlantic cutlassfish.” Accessed: Dec. 19, 2023. [Online]. Available: https://eol.org/pages/46577378
[83] H. Badar Osmany, “Trichiurus lepturus.” Accessed: Dec. 20, 2023. [Online]. Available: https://fishbase.se/photos/UploadedBy.php?autoctr=21102&win=uploaded
[84] B. Yau, “Larimichthys polyactis.” Accessed: Dec. 20, 2023. [Online]. Available: https://www.fishbase.se/photos/PicturesSummary.php?resultPage=2&ID=416&what=species
[85] M. Matsunuma *et al.*, “Checklist of fishes collected from Haruno Fishing Port, Kochi Prefecture, Japan,” *Nature of Kagoshima*, vol. 44, pp. 47–71, 2017.
[86] Chinese Academy of Fishery Sciences, “Paralichthys olivaceus.” Accessed: Dec. 20, 2023. [Online]. Available: https://www.fishbase.se/photos/ThumbnailsSummary.php?ID=1351
[87] Sea World Distribution, “Litopenaeus vannamei.” Accessed: Dec. 20, 2023. [Online]. Available: https://www.seaworld-distribution.com/en/shellfish/prawns/prawn-litopenaeus-vannamei-indonesia/
[88] “Penaeus monodon.” Accessed: Dec. 20, 2023. [Online]. Available: https://commons.wikimedia.org/wiki/File:Penaeus_monodon.jpg
[89] S. Prajapati and N. Ujjania, “Length-weight relationship and condition factor of Pacific whiteleg shrimp (Litopenaeus vannamei, Boone, 1931) cultured in polyethylene lined pond,” *International Journal of Fauna and Biological Studies*, vol. 9, no. 4, pp. 15–18, 2022, doi: 10.22271/23940522.2022.v9.i4a.914.
[90] J. H. Bae and S. Y. Lim, “Comparative study of the concentration of mercury and lead and the chemical characteristics of Japanese and Korean chub mackerel (Scomber japonicas Houttuyn, 1782) in the East China Sea,” *Afr J Agric Res*, vol. 8, no. 3, pp. 269–273, 2013, doi: 10.5897/AJAR12.1219.
[91] J. Gim, “A length-based model for Korean chub mackerel (Scomber japonicus) stock,” Pukyong National University, 2019. Accessed: Dec. 06, 2023. [Online]. Available: https://repository.pknu.ac.kr:8443/bitstream/2021.oak/23443/2/A%20length-

based%20model%20for%20Korean%20chub%20mackerel%20%20%28Scomber%20japonicus%29%20stock.pdf
[92] L. Chen, W. Zeng, Y. Rong, and B. Lou, “Compositions, nutritional and texture quality of wild-caught andcage-cultured small yellow croaker,” *Journal of Food Composition and Analysis*, vol. 107, p. 104370, Apr. 2022, doi: 10.1016/J.JFCA.2021.104370.
[93] Fishbase, “Trachurus japonicus.” Accessed: Dec. 12, 2023. [Online]. Available: https://www.fishbase.se/summary/Trachurus-japonicus.html
[94] Fishbase, “Larimichthys polyactis, yellow croaker.” Accessed: Dec. 12, 2023. [Online]. Available: https://fishbase.mnhn.fr/summary/Larimichthys-polyactis.html
[95] H.-J. Lu, C.-C. Chen, J.-C. Cheng, H.-J. ; Lu, and C.-C. Chen, “Age and growth study of the jack mackerel (Trachurus japonicus) in the northeastern wasters off Taiwan,” *J Mar Sci Technol*, vol. 21, no. 7, pp. 31–40, 2013, doi: 10.6119/JMST-013-1220-1.
[96] S. C. Bai and S. Lee, “Culture of Olive Flounder: Korean Perspective,” 2010, doi: 10.1002/9780813810997.ch9.
[97] FAO, “Penaeus monodon (Fabricius, 1798).” Accessed: Dec. 12, 2023. [Online]. Available: https://firms.fao.org/fi/website/FIRetrieveAction.do?dom=culturespecies&xml=Penaeus_monodon.xml
[98] FAO, “Penaeus vannamei.” Accessed: Dec. 12, 2023. [Online]. Available: https://www.fao.org/fishery/docs/DOCUMENT/aquaculture/CulturedSpecies/file/en/en_whitelegshrimp.htm
[99] Sealifebase, “Portunus trituberculatus, Gazami crab.” Accessed: Dec. 12, 2023. [Online]. Available: https://www.sealifebase.ca/country/CountrySpeciesSummary.php?id=83565&c_code=156
[100] FAO, “Global Production,” Fisheries and Aquaculture Division . Accessed: Dec. 06, 2023. [Online]. Available: https://www.fao.org/fishery/en/collection/global_production?lang=en
[101] J. Kim, “South Korea’s first production of Black Tiger shrimp,” Nov. 01, 2022. Accessed: Dec. 12, 2023. [Online]. Available: https://seafoodnetworkbd.com/south-korean-first-production-of-black-tiger-shrimp
[102] Union Forsea Corp., “South Korean import of black tiger and vannamei shrimp,” Jan. 23, 2023. Accessed: Dec. 12, 2023. [Online]. Available: http://www.fis-net.com/fis/worldnews/worldnews.asp?monthyear=1-2023&day=23&id=121518&l=e&country=0&special=0&ndb=1&df=0
[103] 홍연아 and 윤찬미, “2021년도 식품수급표,” 나주시, Dec. 2022. [Online]. Available: http://www.krei.re.kr
[104] S. Kang, X. Li, J. Fan, and J. Chang, “Hydrothermal conversion of lignin: A review,” *Renewable and Sustainable Energy Reviews*, vol. 27, pp. 546–558, Nov. 2013, doi: 10.1016/J.RSER.2013.07.013.
[105] D. Lachos-Perez, P. César Torres-Mayanga, E. R. Abaide, G. L. Zabot, and F. De Castilhos, “Hydrothermal carbonization and Liquefaction: differences, progress, challenges, and opportunities,” *Bioresour Technol*, vol. 343, p. 126084, Jan. 2022, doi: 10.1016/J.BIORTECH.2021.126084.
[106] Q. Wang *et al.*, “Co-hydrothermal carbonization of organic solid wastes to hydrochar as potential fuel: A review,” *Science of The Total Environment*, vol. 850, p. 158034, Dec. 2022, doi: 10.1016/J.SCITOTENV.2022.158034.

[107] A. A. Peterson, F. Vogel, R. P. Lachance, M. Fröling, M. J. Antal, and J. W. Tester, “Thermochemical biofuel production in hydrothermal media: A review of sub- and supercritical water technologies,” *Energy Environ Sci*, vol. 1, no. 1, pp. 32–65, Jul. 2008, doi: 10.1039/B810100K.

[108] D. Lachos-Perez *et al.*, “Applications of subcritical and supercritical water conditions for extraction, hydrolysis, gasification, and carbonization of biomass: A critical review,” *Biofuel Research Journal*, vol. 4, no. 2. Green Wave Publishing of Canada, pp. 611–626, 2017. doi: 10.18331/BRJ2017.4.2.6.

[109] J. A. Okolie, S. Nanda, A. K. Dalai, F. Berruti, and J. A. Kozinski, “A review on subcritical and supercritical water gasification of biogenic, polymeric and petroleum wastes to hydrogen-rich synthesis gas,” *Renewable and Sustainable Energy Reviews*, vol. 119, p. 109546, Mar. 2020, doi: 10.1016/J.RSER.2019.109546.

[110] Y. Cao, M. He, S. Dutta, G. Luo, S. Zhang, and D. C. W. Tsang, “Hydrothermal carbonization and liquefaction for sustainable production of hydrochar and aromatics,” *Renewable and Sustainable Energy Reviews*, vol. 152, p. 111722, Dec. 2021, doi: 10.1016/J.RSER.2021.111722.

[111] A. A. Azzaz, B. Khiari, S. Jellali, C. M. Ghimbeu, and M. Jeguirim, “Hydrochars production, characterization and application for wastewater treatment: A review,” *Renewable and Sustainable Energy Reviews*, vol. 127, p. 109882, Jul. 2020, doi: 10.1016/J.RSER.2020.109882.

[112] T. Wang, Y. Zhai, Y. Zhu, C. Li, and G. Zeng, “A review of the hydrothermal carbonization of biomass waste for hydrochar formation: Process conditions, fundamentals, and physicochemical properties,” *Renewable and Sustainable Energy Reviews*, vol. 90, pp. 223–247, Jul. 2018, doi: 10.1016/j.rser.2018.03.071.

[113] Z. Zhang, J. Yang, J. Qian, Y. Zhao, T. Wang, and Y. Zhai, “Biowaste hydrothermal carbonization for hydrochar valorization: Skeleton structure, conversion pathways and clean biofuel applications,” *Bioresour Technol*, vol. 324, p. 124686, Mar. 2021, doi: 10.1016/J.BIORTECH.2021.124686.

[114] L. Wang, Y. Chang, and A. Li, “Hydrothermal carbonization for energy-efficient processing of sewage sludge: A review,” *Renewable and Sustainable Energy Reviews*, vol. 108, pp. 423–440, Jul. 2019, doi: 10.1016/J.RSER.2019.04.011.

[115] Q. Wang *et al.*, “Co-hydrothermal carbonization of corn stover and food waste: Characterization of hydrochar, synergistic effects, and combustion characteristic analysis,” *J Environ Chem Eng*, vol. 10, no. 6, p. 108716, Dec. 2022, doi: 10.1016/J.JECE.2022.108716.

[116] K. Byrappa and T. Adschiri, “Hydrothermal technology for nanotechnology,” *Progress in Crystal Growth and Characterization of Materials*, vol. 53, no. 2, pp. 117–166, Jun. 2007, doi: 10.1016/J.PCRYSGROW.2007.04.001.

[117] A. Kruse, A. Funke, and M. M. Titirici, “Hydrothermal conversion of biomass to fuels and energetic materials,” *Curr Opin Chem Biol*, vol. 17, no. 3, pp. 515–521, Jun. 2013, doi: 10.1016/J.CBPA.2013.05.004.

[118] P. V. Gopirajan, K. P. Gopinath, G. Sivaranjani, and J. Arun, “Optimization of hydrothermal gasification process through machine learning approach: Experimental conditions, product yield and pollution,” *J Clean Prod*, vol. 306, p. 127302, Jul. 2021, doi: 10.1016/J.JCLEPRO.2021.127302.

[119] A. S. Jatoi *et al.*, “Hydrothermal Liquefaction of Lignocellulosic and Protein-Containing Biomass: A Comprehensive Review,” *Catalysts 2022, Vol. 12, Page 1621*, vol. 12, no. 12, p. 1621, Dec. 2022, doi: 10.3390/CATAL12121621.
[120] G. Ischia and L. Fiori, “Hydrothermal Carbonization of Organic Waste and Biomass: A Review on Process, Reactor, and Plant Modeling,” *Waste and Biomass Valorization 2020 12:6*, vol. 12, no. 6, pp. 2797–2824, Oct. 2020, doi: 10.1007/S12649-020-01255-3.
[121] S. K. Hoekman, A. Broch, and C. Robbins, “Hydrothermal carbonization (HTC) of lignocellulosic biomass,” *Energy and Fuels*, vol. 25, no. 4, pp. 1802–1810, Apr. 2011, doi: 10.1021/EF101745N.
[122] E. Ahmad and K. K. Pant, “Lignin Conversion: A Key to the Concept of Lignocellulosic Biomass-Based Integrated Biorefinery,” *Waste Biorefinery: Potential and Perspectives*, pp. 409–444, Jan. 2018, doi: 10.1016/B978-0-444-63992-9.00014-8.
[123] J. Akhtar and N. Saidina Amin, “A review on operating parameters for optimum liquid oil yield in biomass pyrolysis,” *Renewable and Sustainable Energy Reviews*, vol. 16, no. 7, pp. 5101–5109, Sep. 2012, doi: 10.1016/J.RSER.2012.05.033.
[124] A. L. Pauline and K. Joseph, “Hydrothermal carbonization of organic wastes to carbonaceous solid fuel – A review of mechanisms and process parameters,” *Fuel*, vol. 279, p. 118472, Nov. 2020, doi: 10.1016/J.FUEL.2020.118472.
[125] A. Funke and F. Ziegler, “Hydrothermal carbonization of biomass: A summary and discussion of chemical mechanisms for process engineering,” *Biofuels, Bioproducts and Biorefining*, vol. 4, no. 2, pp. 160–177, Mar. 2010, doi: 10.1002/BBB.198.
[126] S. Soroush, F. Ronsse, J. Park, and P. M. Heynderickx, “Comparison Study on the Water-to-Biomass Ratio in Hydrothermal Carbonization of Fresh Seaweed,” *Processes*, vol. 11, no. 4, p. 1123, Apr. 2023, doi: 10.3390/PR11041123/S1.
[127] A. L. Tasca *et al.*, “Hydrothermal Carbonization of Sewage Sludge: Analysis of Process Severity and Solid Content,” *Chem Eng Technol*, vol. 43, no. 12, pp. 2382–2392, Dec. 2020, doi: 10.1002/CEAT.202000095.
[128] S. Soroush *et al.*, “Production of solid hydrochar from waste seaweed by hydrothermal carbonization: effect of process variables,” *Biomass Convers Biorefin*, vol. 1, pp. 1–15, Feb. 2022, doi: 10.1007/S13399-022-02365-9/TABLES/5.
[129] M. Watanabe, T. M. Aida, and R. L. Smith, “Review of Biomass Conversion in High Pressure High Temperature Water (HHW) Including Recent Experimental Results (Isomerization and Carbonization),” pp. 249–274, 2014, doi: 10.1007/978-3-642-54458-3_11.
[130] R. Ferrentino, R. Ceccato, V. Marchetti, G. Andreottola, and L. Fiori, “Sewage Sludge Hydrochar: An Option for Removal of Methylene Blue from Wastewater,” *Applied Sciences 2020, Vol. 10, Page 3445*, vol. 10, no. 10, p. 3445, May 2020, doi: 10.3390/APP10103445.
[131] R. Z. Gaur *et al.*, “Hydrothermal carbonization of sewage sludge coupled with anaerobic digestion: Integrated approach for sludge management and energy recycling,” *Energy Convers Manag*, vol. 224, p. 113353, Nov. 2020, doi: 10.1016/J.ENCONMAN.2020.113353.
[132] Q. Li *et al.*, “Co-hydrothermal carbonization of swine and chicken manure: Influence of cross-interaction on hydrochar and liquid characteristics,” *Science of The Total Environment*, vol. 786, p. 147381, Sep. 2021, doi: 10.1016/J.SCITOTENV.2021.147381.
[133] J. D. Marin-Batista, J. A. Villamil, S. V. Qaramaleki, C. J. Coronella, A. F. Mohedano, and M. A. de la Rubia, “Energy valorization of cow manure by hydrothermal carbonization and

anaerobic digestion," *Renew Energy*, vol. 160, pp. 623–632, Nov. 2020, doi: 10.1016/J.RENENE.2020.07.003.
[134] H. Fu *et al.*, "Assessment of livestock manure-derived hydrochar as cleaner products: Insights into basic properties, nutrient composition, and heavy metal content," *J Clean Prod*, vol. 330, p. 129820, Jan. 2022, doi: 10.1016/J.JCLEPRO.2021.129820.
[135] A. M. Smith, S. Singh, and A. B. Ross, "Fate of inorganic material during hydrothermal carbonisation of biomass: Influence of feedstock on combustion behaviour of hydrochar," *Fuel*, vol. 169, pp. 135–145, Apr. 2016, doi: 10.1016/J.FUEL.2015.12.006.
[136] N. D. Berge, K. S. Ro, J. Mao, J. R. V. Flora, M. A. Chappell, and S. Bae, "Hydrothermal carbonization of municipal waste streams," *Environ Sci Technol*, vol. 45, no. 13, pp. 5696–5703, Jul. 2011, doi: 10.1021/ES2004528.
[137] M. Wilk, M. Sliz, and M. Gajek, "The effects of hydrothermal carbonization operating parameters on high-value hydrochar derived from beet pulp," 2021, doi: 10.1016/j.renene.2021.05.112.
[138] N. Patel, B. Acharya, and P. Basu, "Hydrothermal carbonization (Htc) of seaweed (macroalgae) for producing hydrochar," *Energies (Basel)*, vol. 14, no. 7, Apr. 2021, doi: 10.3390/en14071805.
[139] J. Lee, J. Hong, D. Jang, and K. Y. Park, "Hydrothermal carbonization of waste from leather processing and feasibility of produced hydrochar as an alternative solid fuel," *J Environ Manage*, vol. 247, pp. 115–120, Oct. 2019, doi: 10.1016/J.JENVMAN.2019.06.067.
[140] M. A. Islam, J. Paul, J. Akter, M. A. Islam, and S. H. Limon, "Conversion of chicken feather waste via hydrothermal carbonization: process optimization and the effect of hydrochar on seed germination of Acacia auriculiformis," *J Mater Cycles Waste Manag*, vol. 23, no. 3, pp. 1177–1188, May 2021, doi: 10.1007/S10163-021-01209-4/FIGURES/6.
[141] X. Zhuang *et al.*, "Insights into the evolution of chemical structures in lignocellulose and non-lignocellulose biowastes during hydrothermal carbonization (HTC)," *Fuel*, vol. 236, pp. 960–974, Jan. 2019, doi: 10.1016/J.FUEL.2018.09.019.
[142] S. Wu *et al.*, "Insights into the chemical structure evolution and carbonisation mechanism of biomass during hydrothermal treatment," *Journal of the Energy Institute*, vol. 108, p. 101257, Jun. 2023, doi: 10.1016/J.JOEI.2023.101257.
[143] B. M. Kabyemela, T. Adschiri, R. M. Malaluan, and K. Arai, "Kinetics of Glucose Epimerization and Decomposition in Subcritical and Supercritical Water," *Ind Eng Chem Res*, vol. 36, no. 5, pp. 1552–1558, May 1997, doi: 10.1021/ie960250h.
[144] X. Zhuang, J. Liu, Q. Zhang, C. Wang, H. Zhan, and L. Ma, "A review on the utilization of industrial biowaste via hydrothermal carbonization," *Renewable and Sustainable Energy Reviews*, vol. 154, p. 111877, Feb. 2022, doi: 10.1016/J.RSER.2021.111877.
[145] Z. Srokol, A. G. Bouche, A. Van Estrik, R. C. J. Strik, T. Maschmeyer, and J. A. Peters, "Hydrothermal upgrading of biomass to biofuel; studies on some monosaccharide model compounds," *Carbohydr Res*, vol. 339, no. 10, pp. 1717–1726, Jul. 2004, doi: 10.1016/J.CARRES.2004.04.018.
[146] S. M. Changi, J. L. Faeth, N. Mo, and P. E. Savage, "Hydrothermal Reactions of Biomolecules Relevant for Microalgae Liquefaction," *Ind Eng Chem Res*, vol. 54, no. 47, pp. 11733–11758, Nov. 2015, doi: 10.1021/ACS.IECR.5B02771/ASSET/IMAGES/LARGE/IE-2015-027713_0013.JPEG.
[147] F. Wei, J. P. Cao, X. Y. Zhao, J. Ren, B. Gu, and X. Y. Wei, "Formation of aromatics and removal of nitrogen in catalytic fast pyrolysis of sewage sludge: A study of sewage sludge

and model amino acids," *Fuel*, vol. 218, pp. 148–154, Apr. 2018, doi: 10.1016/J.FUEL.2018.01.025.
[148] M. Déniel, G. Haarlemmer, A. Roubaud, E. Weiss-Hortala, and J. Fages, "Energy valorisation of food processing residues and model compounds by hydrothermal liquefaction," *Renewable and Sustainable Energy Reviews*, vol. 54, pp. 1632–1652, Feb. 2016, doi: 10.1016/J.RSER.2015.10.017.
[149] K. Zhao, Y. Li, Y. Zhou, W. Guo, H. Jiang, and Q. Xu, "Characterization of hydrothermal carbonization products (hydrochars and spent liquor) and their biomethane production performance," *Bioresour Technol*, vol. 267, pp. 9–16, Nov. 2018, doi: 10.1016/J.BIORTECH.2018.07.006.
[150] S. E. Kinata, K. Loubar, M. Paraschiv, M. Tazerout, and C. Belloncle, "Catalytic hydroliquefaction of charcoal CCB (copper, chromium and boron)-treated wood for bio-oil production: Influence of CCB salts, residence time and catalysts," *Appl Energy*, vol. 115, pp. 57–64, Feb. 2014, doi: 10.1016/J.APENERGY.2013.10.057.
[151] X. Cui, M. Antonietti, and S. H. Yu, "Structural effects of iron oxide nanoparticles and iron ions on the hydrothermal carbonization of starch and rice carbohydrates," *Small*, vol. 2, no. 6, pp. 756–759, Jun. 2006, doi: 10.1002/SMLL.200600047.
[152] C. Yang *et al.*, "Catalytic hydroprocessing of microalgae-derived biofuels: a review," *Green Chemistry*, vol. 18, no. 13, pp. 3684–3699, Jun. 2016, doi: 10.1039/C6GC01239F.
[153] S. Zhang, X. Zhu, S. Zhou, H. Shang, J. Luo, and D. C. W. Tsang, "Hydrothermal Carbonization for Hydrochar Production and Its Application," *Biochar from Biomass and Waste: Fundamentals and Applications*, pp. 275–294, Jan. 2019, doi: 10.1016/B978-0-12-811729-3.00015-7.
[154] N. Saha, K. McGaughy, and M. T. Reza, "Elucidating hydrochar morphology and oxygen functionality change with hydrothermal treatment temperature ranging from subcritical to supercritical conditions," *J Anal Appl Pyrolysis*, vol. 152, p. 104965, Nov. 2020, doi: 10.1016/J.JAAP.2020.104965.
[155] M. Sevilla and A. B. Fuertes, "Chemical and structural properties of carbonaceous products obtained by hydrothermal carbonization of saccharides," *Chemistry - A European Journal*, vol. 15, no. 16, pp. 4195–4203, Apr. 2009, doi: 10.1002/CHEM.200802097.
[156] C. Qiu, L. Jiang, Y. Gao, and L. Sheng, "Effects of oxygen-containing functional groups on carbon materials in supercapacitors: A review," *Mater Des*, vol. 230, p. 111952, Jun. 2023, doi: 10.1016/J.MATDES.2023.111952.
[157] Y. heng Fei *et al.*, "Feasibility of sewage sludge derived hydrochars for agricultural application: Nutrients (N, P, K) and potentially toxic elements (Zn, Cu, Pb, Ni, Cd)," *Chemosphere*, vol. 236, p. 124841, Dec. 2019, doi: 10.1016/J.CHEMOSPHERE.2019.124841.
[158] M. T. Reza, E. Rottler, L. Herklotz, and B. Wirth, "Hydrothermal carbonization (HTC) of wheat straw: Influence of feedwater pH prepared by acetic acid and potassium hydroxide," *Bioresour Technol*, vol. 182, pp. 336–344, Apr. 2015, doi: 10.1016/J.BIORTECH.2015.02.024.
[159] Z. Heidarinejad, M. H. Dehghani, M. Heidari, G. Javedan, I. Ali, and M. Sillanpää, "Methods for preparation and activation of activated carbon: a review," *Environmental Chemistry Letters 2020 18:2*, vol. 18, no. 2, pp. 393–415, Jan. 2020, doi: 10.1007/S10311-019-00955-0.

[160] M. James, W. Yuan, M. D. Boyette, D. Wang, and A. Kumar, “Characterization of biochar from rice hulls and wood chips produced in a top-lit updraft biomass gasifier,” *Trans ASABE*, vol. 59, no. 3, pp. 749–756, Jan. 2016, doi: 10.13031/TRANS.59.11631.
[161] K. S. W. Sing *et al.*, “Reporting Physisorption Data for Gas/Solid Systems with Special Reference to the Determination of Surface Area and Porosity,” *Pure and Applied Chemistry*, vol. 57, no. 4, pp. 603–619, Jan. 1985, doi: 10.1351/PAC198557040603/MACHINEREADABLECITATION/RIS.
[162] R. Khoshbouy, F. Takahashi, and K. Yoshikawa, “Preparation of high surface area sludge-based activated hydrochar via hydrothermal carbonization and application in the removal of basic dye,” *Environ Res*, vol. 175, pp. 457–467, Aug. 2019, doi: 10.1016/J.ENVRES.2019.04.002.
[163] N. U. Saqib, S. Baroutian, and A. K. Sarmah, “Physicochemical, structural and combustion characterization of food waste hydrochar obtained by hydrothermal carbonization,” *Bioresour Technol*, vol. 266, pp. 357–363, Oct. 2018, doi: 10.1016/J.BIORTECH.2018.06.112.
[164] W. Stumm and J. Morgan, *Aquatic chemistry: chemical equilibria and rates in natural waters*. 2012. Accessed: Dec. 07, 2023. [Online]. Available: https://books.google.com/books?hl=en&lr=&id=NLV_yfulgkQC&oi=fnd&pg=PT14&ots=cMYW3pe7JB&sig=evCRo6NFokQ2OGBVdvj-jZ1nNqo
[165] L. W. Zelazny, L. He, and A. M. Vanwormhoudt, “Charge analysis of soils and anion exchange,” *Methods of Soil Analysis, Part 3: Chemical Methods*, pp. 1231–1253, Jan. 2018, doi: 10.2136/SSSABOOKSER5.3.C41.
[166] G. Sposito, *The chemistry of soils*. 2008. Accessed: Dec. 07, 2023. [Online]. Available: https://books.google.com/books?hl=en&lr=&id=XCJnDAAAQBAJ&oi=fnd&pg=PR9&ots=Ilk4b0A24v&sig=mDZCWIsCA_vqUwRO6KfD-4cc8XE
[167] E. N. Bakatula, D. Richard, C. M. Neculita, and G. J. Zagury, “Determination of point of zero charge of natural organic materials,” *Environmental Science and Pollution Research*, vol. 25, no. 8, pp. 7823–7833, Mar. 2018, doi: 10.1007/S11356-017-1115-7/FIGURES/4.
[168] G. Sposito, “On points of zero charge,” *Environ Sci Technol*, vol. 32, no. 19, pp. 2815–2819, Oct. 1998, doi: 10.1021/ES9802347.
[169] T. Mahmood, M. T. Saddique, A. Naeem, P. Westerhoff, S. Mustafa, and A. Alum, “Comparison of different methods for the point of zero charge determination of NiO,” *Ind Eng Chem Res*, vol. 50, no. 17, pp. 10017–10023, Sep. 2011, doi: 10.1021/IE200271D/ASSET/IMAGES/LARGE/IE-2011-00271D_0011.JPEG.
[170] W. F. Tan, S. J. Lu, F. Liu, X. H. Feng, J. Z. He, and L. K. Koopal, “Determination of the point-of-zero charge of manganese oxides with different methods including an improved salt titration method,” *Soil Sci*, vol. 173, no. 4, pp. 277–286, Apr. 2008, doi: 10.1097/SS.0B013E31816D1F12.
[171] van Krevelen DW, “Graphical-statistical model for the study of structure and reaction processes of coal,” *Fuel*, vol. 29, pp. 269–284, 1950.
[172] Z. Liu, A. Quek, S. Kent Hoekman, and R. Balasubramanian, “Production of solid biochar fuel from waste biomass by hydrothermal carbonization,” *Fuel*, vol. 103, pp. 943–949, Jan. 2013, doi: 10.1016/J.FUEL.2012.07.069.
[173] EBC, “European Biochar Certificate - Guidelines for a Sustainable Production of Biochar,” Frick, Switzerland, Apr. 2023.

[174] W. Plazinski and W. Rudzinski, “Kinetics of Adsorption at Solid/Solution Interfaces Controlled by Intraparticle Diffusion: A Theoretical Analysis,” *Journal of Physical Chemistry C*, vol. 113, no. 28, pp. 12495–12501, Jul. 2009, doi: 10.1021/JP902914Z.
[175] J. P. Vareda, “On validity, physical meaning, mechanism insights and regression of adsorption kinetic models,” *J Mol Liq*, vol. 376, p. 121416, Apr. 2023, doi: 10.1016/J.MOLLIQ.2023.121416.
[176] D. M. Ruthven, “Fundamentals of adsorption equilibrium and kinetics in microporous solids,” *Molecular Sieves - Science and Technology*, vol. 7, pp. 1–43, 2008, doi: 10.1007/3829_007/COVER.
[177] J. S. Piccin, T. R. S. A. Cadaval, L. A. A. De Pinto, and G. L. Dotto, “Adsorption isotherms in liquid phase: Experimental, modeling, and interpretations,” *Adsorption Processes for Water Treatment and Purification*, pp. 19–51, Jul. 2017, doi: 10.1007/978-3-319-58136-1_2/FIGURES/7.
[178] M. Niinipuu, “Tailoring residue-derived carbon materials for the removal of wastewater contaminants,” Umea University, Umea, 2019.
[179] C. Pelekani and V. L. Snoeyink, “Competitive adsorption between atrazine and methylene blue on activated carbon: the importance of pore size distribution,” *Carbon N Y*, vol. 38, no. 10, pp. 1423–1436, Jan. 2000, doi: 10.1016/S0008-6223(99)00261-4.
[180] Pubchem, “Methylene Blue.” Accessed: Dec. 28, 2023. [Online]. Available: https://pubchem.ncbi.nlm.nih.gov/compound/6099#section=Computed-Properties
[181] A. Bensedira, N. Haddaoui, R. Doufnoune, O. Meziane, and N. S. Labidi, “Study of methylene blue dye elimination from water using polyaniline (PANI) and PANI/SiO_2 composite,” *Polymers and Polymer Composites*, vol. 30, p. 096739112211417, Jan. 2022, doi: 10.1177/09673911221141747.
[182] Y. Y. Lau, Y. S. Wong, T. T. Teng, N. Morad, M. Rafatullah, and S. A. Ong, “Degradation of cationic and anionic dyes in coagulation-flocculation process using bi-functionalized silica hybrid with aluminum-ferric as auxiliary agent,” *RSC Adv*, vol. 5, no. 43, pp. 34206–34215, 2015, doi: 10.1039/C5RA01346A.
[183] Pubchem, “Methyl orange .” Accessed: Dec. 28, 2023. [Online]. Available: https://pubchem.ncbi.nlm.nih.gov/compound/Methyl-orange
[184] Y. Sun *et al.*, “Effects of feedstock type, production method, and pyrolysis temperature on biochar and hydrochar properties,” 2013, doi: 10.1016/j.cej.2013.10.081.
[185] J. Fang, B. Gao, J. Chen, and A. R. Zimmerman, “Hydrochars derived from plant biomass under various conditions: Characterization and potential applications and impacts,” 2015, doi: 10.1016/j.cej.2015.01.026.
[186] I. Bargmann, M. C. Rillig, W. Buss, A. Kruse, and M. Kuecke, “Hydrochar and biochar effects on germination of spring barley,” *J Agron Crop Sci*, vol. 199, no. 5, pp. 360–373, Oct. 2013, doi: 10.1111/JAC.12024.
[187] W. Buss and M. Sek, “Mobile organic compounds in biochar - A potential source of contamination - Phytotoxic effects on cress seed (Lepidium sativum) germination,” *J Environ Manage*, vol. 137, pp. 111–119, 2014, doi: 10.1016/j.jenvman.2014.01.045.
[188] K. Sun, K. Ro, M. Guo, J. Novak, H. Mashayekhi, and B. Xing, “Sorption of bisphenol A, 17a-ethinyl estradiol and phenanthrene on thermally and hydrothermally produced biochars,” 2011, doi: 10.1016/j.biortech.2011.03.038.
[189] L. Han *et al.*, “New evidence for high sorption capacity of hydrochar for hydrophobic organic pollutants,” *Environ Sci Technol*, vol. 50, no. 24, pp. 13274–13282, Dec. 2016, doi: 10.1021/ACS.EST.6B02401/SUPPL_FILE/ES6B02401_SI_001.PDF.

[190] J. Fang, L. Zhan, Y. S. Ok, and B. Gao, “Minireview of potential applications of hydrochar derived from hydrothermal carbonization of biomass,” *Journal of Industrial and Engineering Chemistry*, vol. 57, pp. 15–21, Jan. 2018, doi: 10.1016/J.JIEC.2017.08.026.
[191] X. Zhu, F. Qian, Y. Liu, S. Zhang, and J. Chen, “Environmental performances of hydrochar-derived magnetic carbon composite affected by its carbonaceous precursor,” *RSC Adv*, vol. 5, no. 75, pp. 60713–60722, Jan. 2015, doi: 10.1039/c5ra07339a.
[192] M. Zhang, B. Gao, J. Fang, A. E. Creamer, and J. L. Ullman, “Self-assembly of needle-like layered double hydroxide (LDH) nanocrystals on hydrochar: characterization and phosphate removal ability,” *RSC Adv*, vol. 4, no. 53, pp. 28171–28175, Jun. 2014, doi: 10.1039/C4RA02332C.
[193] X. Zhu, Y. Liu, F. Qian, C. Zhou, S. Zhang, and J. Chen, “Role of Hydrochar Properties on the Porosity of Hydrochar-based Porous Carbon for Their Sustainable Application,” *ACS Sustain Chem Eng*, vol. 3, no. 5, pp. 833–840, May 2015, doi: 10.1021/ACSSUSCHEMENG.5B00153/SUPPL_FILE/SC5B00153_SI_001.PDF.
[194] M. Sevilla and A. B. Fuertes, “A Green Approach to High-Performance Supercapacitor Electrodes: The Chemical Activation of Hydrochar with Potassium Bicarbonate,” *ChemSusChem*, vol. 9, no. 14, pp. 1880–1888, Jul. 2016, doi: 10.1002/CSSC.201600426.
[195] X. Zhu, Y. Liu, G. Luo, F. Qian, S. Zhang, and J. Chen, “Facile fabrication of magnetic carbon composites from hydrochar via simultaneous activation and magnetization for triclosan adsorption,” *Environ Sci Technol*, vol. 48, no. 10, pp. 5840–5848, May 2014, doi: 10.1021/ES500531C/SUPPL_FILE/ES500531C_SI_001.PDF.
[196] K. Sun, J. Tang, Y. Gong, and H. Zhang, “Characterization of potassium hydroxide (KOH) modified hydrochars from different feedstocks for enhanced removal of heavy metals from water,” *Environmental Science and Pollution Research*, vol. 22, no. 21, pp. 16640–16651, Jun. 2015, doi: 10.1007/S11356-015-4849-0/FIGURES/9.
[197] J. Fang, B. Gao, A. R. Zimmerman, K. S. Ro, and J. Chen, “Physically (CO2) activated hydrochars from hickory and peanut hull: Preparation, characterization, and sorption of methylene blue, lead, copper, and cadmium,” *RSC Adv*, vol. 6, no. 30, pp. 24906–24911, Jan. 2016, doi: 10.1039/c6ra01644h.
[198] F. Qian *et al.*, “Synthesis, characterization and adsorption capacity of magnetic carbon composites activated by CO 2 : implication for the catalytic mechanisms of iron salts †,” 2016, doi: 10.1039/c6ta06614c.
[199] Q. Zhu *et al.*, “Biochar derived from hydrolysis of sewage sludge influences soil properties and heavy metals distributed in the soil,” *J Hazard Mater*, vol. 442, p. 130053, Jan. 2023, doi: 10.1016/J.JHAZMAT.2022.130053.
[200] J. Huang *et al.*, “A bibliographic study reviewing the last decade of hydrochar in environmental application: history, status quo, and trending research paths,” *Biochar 2023 5:1*, vol. 5, no. 1, pp. 1–27, Mar. 2023, doi: 10.1007/S42773-023-00210-4.
[201] Y. Yao, B. Gao, J. Chen, and L. Yang, “Engineered biochar reclaiming phosphate from aqueous solutions: Mechanisms and potential application as a slow-release fertilizer,” *Environ Sci Technol*, vol. 47, no. 15, pp. 8700–8708, Aug. 2013, doi: 10.1021/ES4012977/SUPPL_FILE/ES4012977_SI_001.PDF.
[202] I. Bargmann, M. C. Rillig, A. Kruse, J. M. Greef, and M. Kücke, “Initial and subsequent effects of hydrochar amendment on germination and nitrogen uptake of spring barley,” *Journal of Plant Nutrition and Soil Science*, vol. 177, no. 1, pp. 68–74, Feb. 2014, doi: 10.1002/JPLN.201300160.

[203] A. Gajić and H.-J. Koch, “Sugar Beet (Beta vulgaris L.) Growth Reduction Caused by Hydrochar Is Related to Nitrogen Supply,” *J Environ Qual*, vol. 41, no. 4, pp. 1067–1075, Jul. 2012, doi: 10.2134/JEQ2011.0237.
[204] C. Naisse *et al.*, “Can biochar and hydrochar stability be assessed with chemical methods?,” 2013, doi: 10.1016/j.orggeochem.2013.04.011.
[205] M. Schulze, J. Mumme, A. Funke, and J. Kern, “Effects of selected process conditions on the stability of hydrochar in low-carbon sandy soil,” 2016, doi: 10.1016/j.geoderma.2015.12.018.
[206] Z. Liu, Y. Guo, R. Balasubramanian, and S. K. Hoekman, “Mechanical stability and combustion characteristics of hydrochar/lignite blend pellets,” 2015, doi: 10.1016/j.fuel.2015.10.004.
[207] J. W. Chung, J. W. Foppen, G. Gerner, R. Krebs, and P. N. L. Lens, “Removal of rotavirus and adenovirus from artificial ground water using hydrochar derived from sewage sludge,” *J Appl Microbiol*, vol. 119, no. 3, pp. 876–884, Sep. 2015, doi: 10.1111/JAM.12863.
[208] J.-H. Zhang, Q.-M. Lin, and X.-R. Zhao, “The Hydrochar Characters of Municipal Sewage Sludge Under Different Hydrothermal Temperatures and Durations,” *J Integr Agric*, vol. 13, no. 3, pp. 471–482, 2014, doi: 10.1016/S2095-3119(13)60702-9.
[209] S. Abel, A. Peters, S. Trinks, H. Schonsky, M. Facklam, and G. Wessolek, “Impact of biochar and hydrochar addition on water retention and water repellency of sandy soil,” *Geoderma*, vol. 202–203, pp. 183–191, Jul. 2013, doi: 10.1016/J.GEODERMA.2013.03.003.
[210] A. D. Igalavithana *et al.*, “Effect of Corn Residue Biochar on the Hydraulic Properties of Sandy Loam Soil,” *Sustainability 2017, Vol. 9, Page 266*, vol. 9, no. 2, p. 266, Feb. 2017, doi: 10.3390/SU9020266.
[211] D. Bona *et al.*, “Evaluating the potential of hydrochar as a soil amendment,” *Waste Management*, vol. 159, pp. 75–83, Mar. 2023, doi: 10.1016/J.WASMAN.2023.01.024.
[212] D. Wüst, C. R. Correa, D. Jung, M. Zimmermann, A. Kruse, and L. Fiori, “Understanding the influence of biomass particle size and reaction medium on the formation pathways of hydrochar,” *Biomass Convers Biorefin*, vol. 10, no. 4, pp. 1357–1380, Dec. 2020, doi: 10.1007/S13399-019-00488-0/FIGURES/13.
[213] M. Lucian, M. Volpe, L. Gao, G. Piro, J. L. Goldfarb, and L. Fiori, “Impact of hydrothermal carbonization conditions on the formation of hydrochars and secondary chars from the organic fraction of municipal solid waste,” 2018, doi: 10.1016/j.fuel.2018.06.060.
[214] A. R. Zimmerman, B. Gao, and M.-Y. Ahn, “Positive and negative carbon mineralization priming effects among a variety of biochar-amended soils,” 2011, doi: 10.1016/j.soilbio.2011.02.005.
[215] S. Mandal *et al.*, “Designing advanced biochar products for maximizing greenhouse gas mitigation potential,” *Crit Rev Environ Sci Technol*, vol. 46, no. 17, pp. 1367–1401, Sep. 2016, doi: 10.1080/10643389.2016.1239975.
[216] S. Malghani, G. Gleixner, and S. E. Trumbore, “Chars produced by slow pyrolysis and hydrothermal carbonization vary in carbon sequestration potential and greenhouse gases emissions,” *Soil Biol Biochem*, vol. 62, pp. 137–146, Jul. 2013, doi: 10.1016/J.SOILBIO.2013.03.013.
[217] C. Kammann, S. Ratering, C. Eckhard, and C. Müller, “Biochar and Hydrochar Effects on Greenhouse Gas (Carbon Dioxide, Nitrous Oxide, and Methane) Fluxes from Soils,” *J Environ Qual*, vol. 41, no. 4, pp. 1052–1066, Jul. 2012, doi: 10.2134/JEQ2011.0132.

[218] S. Baronti *et al.*, “Hydrochar enhances growth of poplar for bioenergy while marginally contributing to direct soil carbon sequestration,” *GCB Bioenergy*, vol. 9, no. 11, pp. 1618–1626, Nov. 2017, doi: 10.1111/gcbb.12450.
[219] J. Jia *et al.*, “Functionalization of supercapacitors electrodes oriented hydrochar from cornstalk: A new vision via biomass fraction,” *Biomass Bioenergy*, vol. 175, p. 106858, Aug. 2023, doi: 10.1016/J.BIOMBIOE.2023.106858.
[220] J. Liu, X. Chen, S. Cao, and H. Yang, “Overview on hybrid solar photovoltaic-electrical energy storage technologies for power supply to buildings,” *Energy Convers Manag*, vol. 187, pp. 103–121, May 2019, doi: 10.1016/J.ENCONMAN.2019.02.080.
[221] J. Libich, J. Máca, J. Vondrák, O. Čech, and M. Sedlaříková, “Supercapacitors: Properties and applications,” *J Energy Storage*, vol. 17, pp. 224–227, Jun. 2018, doi: 10.1016/J.EST.2018.03.012.
[222] X. Li, J. Zhang, B. Liu, and Z. Su, “A critical review on the application and recent developments of post-modified biochar in supercapacitors,” *J Clean Prod*, vol. 310, p. 127428, 2021, doi: 10.1016/j.jclepro.2021.127428.
[223] L. Ding, Z. Wang, Y. Li, Y. Du, H. Liu, and Y. Guo, “A novel hydrochar and nickel composite for the electrochemical supercapacitor electrode material,” *Mater Lett*, vol. 74, pp. 111–114, May 2012, doi: 10.1016/J.MATLET.2012.01.070.
[224] J. Lu *et al.*, “Hierarchical porous carbon for high-performance capacitor derived from sewage sludge by KHCO3 activation,” *J Energy Storag*e, vol. 50, p. 104644, Jun. 2022, doi: 10.1016/J.EST.2022.104644.
[225] X. Cao, S. Sun, and R. Sun, “Application of biochar-based catalysts in biomass upgrading: a review,” *RSC Adv*, vol. 7, no. 77, pp. 48793–48805, Oct. 2017, doi: 10.1039/C7RA09307A.
[226] C. A. Che and P. M. Heynderickx, “Hydrothermal carbonization of plastic waste: A review of its potential in alternative energy applications,” *Fuel Communications*, vol. 18, p. 100103, Mar. 2024, doi: 10.1016/J.JFUECO.2023.100103.
[227] N. Saha, A. Saba, and M. T. Reza, “Effect of hydrothermal carbonization temperature on pH, dissociation constants, and acidic functional groups on hydrochar from cellulose and wood,” *J Anal Appl Pyrolysis*, vol. 137, pp. 138–145, Jan. 2019, doi: 10.1016/J.JAAP.2018.11.018.
[228] B. Ghanim *et al.*, “Application of KOH modified seaweed hydrochar as a biosorbent of Vanadium from aqueous solution: Characterisations, mechanisms and regeneration capacity,” *J Environ Chem Eng*, vol. 8, no. 5, p. 104176, Oct. 2020, doi: 10.1016/J.JECE.2020.104176.
[229] “Propagation of uncertainty - Wikipedia.” Accessed: Jan. 31, 2024. [Online]. Available: https://en.wikipedia.org/wiki/Propagation_of_uncertainty#cite_note-17
[230] S. A. Channiwala and P. P. Parikh, “A unified correlation for estimating HHV of solid, liquid and gaseous fuels,” *Fuel*, vol. 81, no. 8, pp. 1051–1063, May 2002, doi: 10.1016/S0016-2361(01)00131-4.
[231] R.-F. Chen *et al.*, “Effect of Organic Substances on Nutrients Recovery by Struvite Electrochemical Precipitation from Synthetic Anaerobically Treated Swine Wastewater,” 2021, doi: 10.3390/membranes.
[232] E. T. Urbansky and M. R. Schock, “Understanding, Deriving, and Computing Buffer Capacity,” *Journal of Chemical Education* •, vol. 77, no. 12, 2000, [Online]. Available: https://pubs.acs.org/sharingguidelines

[233] R. De Levie, “Estimating Parameter Precision in Nonlinear Least Squares with Excel’s Solver,” *J Chem Educ*, vol. 76, no. 11, pp. 1594–1598, 1999, doi: 10.1021/ED076P1594.
[234] J. Debord, M. Harel, J. C. Bollinger, and K. H. Chu, “The Elovich isotherm equation: Back to the roots and new developments,” *Chem Eng Sci*, vol. 262, p. 118012, Nov. 2022, doi: 10.1016/J.CES.2022.118012.
[235] I. Langmuir, “The adsorption of gases on plane surfaces of glass, mica and platinum,” *J Am Chem Soc*, vol. 40, no. 9, pp. 1361–1403, Sep. 1918, doi: 10.1021/JA02242A004/ASSET/JA02242A004.FP.PNG_V03.
[236] M. T. Yagub, T. K. Sen, S. Afroze, and H. M. Ang, “Dye and its removal from aqueous solution by adsorption: A review,” *Adv Colloid Interface Sci*, vol. 209, pp. 172–184, Jul. 2014, doi: 10.1016/J.CIS.2014.04.002.
[237] J. De Smedt, P. M. Heynderickx, P. J. Arauzo, and F. Ronsse, “Adsorption mechanism of different dyes on chemical activated carbon as quantitative assessment for wastewater treatment: Comparative study between ZnCl2 and its eutectic,” *Sep Purif Technol*, vol. 334, p. 126002, Apr. 2024, doi: 10.1016/J.SEPPUR.2023.126002.
[238] P. Ehiomogue, I. I. Ahuchaogu, and I. E. Ahaneku, “Review of Adsorption Isotherms Models,” *ACTA TECHNICA CORVINIENSIS - Bulletin of Engineering*, vol. XIV, Oct. 2021.
[239] N. Ayawei, A. N. Ebelegi, and D. Wankasi, “Modelling and Interpretation of Adsorption Isotherms,” *J Chem*, vol. 2017, 2017, doi: 10.1155/2017/3039817.
[240] J. Wang and X. Guo, “Adsorption kinetic models: Physical meanings, applications, and solving methods,” *J Hazard Mater*, vol. 390, p. 122156, May 2020, doi: 10.1016/J.JHAZMAT.2020.122156.
[241] N. Khan, S. Mohan, and P. Dinesha, “Regimes of hydrochar yield from hydrothermal degradation of various lignocellulosic biomass: A review,” *J Clean Prod*, vol. 288, p. 125629, Mar. 2021, doi: 10.1016/J.JCLEPRO.2020.125629.
[242] J. Akhtar and N. A. S. Amin, “A review on process conditions for optimum bio-oil yield in hydrothermal liquefaction of biomass,” *Renewable and Sustainable Energy Reviews*, vol. 15, no. 3, pp. 1615–1624, Apr. 2011, doi: 10.1016/J.RSER.2010.11.054.
[243] J. M. Novak *et al.*, “Characterization of Designer Biochar Produced at Different Temperatures and Their Effects on a Loamy Sand,” *Annals of Environmental Science*, vol. 3, pp. 195–206, Nov. 2009, Accessed: Jan. 23, 2024. [Online]. Available: https://openjournals.neu.edu/aes/journal/article/view/v3art5
[244] Y. Shinogi and Y. Kanri, “Pyrolysis of plant, animal and human waste: physical and chemical characterization of the pyrolytic products,” *Bioresour Technol*, vol. 90, no. 3, pp. 241–247, Dec. 2003, doi: 10.1016/S0960-8524(03)00147-0.
[245] O. S. Djandja *et al.*, “Catalytic hydrothermal carbonization of wet organic solid waste: A review,” *Science of The Total Environment*, vol. 873, p. 162119, May 2023, doi: 10.1016/J.SCITOTENV.2023.162119.
[246] X. Xu *et al.*, “The correlation of physicochemical properties and combustion performance of hydrochar with fixed carbon index,” *Bioresour Technol*, vol. 294, p. 122053, Dec. 2019, doi: 10.1016/J.BIORTECH.2019.122053.
[247] H. Y. Ismail *et al.*, “ANN-Kriging hybrid model for predicting carbon and inorganic phosphorus recovery in hydrothermal carbonization,” *Waste Management*, vol. 85, pp. 242–252, Feb. 2019, doi: 10.1016/J.WASMAN.2018.12.044.
[248] M. J. Alhnidi, D. Wüst, A. Funke, L. Hang, and A. Kruse, “Fate of Nitrogen, Phosphate, and Potassium during Hydrothermal Carbonization and the Potential for Nutrient Recovery,”

ACS Sustain Chem Eng, vol. 8, no. 41, pp. 15507–15516, Oct. 2020, doi: 10.1021/ACSSUSCHEMENG.0C04229/ASSET/IMAGES/LARGE/SC0C04229_0005.JPEG.

[249] X. Zhu *et al.*, "Machine learning-assisted exploration for carbon neutrality potential of municipal sludge recycling via hydrothermal carbonization," *Bioresour Technol*, vol. 369, p. 128454, Feb. 2023, doi: 10.1016/J.BIORTECH.2022.128454.

[250] S. Hosokai, K. Matsuoka, K. Kuramoto, and Y. Suzuki, "Modification of Dulong's formula to estimate heating value of gas, liquid and solid fuels," *Fuel Processing Technology*, vol. 152, pp. 399–405, Nov. 2016, doi: 10.1016/J.FUPROC.2016.06.040.

[251] Y. Gao, J. Remón, and A. S. Matharu, "Microwave-assisted hydrothermal treatments for biomass valorisation: a critical review," *Green Chemistry*, vol. 23, no. 10, pp. 3502–3525, 2021, doi: 10.1039/D1GC00623A.

[252] I. Zambon *et al.*, "An Innovative Agro-Forestry Supply Chain for Residual Biomass: Physicochemical Characterisation of Biochar from Olive and Hazelnut Pellets," *Energies 2016, Vol. 9, Page 526*, vol. 9, no. 7, p. 526, Jul. 2016, doi: 10.3390/EN9070526.

[253] J. Xu, J. Zhang, J. Huang, W. He, and G. Li, "Conversion of phoenix tree leaves into hydro-char by microwave-assisted hydrothermal carbonization," *Bioresour Technol Rep*, vol. 9, p. 100353, Feb. 2020, doi: 10.1016/J.BITEB.2019.100353.

[254] S. Kang, X. Li, J. Fan, and J. Chang, "Characterization of hydrochars produced by hydrothermal carbonization of lignin, cellulose, d-xylose, and wood meal," *Ind Eng Chem Res*, vol. 51, no. 26, pp. 9023–9031, Jul. 2012, doi: 10.1021/IE300565D/ASSET/IMAGES/LARGE/IE-2012-00565D_0011.JPEG.

[255] B. Singh, M. M. Dolk, Q. Shen, and M. Camps-Arbestain, "Biochar pH, electrical conductivity and liming potential," *Biochar: A Guide to Analytical Methods*, no. June 2018, pp. 23–38, 2017, Accessed: Jan. 21, 2024. [Online]. Available: https://ebooks.publish.csiro.au/content/ISBN/9781486305100

[256] V. C. Farmer, "The Infrared Spectra of Minerals," *Mineralogical Society, London*, 1974, doi: 10.1180/MONO-4.

[257] J. Coates, "Interpretation of Infrared Spectra, A Practical Approach," in *Encyclopedia of Analytical Chemistry*, Wiley, 2006. doi: 10.1002/9780470027318.a5606.

[258] M. Keiluweit, P. S. Nico, M. Johnson, and M. Kleber, "Dynamic molecular structure of plant biomass-derived black carbon (biochar)," *Environ Sci Technol*, vol. 44, no. 4, pp. 1247–1253, 2010, doi: 10.1021/ES9031419/SUPPL_FILE/ES9031419_SI_001.PDF.

[259] W. M. Davis, C. L. Erickson, C. T. Johnston, J. J. Delfino, and J. E. Porter, "Quantitative Fourier Transform Infrared spectroscopic investigation humic substance functional group composition," *Chemosphere*, vol. 38, no. 12, pp. 2913–2928, May 1999, doi: 10.1016/S0045-6535(98)00486-X.

[260] T. R. Filley *et al.*, "Comparison of the chemical alteration trajectory of Liriodendron tulipifera L. leaf litter among forests with different earthworm abundance," 2008, Accessed: Jan. 21, 2024. [Online]. Available: http://repository.si.edu/xmlui/handle/10088/18119

[261] S. J. Parikh and J. Chorover, "ATR-FTIR study of lipopolysaccharides at mineral surfaces," *Colloids Surf B Biointerfaces*, vol. 62, no. 2, pp. 188–198, Apr. 2008, doi: 10.1016/J.COLSURFB.2007.10.002.

[262] S. J. Parikh, K. W. Goyne, A. J. Margenot, F. N. D. Mukome, and F. J. Calderón, "Soil chemical insights provided through vibrational spectroscopy," *Advances in Agronomy*, vol. 126, pp. 1–148, 2014, doi: 10.1016/B978-0-12-800132-5.00001-8.

[263] G. Socrates, “Infrared and Raman characteristic group frequencies : tables and charts,” 2001.
[264] G. B. Deacon and R. J. Phillips, “Relationships between the carbon-oxygen stretching frequencies of carboxylato complexes and the type of carboxylate coordination,” *Coord Chem Rev*, vol. 33, no. 3, pp. 227–250, Oct. 1980, doi: 10.1016/S0010-8545(00)80455-5.
[265] S. Krimm, “Vibrational analysis of conformation in peptides, polypeptides, and proteins,” *Biopolymers*, vol. 22, no. 1, pp. 217–225, Jan. 1983, doi: 10.1002/BIP.360220130.
[266] C. T. Johnston, B. Khan, E. F. Barth, S. Chattopadhyay, and S. A. Boyd, “Nature of the interlayer environment in an organoclay optimized for the sequestration of dibenzo-p-dioxin,” *Environ Sci Technol*, vol. 46, no. 17, pp. 9584–9591, Sep. 2012, doi: 10.1021/ES300699Y.
[267] O. R. Harvey, B. E. Herbert, L. J. Kuo, and P. Louchouarn, “Generalized two-dimensional perturbation correlation infrared spectroscopy reveals mechanisms for the development of surface charge and recalcitrance in plant-derived biochars,” *Environ Sci Technol*, vol. 46, no. 19, pp. 10641–10650, Oct. 2012, doi: 10.1021/ES302971D.
[268] Y. Bulut and H. Aydın, “A kinetics and thermodynamics study of methylene blue adsorption on wheat shells,” 2006, doi: 10.1016/j.desal.2005.10.032.
[269] B. K. Nandi, A. Goswami, and M. K. Purkait, “Removal of cationic dyes from aqueous solutions by kaolin: Kinetic and equilibrium studies,” *Appl Clay Sci*, vol. 42, no. 3–4, pp. 583–590, Jan. 2009, doi: 10.1016/J.CLAY.2008.03.015.

8. APPENDICES

8.1. Appendix A: Figures

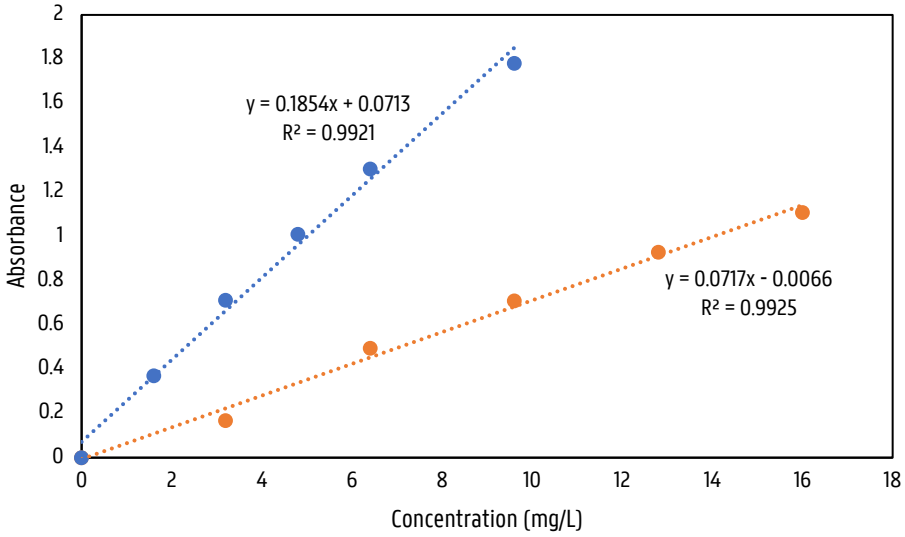

Figure A.1: Calibration curve MB and MO.

(a)

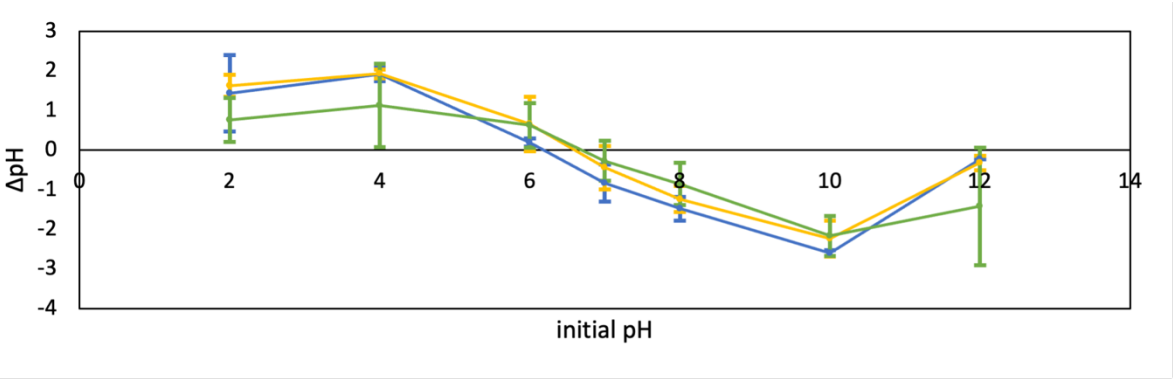
3
2
1
0
-1
-2
-3
-4
ΔpH
0
2
4
6
8
10
12
14
initial pH

(b)

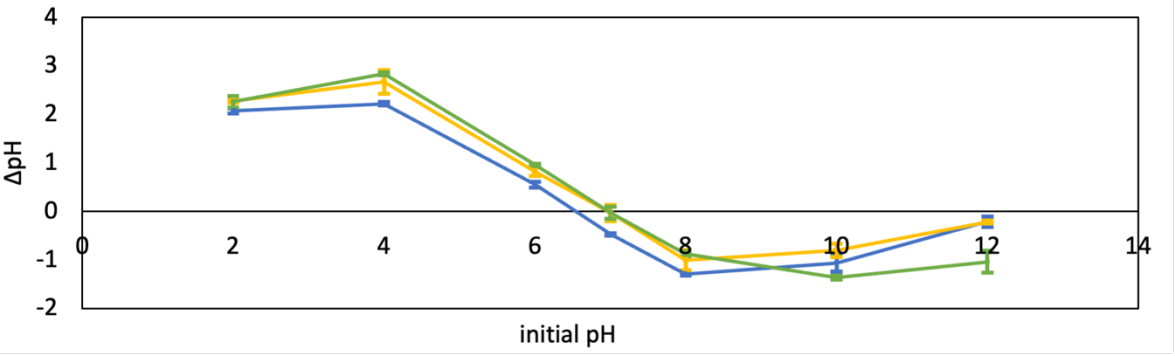
4
3
2
1
0
-1
-2
ΔpH
0
2
4
6
8
10
12
14
initial pH

(c)

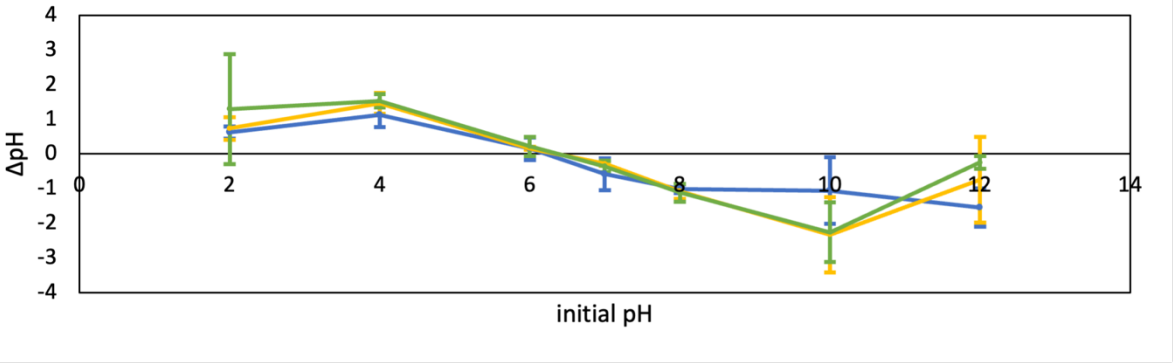
4
3
2
1
0
-1
-2
-3
-4
ΔpH
0
2
4
6
8
10
12
14
initial pH

(d)

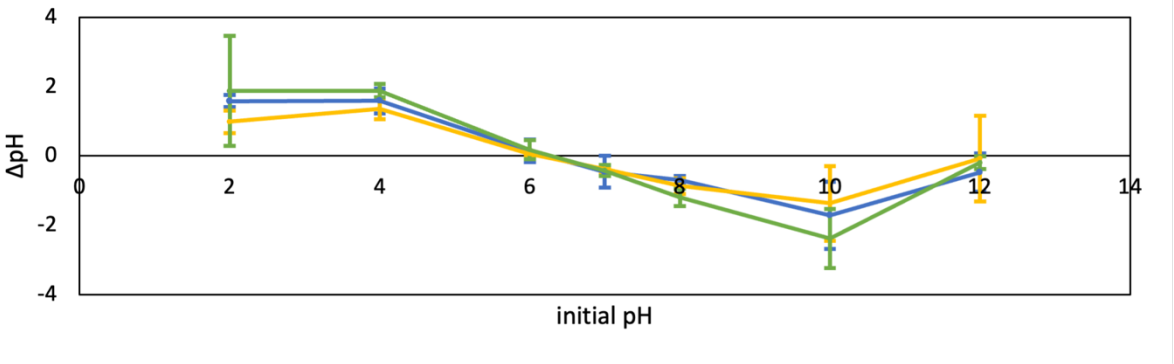
4
2
0
-2
-4
ΔpH
0
2
4
6
8
10
12
14
initial pH

(e)

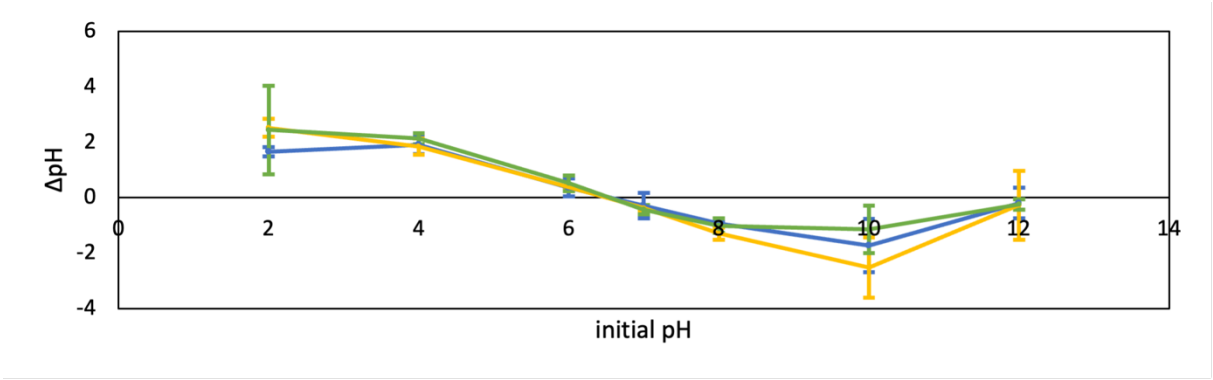

(f)

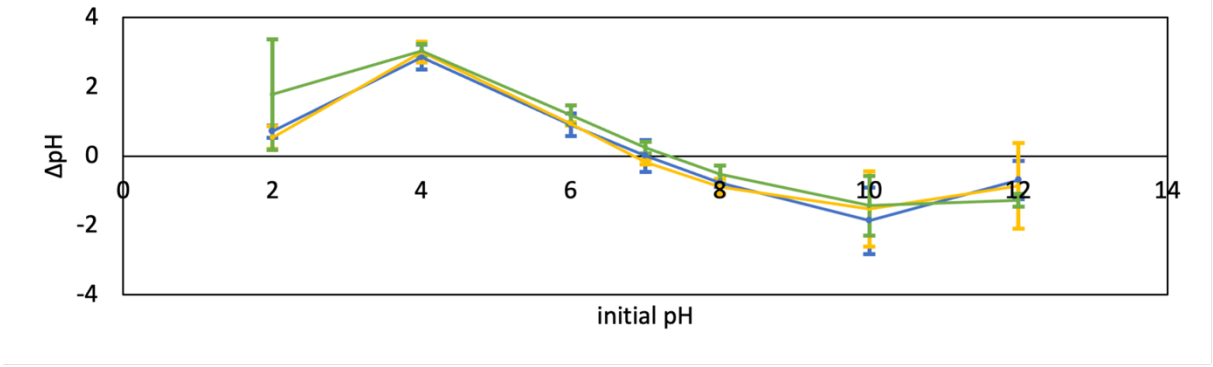

(g)

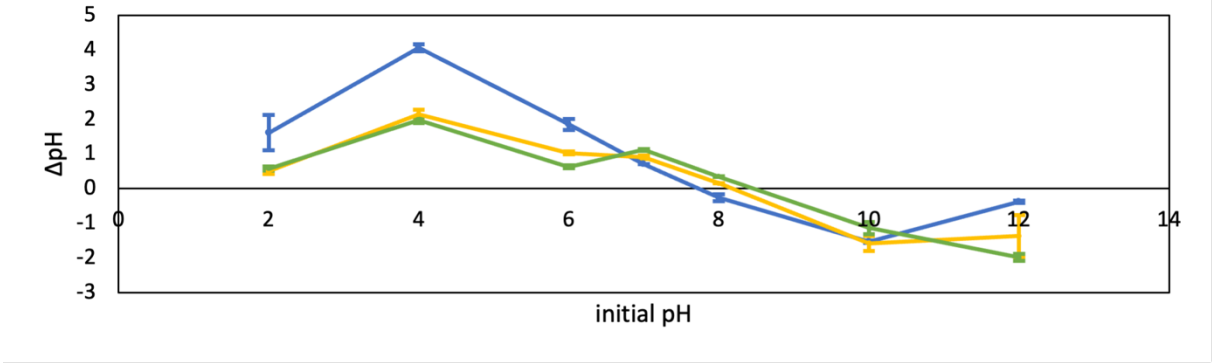

(h)

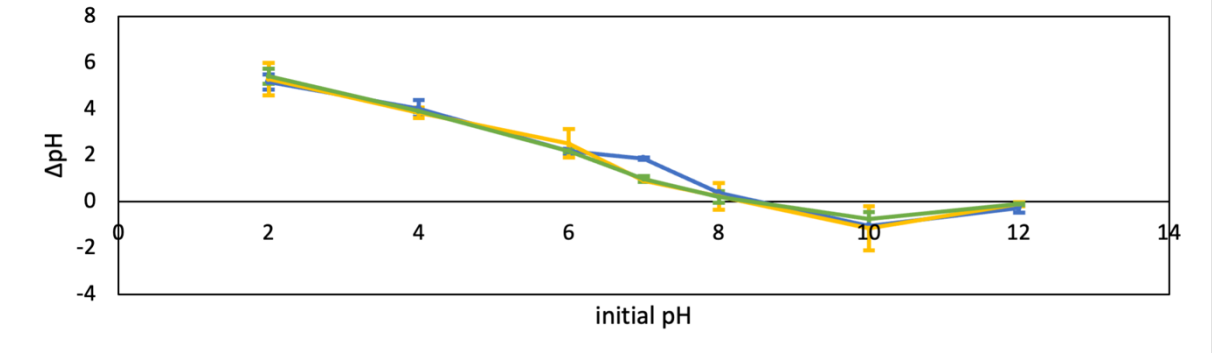

Figure A.2: Point of zero charge graphs (200°C, 220°C, 240°C). (a) chub mackerel, (b) hairtail, (c) yellow corvina, (d) horse mackerel, (e) olive flounder, (f) whiteleg shrimp, (g) tiger prawn, (h) Gazami crab.

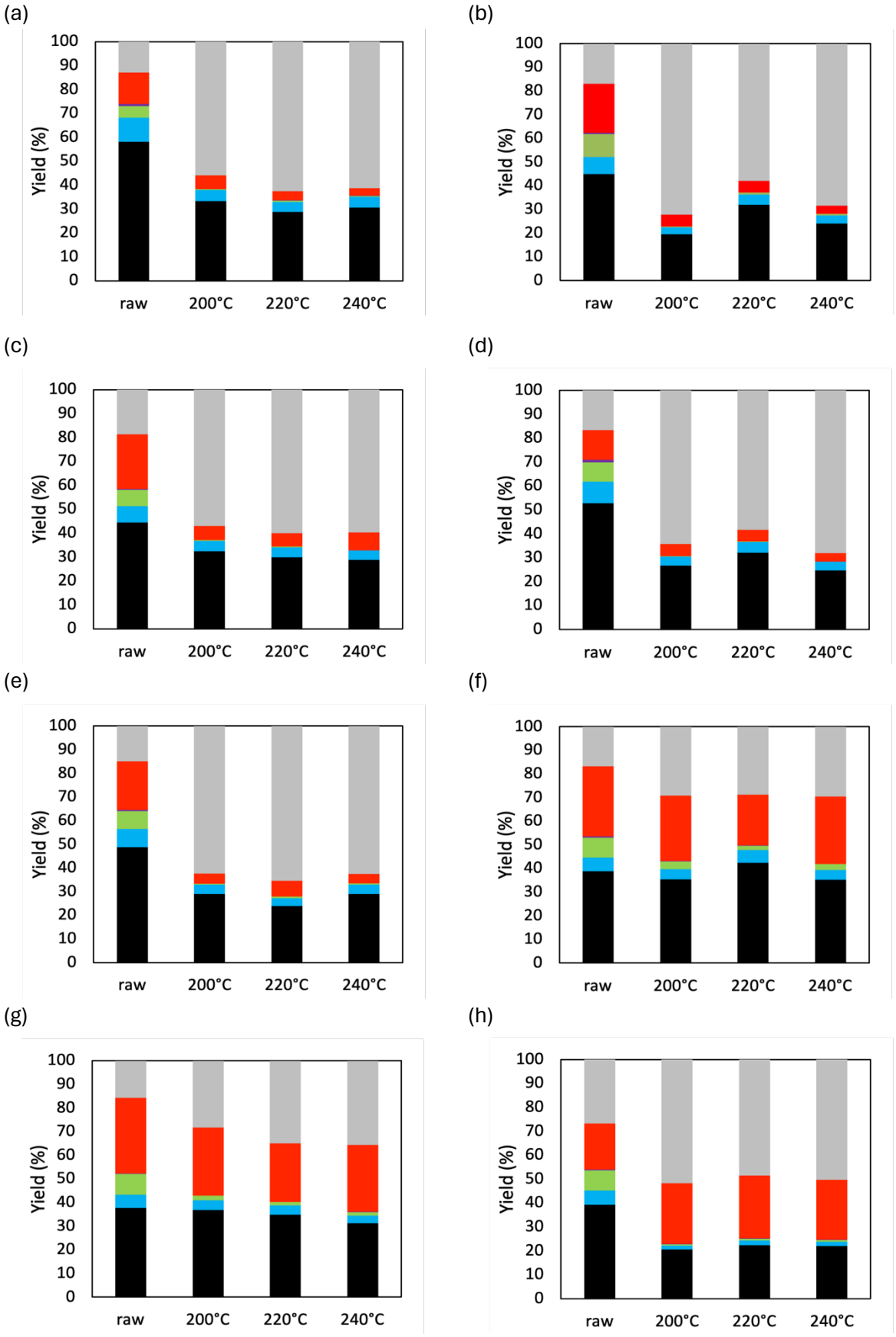

Figure A.3: Elemental analysis of produced hydrochars: carbon (■), hydrogen (■), nitrogen (■), sulphur (■), oxygen (■) and ash (■). (a) chub mackerel, (b) hairtail, (c) yellow corvina, (d) horse mackerel, (e) olive flounder, (f) whiteleg shrimp, (g) tiger prawn, (h) Gazami crab.

(a)

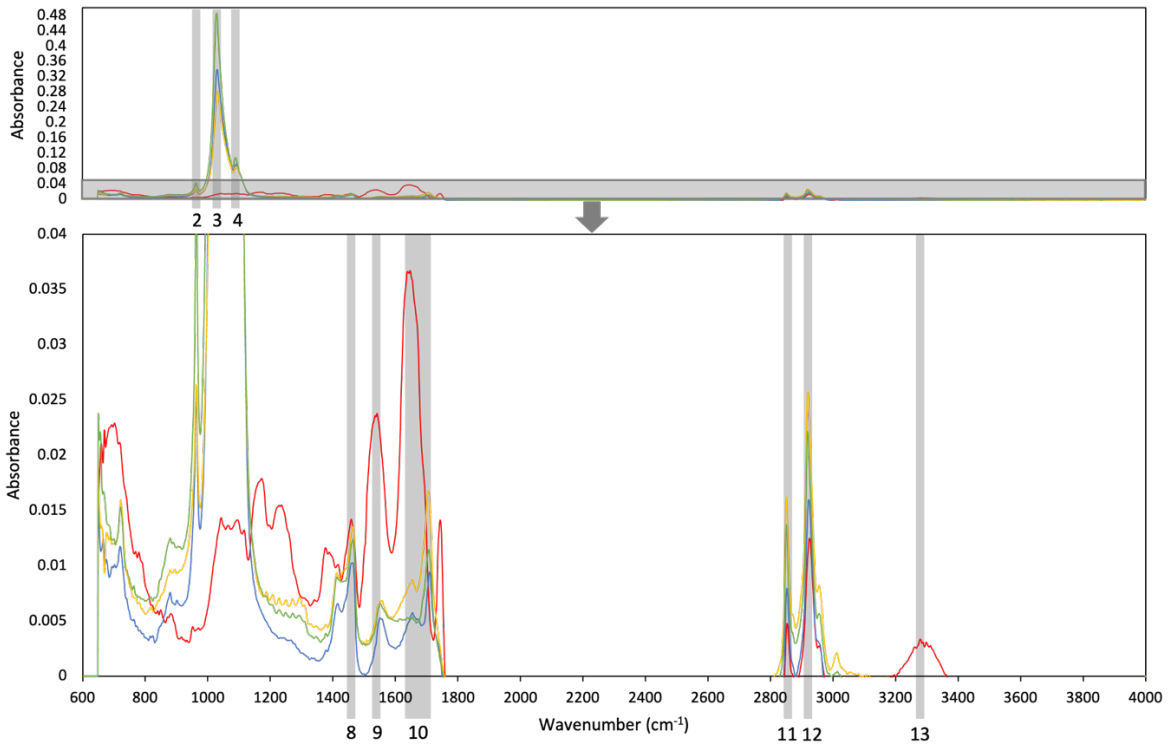
Absorbance
0.48
0.44
0.4
0.36
0.32
0.28
0.24
0.2
0.16
0.12
0.08
0.04
0
2 3 4
0.04
0.035
0.03
0.025
0.02
0.015
0.01
0.005
0
600 800 1000 1200 1400 1600 1800 2000 2200 2400 2600 2800 3000 3200 3400 3600 3800 4000
Wavenumber (cm-1)
8 9 10
11 12
13

(b)

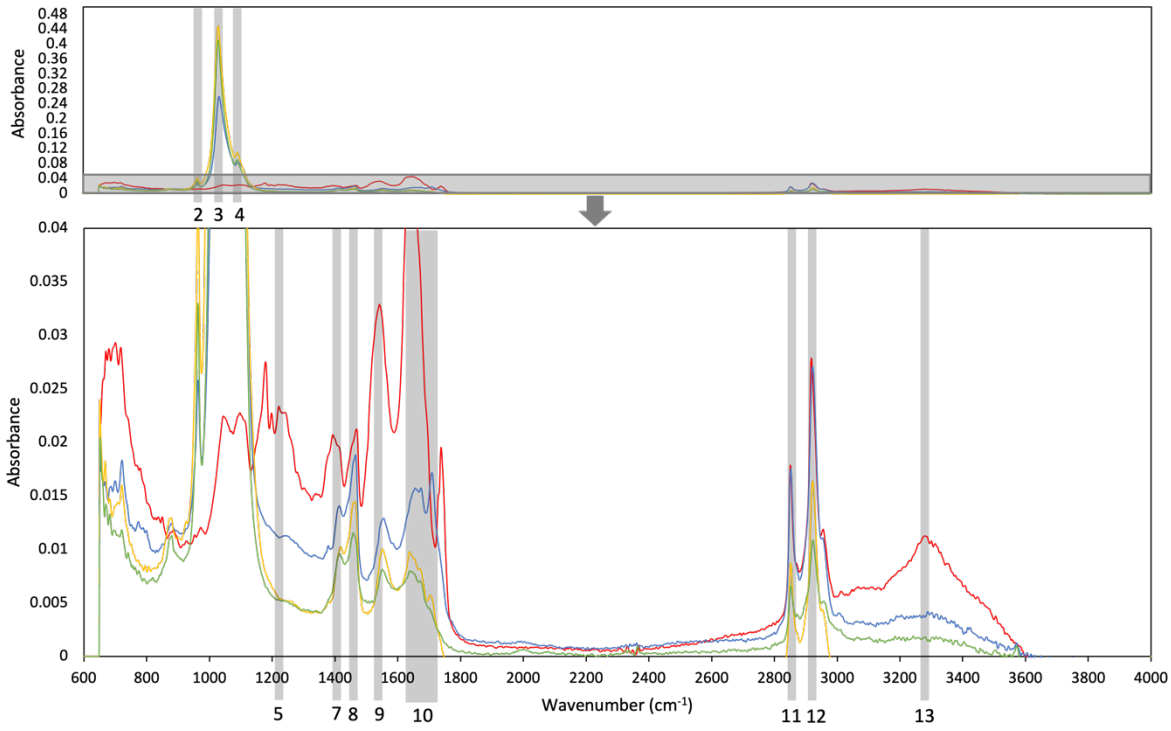
Absorbance
0.48
0.44
0.4
0.36
0.32
0.28
0.24
0.2
0.16
0.12
0.08
0.04
0
2 3 4
0.04
0.035
0.03
0.025
0.02
0.015
0.01
0.005
0
600 800 1000 1200 1400 1600 1800 2000 2200 2400 2600 2800 3000 3200 3400 3600 3800 4000
Wavenumber (cm-1)
5
7 8 9 10
11 12
13

(c)

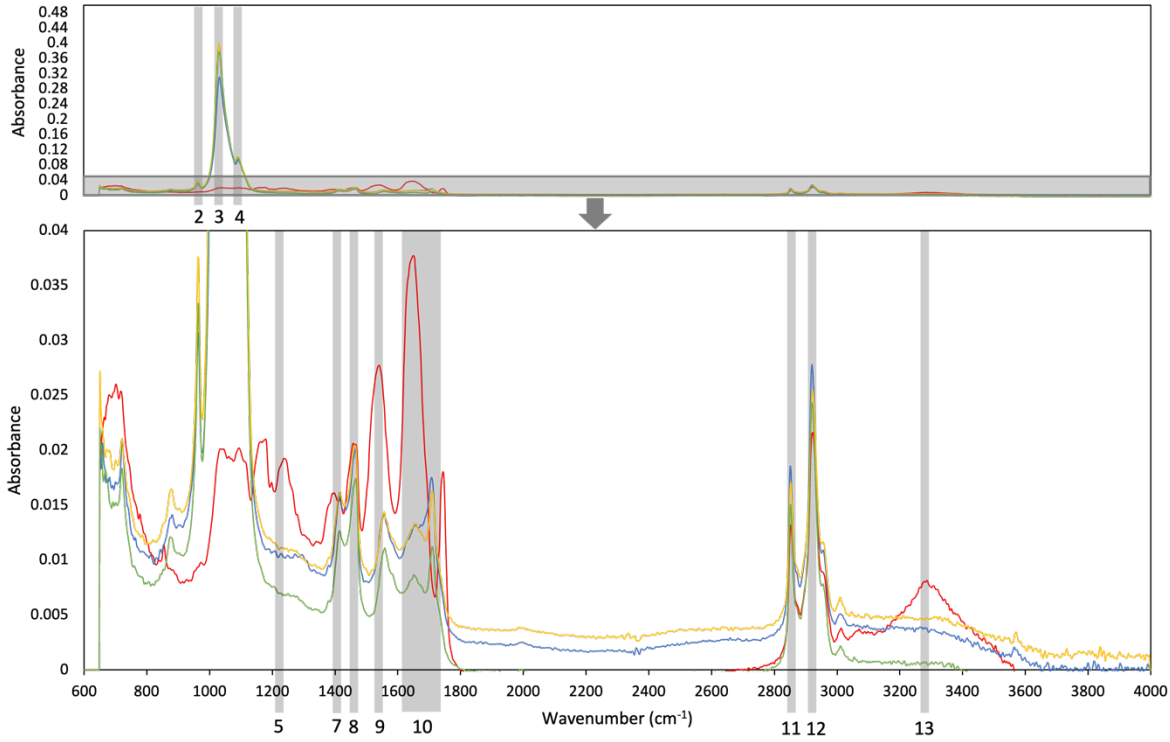
Absorbance
0.48
0.44
0.4
0.36
0.32
0.28
0.24
0.2
0.16
0.12
0.08
0.04
0
2 3 4
0.04
0.035
0.03
0.025
0.02
0.015
0.01
0.005
0
600 800 1000 1200 1400 1600 1800 2000 2200 2400 2600 2800 3000 3200 3400 3600 3800 4000
Wavenumber (cm-1)
5 7 8 9 10 11 12 13

(d)

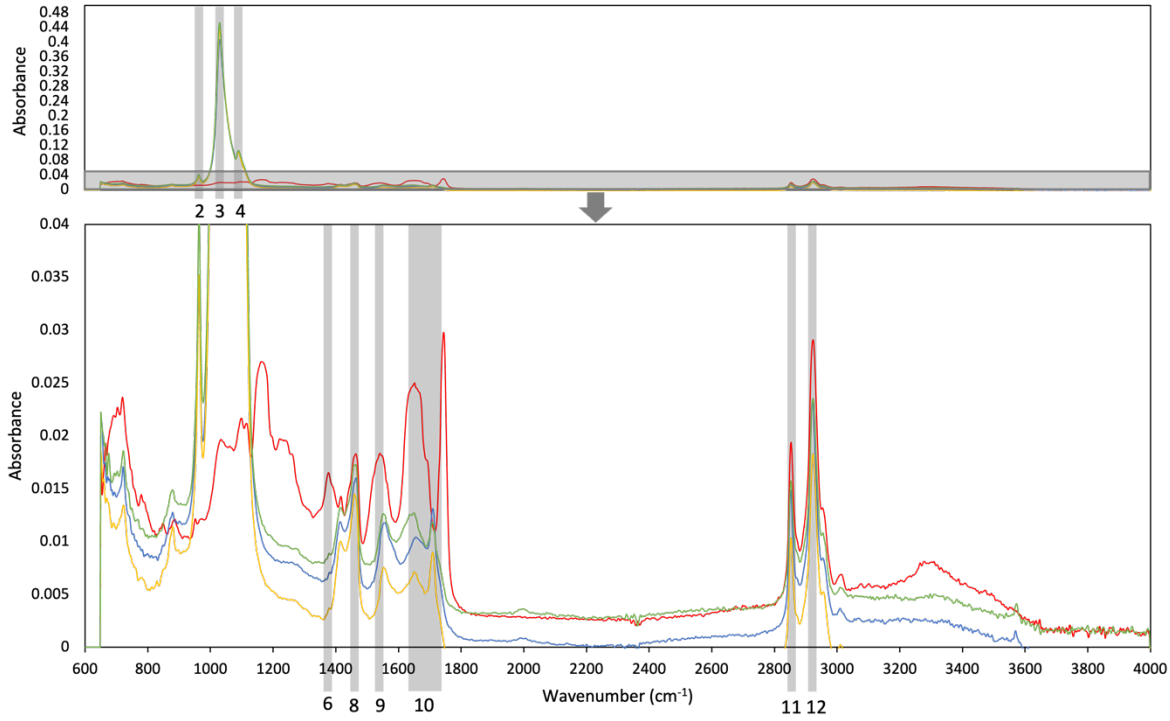
Absorbance
0.48
0.44
0.4
0.36
0.32
0.28
0.24
0.2
0.16
0.12
0.08
0.04
0
2 3 4
0.04
0.035
0.03
0.025
0.02
0.015
0.01
0.005
0
600 800 1000 1200 1400 1600 1800 2000 2200 2400 2600 2800 3000 3200 3400 3600 3800 4000
Wavenumber (cm-1)
6 8 9 10 11 12

(e)

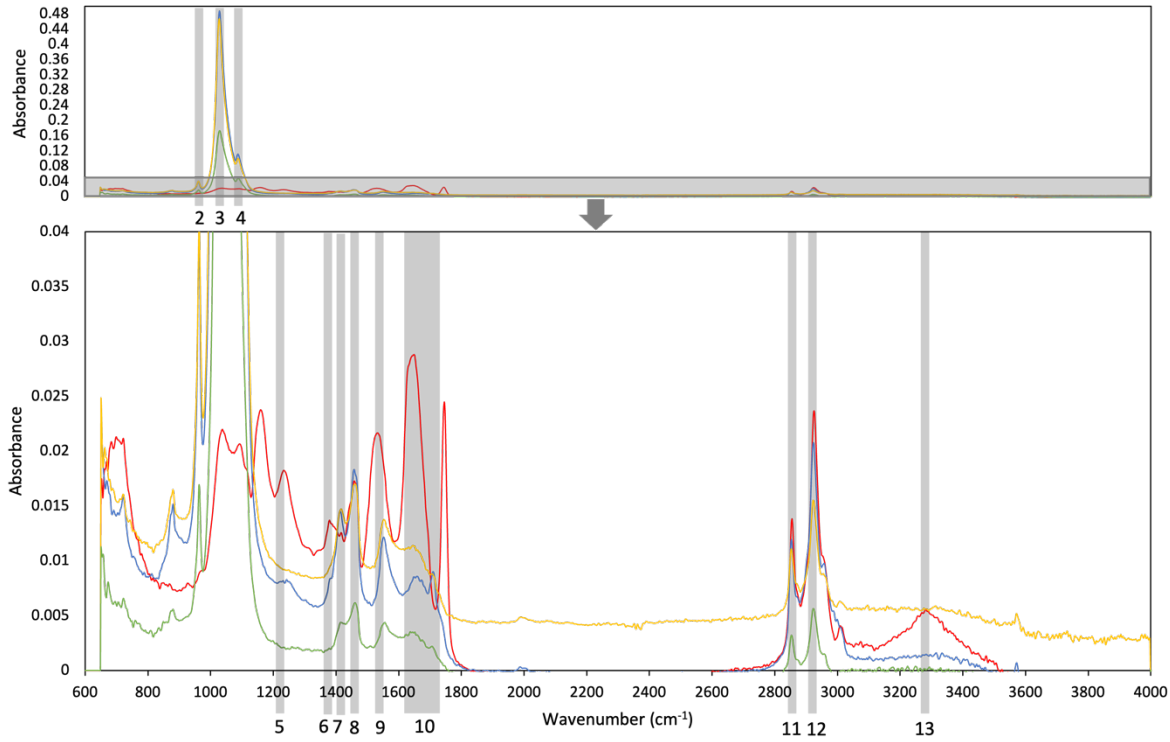
Absorbance
0.48
0.44
0.4
0.36
0.32
0.28
0.24
0.2
0.16
0.12
0.08
0.04
0
2 3 4
0.04
0.035
0.03
0.025
0.02
0.015
0.01
0.005
0
600 800 1000 1200 1400 1600 1800 2000 2200 2400 2600 2800 3000 3200 3400 3600 3800 4000
Wavenumber (cm-1)
5 6 7 8 9 10 11 12 13

(f)

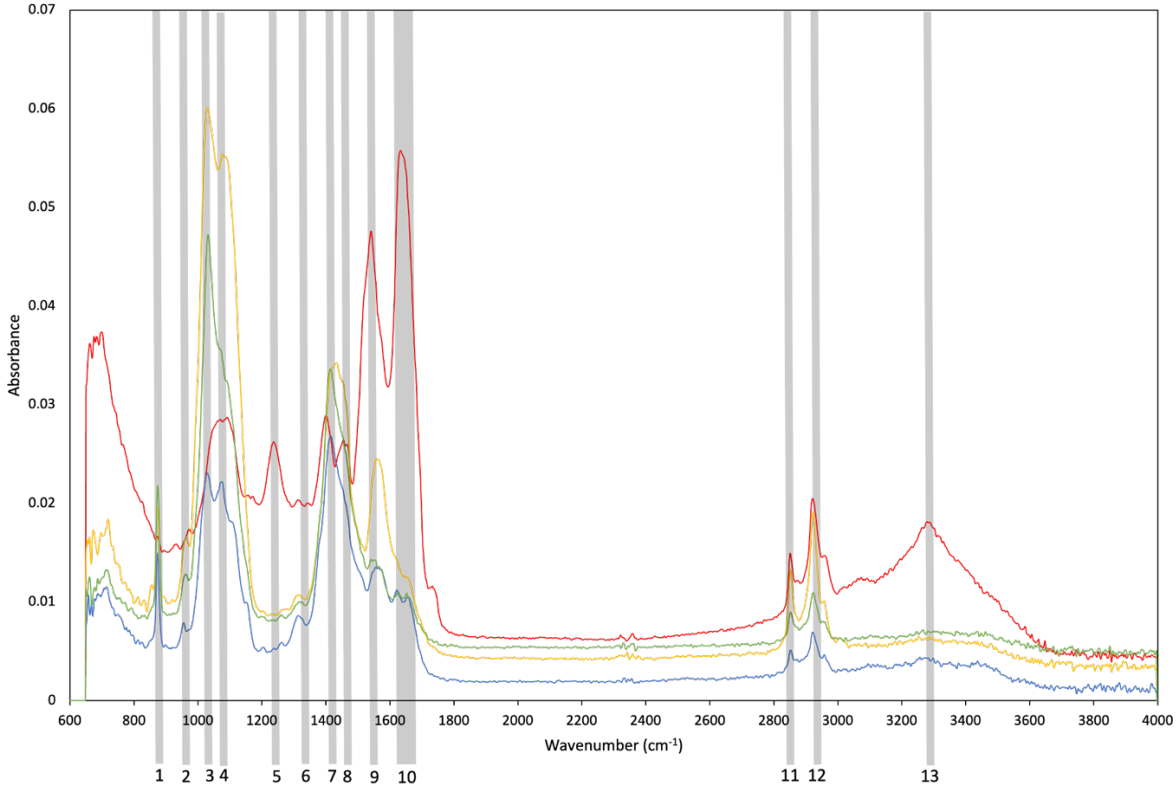
Absorbance
0.07
0.06
0.05
0.04
0.03
0.02
0.01
0
600 800 1000 1200 1400 1600 1800 2000 2200 2400 2600 2800 3000 3200 3400 3600 3800 4000
Wavenumber (cm-1)
1 2 3 4 5 6 7 8 9 10 11 12 13

(g)

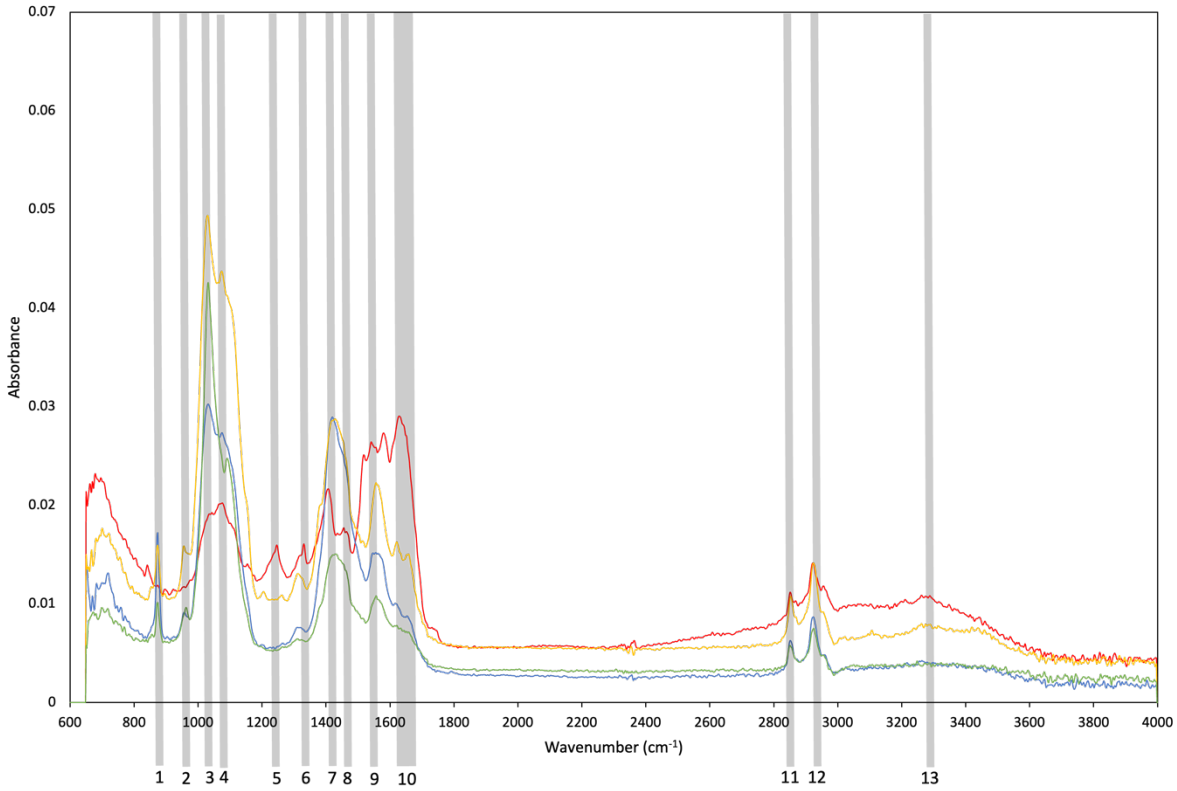

(h)

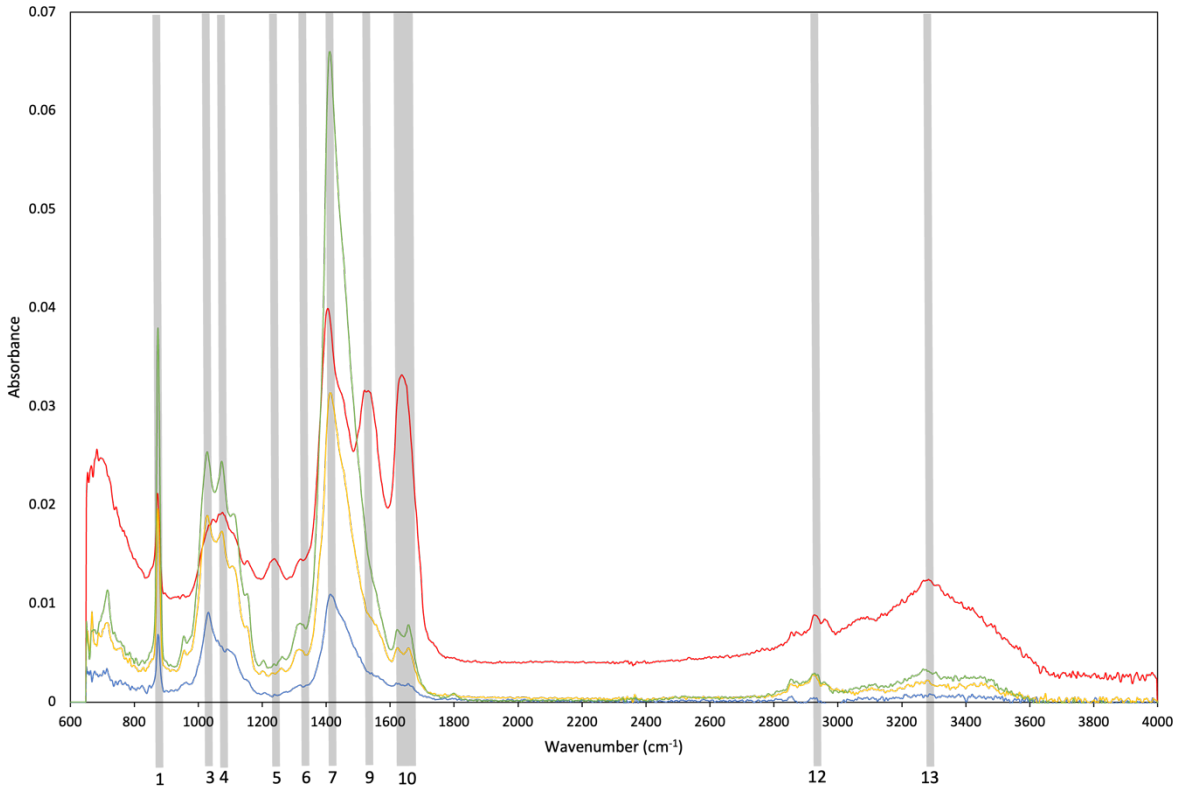

Figure A.4: FTIR spectrum of raw feedstock and hydrochar produced at 200°C, 220°C, 240°C. (a) chub mackerel, (b) hairtail, (c) yellow corvina, (d) horse mackerel, (e) olive flounder, (f) whiteleg shrimp, (g) tiger prawn, (h) Gazami crab.

8.2. Appendix B: Tables

Table B.1: Moisture content of different species

Species	Moisture content (%)
Chub mackerel	71 ± 2
Hairtail	73 ± 3
Yellow corvina	70 ± 4
Horse mackerel	67 ± 2
Olive flounder	71 ± 4
Whiteleg shrimp	77 ± 4
Tiger prawn	81 ± 1
Gazami crab	75 ± 3

Table B.2: Hydrochar yield of the different marine species.

Hydrochar yield (%)	180°C	200°C	220°C	240°C
Chub mackerel	-	15 ± 3	16 ± 2	15 ± 1
Hairtail	-	21 ± 2	22 ± 4	6 ± 2
Yellow corvina	-	19 ± 2	20 ± 2	17 ± 1
Horse mackerel	-	16 ± 1	20 ± 1	19 ± 1
Olive flounder	-	16 ± 5	19 ± 4	17 ± 0.5
Whiteleg shrimp	37 ± 1	48 ± 1	40 ± 4	38 ± 4
Tiger prawn	44 ± 3	62 ± 1	45 ± 2	52 ± 1
Gazami Crab	69 ± 6	68 ± 8	60 ± 4	58 ± 8

Table B.3: Oil yield of the different fish species hydrochars on a wet feedstock basis.

Oil yield (%)	200°C	220°C	240°C
Chub mackerel	24.96	26.35	27.38
Hairtail	19.76	20.82	21.31
Yellow corvina	17.78	18.15	19.20
Horse mackerel	28.29	29.45	29.78
Olive flounder	18.32	20.25	24.11

Table B.4: Elemental analysis of the raw species and the obtained hydrochars.

Sample	T (°C)	C (%)	H (%)	N (%)	S (%)	O (%)	Ash (%)	HHV (kJ/g)
Chub mackerel	raw	58.06	10.10	4.84	0.86	13.24	12.90	31.9
	200	33.36	4.69	0.19	0.00	5.93	55.82	17.0
	220	28.89	4.09	0.44	0.32	3.72	62.55	15.0
	240	30.69	4.40	0.37	0.09	3.13	61.32	16.2
Hairtail	raw	44.98	7.09	9.81	0.42	20.67	17.04	21.8
	200	19.58	2.81	0.36	0.06	4.94	72.26	9.8
	220	31.94	4.33	0.85	0.10	4.85	57.93	16.2
	240	24.10	3.28	0.72	0.04	3.50	68.37	12.2
Yellow corvina	raw	44.38	6.84	6.91	0.36	22.81	18.71	20.8
	200	32.35	4.40	0.36	0.01	5.83	57.06	16.2
	220	29.83	4.11	0.36	0.03	5.71	59.97	15.0
	240	28.71	4.09	0.00	0.00	7.41	59.79	14.3
Horse mackerel	raw	52.81	8.94	8.02	1.17	12.42	16.65	28.6
	200	26.73	3.75	0.12	0.00	5.06	64.34	13.5
	220	32.12	4.47	0.24	0.01	4.71	58.45	16.5
	240	24.77	3.49	0.13	0.00	3.59	68.03	12.8
Olive flounder	raw	48.64	7.82	7.55	0.57	20.56	14.88	24.1
	200	28.98	3.96	0.33	0.02	4.24	62.47	14.8
	220	23.90	3.27	0.66	0.02	6.65	65.50	11.6
	240	29.02	3.89	0.59	0.02	3.87	62.62	14.7
Whiteleg shrimp	raw	38.75	5.81	8.49	0.58	29.63	16.75	16.2
	200	35.40	4.27	3.34	0.18	27.61	29.21	13.2
	220	35.36	4.31	1.92	0.11	21.35	36.95	14.3
	240	35.30	4.07	2.41	0.11	28.64	29.47	12.7
Tiger prawn	raw	37.68	5.66	8.67	0.21	32.12	15.68	15.1
	200	36.72	4.21	1.91	0.06	28.81	28.29	13.3
	220	34.81	3.92	1.39	0.12	24.71	35.05	13.0
	240	31.19	3.28	1.49	0.08	28.24	35.72	10.2
Gazami crab	raw	39.21	5.91	8.51	0.32	19.23	26.82	18.4
	200	20.56	1.64	0.59	0.06	25.40	51.76	4.7
	220	22.32	1.99	0.83	0.07	26.36	48.44	5.7
	240	22.03	1.84	0.69	0.06	25.03	50.35	5.6

Table B.5: Proximate analysis of the raw species and the obtained hydrochars.

Sample	T (°C)	Volatile Matter (%)	Fixed Carbon (%)	Ash (%)
Chub mackerel	raw	79.2	7.3	13.4
	200	34.9	6.5	58.5
	220	46.9	0.5	52.6
	240	39.5	0.0	60.5
Hairtail	raw	70.8	11.4	17.8
	200	36.2	0.3	63.5
	220	36.0	0.0	64.0
	240	19.8	1.0	79.2
Yellow corvina	raw	73.7	6.8	19.5
	200	43.2	0.0	56.8
	220	48.1	0.0	51.9
	240	41.0	0.0	59.0
Horse mackerel	raw	75.3	6.8	17.9
	200	39.2	0.0	60.8
	220	38.6	0.0	61.4
	240	37.5	0.7	61.8
Olive flounder	raw	76.4	8.8	14.9
	200	32.9	0.0	67.1
	220	22.6	0.0	77.4
	240	20.2	1.1	78.8
Whiteleg shrimp	raw	73.3	8.8	17.9
	200	68.6	3.4	28.1
	220	68.4	3.9	27.7
	240	71.9	3.6	24.5
Tiger prawn	raw	73.5	8.9	17.6
	200	67.2	4.6	28.2
	220	65.7	3.3	31.1
	240	63.8	4.0	32.3
Gazami crab	raw	67.3	3.9	28.8
	200	56.4	0.0	43.6
	220	58.5	0.0	41.5
	240	57.1	0.0	42.9

Table B.6: Main functional groups present in the FTIR spectra on the raw feedstock (✓) and the produced hydrochars (✓) of the fish; chub mackerel (CM), hairtail (H), yellow corvina (YC), horse mackerel (HM), olive flounder (OF).

	Range (cm^{-1})	Type of functional group	Ref.	CM	H	YC	HM	OF
1	820 – 940	O-H bending bands from clay minerals associated with hydrochar	[256]	-	-	-	-	-
2	960-970	Alkene trans-C-H out-of-plane bend	[257]	✓	✓	✓	✓	✓
3	1020-1030	OH representative of oxygenated functional groups of polysaccharides	[258]	✓	✓	✓✓	✓✓	✓✓
4	1020 – 1160	C-O from polysaccharide, carbohydrate region	[259], [260], [261]	✓✓	✓✓	✓✓	✓✓	✓✓
5	1200 – 1280	Carboxylic acid C-OH stretch, O-H deformation	[260], [262]	-	✓	✓	-	✓
6	1310-1390	Phenolic O-H bend, -$C(CH_3)$ C-H deformation	[263]	-	-	-	✓	✓
7	1400-1450	Carbonate (v3; asymmetric stretch)	[256]		✓	✓✓		✓
8	1440-1480	CH_2 deformation (scissor vibration)	[263]	✓✓	✓✓	✓✓	✓✓	✓✓
9	1520 – 1590	COO- carboxylate anions	[264], [265]	✓	✓✓	✓✓	✓✓	✓✓
10	1650 – 1740	C=O from carboxylic acids, esters, and ketones	[263]	✓✓	✓✓	✓✓	✓✓	✓
11	2840 – 2870	Symmetric aliphatic CH from terminal CH_3 groups	[263], [266], [267]	✓✓	✓✓	✓✓	✓✓	✓✓
12	2920 – 2950	Asymmetric aliphatic CH from terminal CH_2 groups	[263]	✓✓	✓✓	✓✓	✓✓	✓✓
13	3200 - 3600	OH from sorbed water and hydrogen-bonded hydrochar O-H groups	[258]	✓	✓	✓	-	✓

Table B.7: Main functional groups present in the FTIR spectra on the raw feedstock (✓✓) and the produced hydrochars (✓) of the crustaceans; whiteleg shrimp (WS), tiger prawn (TP), Gazami crab (GC).

	Range (cm^{-1})	Type of functional group	Ref.	WS	TP	GC
1	820 – 940	O-H bending bands from clay minerals associated with hydrochar	[256]	✓	✓	✓✓
2	960-970	Alkene trans-C-H out-of-plane bend	[257]	✓	✓	-
3	1020-1030	OH representative of oxygenated functional groups of polysaccharides	[258]	✓	✓	✓
4	1020 – 1160	C-O from polysaccharide, carbohydrate region	[259], [260], [261]	✓	✓✓	✓✓
5	1200 – 1280	Carboxylic acid C-OH stretch, O-H deformation	[260], [262]	✓	✓	✓
6	1310-1390	Phenolic O-H bend, -C(CH_3) C-H deformation	[263]	✓	✓✓	✓
7	1400-1450	Carbonate (v3; asymmetric stretch)	[256]	✓✓	✓✓	✓✓
8	1440-1480	CH_2 deformation (scissor vibration)	[263]	✓	✓	-
9	1520 – 1590	COO- carboxylate anions	[264], [265]	✓✓	✓✓	✓
10	1650 – 1740	C=O from carboxylic acids, esters, and ketones	[263]	✓✓	✓✓	✓✓
11	2840 – 2870	Symmetric aliphatic CH from terminal CH_3 groups	[263], [266], [267]	✓✓	✓✓	-
12	2920 – 2950	Asymmetric aliphatic CH from terminal CH_2 groups	[263]	✓✓	✓✓	✓✓
13	3200 - 3600	OH from sorbed water and hydrogen-bonded hydrochar O-H groups	[258]	✓	-	✓